Titre: Title:	Towards Single Bacterium Detection: A Microelectronic/Microfluidic Hybrid System Based on a CMOS Technology
Auteur: Author:	Zhao Lu
Date:	2012
Type:	Mémoire ou thèse / Dissertation or Thesis
Référence: Citation:	Lu, Z. (2012). Towards Single Bacterium Detection: A Microelectronic/Microfluidic Hybrid System Based on a CMOS Technology [Ph.D. thesis, École Polytechnique de Montréal]. PolyPublie. https://publications.polymtl.ca/836/

URL de PolyPublie: PolyPublie URL:	https://publications.polymtl.ca/836/
Directeurs de recherche: Advisors:	Sylvain Martel, & Yvon Savaria
Programme: Program:	Génie informatique

UNIVERSITÉ DE MONTRÉAL

TOWARDS SINGLE BACTERIUM DETECTION: A MICROELECTRONIC/MICROFLUIDIC HYBRID SYSTEM BASED ON A CMOS TECHNOLOGY

ZHAO LU
DÉPARTEMENT DE GÉNIE INFORMATIQUE ET GÉNIE LOGICIEL
ÉCOLE POLYTECHNIQUE DE MONTRÉAL

THÈSE PRÉSENTÉE EN VUE DE L'OBTENTION
DU DIPLÔME DE PHILOSOPHIE DOCTOR
(GÉNIE INFORMATIQUE)
AVRIL 2012

UNIVERSITÉ DE MONTRÉAL

ÉCOLE POLYTECHNIQUE DE MONTRÉAL

Cette thèse intitulée:

TOWARDS SINGLE BACTERIUM DETECTION: A MICROELECTRONIC/MICROFLUIDIC HYBRID SYSTEM BASED ON A CMOS TECHNOLOGY

présentée par: LU Zhao
en vue de l'obtention du diplôme de : Philosophiae Doctor
a été dûment acceptée par le jury d'examen constitué de :

M. LANGLOIS, J.M. Pierre, Ph.D., président
M. MARTEL, Sylvain, Ph.D., membre et directeur de recherche
M. SAVARIA, Yvon, Ph.D., membre et codirecteur de recherche
M. PETER, Yves-Alain, Dr. Sc., membre
M. PACKIRISAMY, Muthukumaran, Ph.D., membre

DEDICATION

My Parents

ACKNOWLEDGMENT

I would first like to thank my principal supervisor, Prof. Sylvain Martel, for his enthusiasm in science and engineering and spirit of innovation. Sylvain served as role model for what can be accomplished by hard work and creative thinking. He always encourages his students thinking out of the box and to be the best of the world. I would also like to thank my co-supervisor, Prof. Yvon Savaria, I very appreciate his endless support and deep technical insights. Without his help, I would not have been able to complete this thesis. His heart for students and attitude to research will have deep impact in my life and career.

Additionally, I would like to express thanks and gratitude to the members of the Nanorobotics Laboratory. Every member repeatedly demonstrated a willingness to help each other. Neila Kaou, Mahmood Mohammadi, Charles C. Tremblay,Walder André, Ouajdi Felfoul, et al.,contributed to the completion of this work and in making it an enjoyable experience.

So many people helped for the fabrication of the device. Especially, I want to thank the members of the LMF and Polystim laboratory, Marie-Hélène Bernier, Philippe Vasseur, Souleymane Bah. I am much obliged to Laurent Mouden, he has never said "No" to my always urgent request of chip bonding. I would like to thank Ryan Denomme for his contribution to the proof of concept and friendship. I also want to thank my dear collaborator, Jaouad El-Fouladi for his efforts in our two generations of IC chips.

I want to thank my parents (Lu Junzhu and Huang Kunning)) for their endless love and devotion. Without my parents' early support for my curiosity and my education and my older brother Lu Ming's encouragement, this work would not have been possible.

Finally to my family, the smile of my son, Lu Yueran (Taotao) and my daughter, Lu Yiran (Yaoyao), are the greatest motivation and happiness of all in my PhD life. To my wife, Liu Guoyuan, I thank you for all your sacrifice, patience and support and most of all, for your love.

RÉSUMÉ

Cette thèse porte sur le développement d'un biocapteur hybride CMOS microfluidique capable de détecter des bactéries pathogènes une à une en temps réel basé sur un principe de spectroscope impédimétrique. Le biocapteur proposé se compose d'une matrice de capteurs qui comportent une matrice de microélectrodes, desmultiplexeurs à commande numérique, et des circuits de détection intégrés sur une puce de silicium CMOS. Cette recherche propose une nouvelle structure de microélectrodes qui permet à une structure de microélectrodes face à face à haute densité intégrable par post-traitement d'une puce CMOS. Au lieu d'être créée par le dépôt et la gravure de couches métalliques supplémentaires, la structure de microélectrodes face à face est construite en exploitant un empilement de couches métalliques disponible avec la technologie CMOS adoptée. Les détecteurs sont obtenus en construisant des microcanaux qui traversent le substrat. Ces microcanaux passent entre les microélectrodes face à face. Lorsque les fluides où se trouvent les échantillons traversent le microcanal, le système détecte de façon continue les changements d'impédance entre les microélectrodes induits par le passage de chaque bactérie.

Cette thèse étudie le processus de microfabrication qui permet de libérer la matrice de microélectrodes et de fabriquer les microcanaux traversant le substrat. Les techniques dites de FIB (focused ion beam) et de DRIE (deep reactive ion etching) sont utilisées. Les forces et faiblesses de chaque technologie sont analysées et des recettes de processus optimisés sont étudiées. La matrice de microélectrodes a été réalisée avec succès par les deux technologies. Comme preuve de concept, plusieurs microcanaux traversant le substrat sont également formés en utilisant la technologie FIB.

Cette thèse propose également un nouveau circuit de détection. Réalisé grâce à la micro-électronique, ce circuit est capable de détecter les changements d'impédance causés par le passage d'une seule bactérie dans un milieu conducteur. Sans conditionnement de signaux et de circuit de traitement complexes, tels que des amplificateurs de haute précision, des filtres ou des convertisseurs analogue à numérique ou numérique à analogique, le circuit de détection offre une bonne sensibilité et une configurabilité qui permet de l'adapter à diverses conditions de détection. Une technique de mise en boîtier biocompatible est également mise en oeuvre pour encapsuler le

capteur intégré tout en fournissant des interfaces fluidiques et électriques pour l'injection d'échantillons et de signaux électriques.

Une nouvelle approche pour améliorer la sélectivité de détection basée sur l'utilisation de bactéries magnétotactiques est également proposée dans cette thèse. Sous le contrôle d'un champ magnétique extérieur, les bactéries magnétotactiques sont utilisés comme bio-transporteurs, qui peuvent chercher activement et capturer les bactéries pathogènes cibles afin de les amener à la zone de détection.

Une puce microfluidique est fabriquée grâce à des techniques de prototypage rapide afin de valider les idées proposées et de fournir des guides de conception d'une puce plus avancés. Les résultats de microfabrication et les résultats des tests préliminaires montrent que l'intégration monolithique des technologies CMOS et microfluidique est possible et qu'elle permet la réalisation de microélectrodes face à face dans une plate-forme capable de détecter le passage d'une seule bactérie en isolation.

ABSTRACT

This thesis reports on the development of a CMOS Microfluidic hybrid biosensor technology that is proposed to detect single pathogenic bacterium in real time based on impedimetric spectroscopy. The proposed biosensor consists of a CMOS silicon die that incorporates a microelectrode array, digitally controlled multiplexers, and sensing circuits. This research proposes a novel microelectrode structure, which is obtained by first manufacturing high density face to face microelectrodes on a CMOS die, possible by a relatively simple CMOS post-processing. Instead of deposition and patterning of additional metal layers, theface to face microelectrode array is constructed by stacking metal and via layers of the adopted CMOS technology. By constructing through substrate microchannels in between pairs of face to face microelectrodes, when a fluid sample flows through the microchannel, the microelectrodes on the wall detect the impedance change induced by bacterium in the fluid in a continuous way.

This thesis investigates the microfabrication process of releasing microelectrode arrays and constructing through substrate microchannels. FIB (Focused Ion Beam) and DRIE (Deep Reactive Ion Etching) technologies are utilized. The strength and weakness of each technology are analyzed and optimized process recipes are investigated. Microelectrode array were successfully released using both process technologies. As a proof of concept, several through substrate microchannels were also formed by using the FIB technology.

This thesis also proposes a novel sensing microelectronic circuit, which is able to sense the impedance change caused by a single bacterium in a conductive medium. The system does not require complex signal conditioning and processing circuits, such as high precision amplifiers, filters or ADC/DAC. The proposed simple sensing structure offer high sensitivity, reliability and configurability. A dedicated biocompatible packaging is also implemented to encapsulate the CMOS die and provide a microchamber, fluidic and electrical interfaces for sample injection and signal interfaces.

A new approach to achieve detection selectivity or specificity assisted by magnetotactic bacterium is also proposed in this thesis. Under the control of an external magnetic field, the

magnetotactic bacteria are used as bio-carriers, which can actively search and capture some target pathogenic bacteria and bring them to the sensing area.

A microfluidic chip is fabricated by rapid prototyping techniques to validate the proposed idea and to provide design guides for a more advanced and highly integrated CMOS chip. The achieved microfabrication results and preliminary testing results show that the monolithic integration of CMOS and microfluidic technology, especially the face to face microelectrode structure is a suitable platform for single bacterium detection and analysis.

TABLE OF CONTENTS

LIST OF TABLES

LIST OF FIGURES

LIST OF ABBREVIATIONS

AC	Alternating current
ADC	Analog to digital converter
AOE	Advanced oxide etch
ASE	Advanced silicon etch
CFU	Colony forming unit
CMOS	Complementary-symmetry metal–oxide–semiconductor
DAC	Digital to analog converter
DC	Direct current
DEP	Dielectrophoresis
DFP	Dry film photoresist
DNA	Deoxyribonucleic acid
DPX	Diparaxylylene
DRIE	Deep reactive ion etching
EDP	Ethylene diamine pyrochatechol
EIS	Electrochemical impedance spectroscopy
ELISA	Enzyme-linked immunosorbent assay
FEM	Finite element model
FIB	Focused ion beam
GIS	Gas injection system
FRA	Frequency response analyzer
IMS	Immunomagnetic separation
ISFET	Ion selective field effect transistors

LIF	Laser induced fluorescence
MTB	Magnetotactic bacteria
MP	Magetophoresis
NMOS	N-type metal-oxide-semiconductor
PCB	Printed circuit board
PCR	Polymerase chain reaction
PDMS	Polydimethylsiloxane
PMOS	P-type metal-oxide-semiconductor
PMT	Photomultiplier tube
RBC	Red blood cell
RIE	Reactive-ion etching
SAW	Surface acoustic wave
SEM	Scanning electron microscope
SPR	Surface plasmon resonance
TEM	Transmission electron microscopy
TMAH	Tetramethylammonium hydroxide
TSMC	Taiwan semiconductor manufacturing company
TSV	Through silicon via

LIST OF APPENDIX

CHAPTER 1 INTRODUCTION

1.1 Background and motivation

Rapid and on-site bacteria detection and identification, especially for pathogenic bacteria, are becoming a global issue. Diseases caused by pathogenic bacteria are a major cause of human death, accounting for nearly 40% of the total 50 million annual estimated deaths worldwide. Only in the United States, each year, around 76 million people suffer from food-borne illnesses caused by pathogenic bacteria such as *Salmonella typhimurium, Escherichia Coli, Staphylococcus aureus*, and *Campylobacter jejuni* [1]. For *salmonella* only, which is a very dangerous food borne pathogen, approximately 5 million analytical tests are performed annually with the cost of $1billion [2]. *E.Coli O157:H7* is a rare strain of *E.Coli* that is considered to be one of the most dangerous food borne pathogens. It causes 20 000 illnesses and 500 deaths per year in USA [3]. Moreover, pathogenic bacteria are generally present at very low concentrations. For example, the infectious dosage of *E.Coli O157:H7* or *Salmonella* is as low as 10 cells，and the existing standard for maximum concentration *E.Coli* in drinking water is 4 cells/100 ml. Thus, rapidly identifying low concentrations of pathogenic bacteria down to single bacterium is critical to control and prevent such diseases.

Some conventional bacteria identification methods can detect a single bacterium. For example, a well known technique is based on amplification of the number of bacteria. It generally includes four steps [4,5]: 1) pre-enrichment or pre-amplification: to allow growth and reproduction of all the micro-organisms; 2) selective enrichment: to grow the targeted micro-organisms population to a detectable level; 3) isolation; and 4) confirmation: serological and biochemical analysis to confirm the presence of the targeted pathogenic bacteria. Typically, the whole procedure may require from at least 16 hours to several days. In these cases, by the time the pathogen or undesired microorganisms are identified, the contaminated food, water or other products would probably have been fabricated or shipped to customers. Furthermore, detection of a few pathogens in a clinical sample, food, water, or cosmetics requires a lot of work from highly skilled professional laboratory personnel.

During the last decade, considerable efforts were dedicated to design more automated, faster, and more sensitive detection approaches. Currently, the most sensitive technology is DNA analysis which uses the polymerase chain reaction (PCR) to amplify small quantities of genetic material to determine the presence of bacteria. Optical biosensors, especially the bioluminescence sensors, show extremely high specificity, and can distinguish viable from non viable bacteria. Blasco et al.[6] reported a method to detect *Salmonella Newport* and *E.Coli* by measuring the ATP bioluminescence. The sensitivity can reach 10^4cells/ml. Both technologies usually take hours to produce results.

One common automated bacterial detection technology is based on the changes of electrical characteristics of a medium where the bacteria are cultivated. Electrodes are generally immersed in an aqueous media and connected with an AC or DC power source. The presence of the bacteria is indicated when the measured impedance changes beyond a certain threshold.

However, for all the work reported in literature dealing with impedance detection methods, the detection time depends on the diffusion rate of the target bacteria or the ionic metabolite that the bacteria release in the media (usually, it takes several hours to 7 days). Also, generally, most of the bacteria are not motile. Furthermore, the diffusion rate of the bacteria and their metabolite are very slow, especially under the condition of low-Reynold number laminar fluidics [7, 8, 9]. If the target sample only contains a few bacteria, it takes a long amplifying time for bacteria to reach the detectable level or reach the detection area. Moreover, this method does not guarantee sensitivity and specificity. Some technologies were developed to reduce the time to target bio-entities approaching the electrode array.

Magnetophoresis (MP), optical fields, flow-driven methods, and dielectrophoresis (DEP) have been demonstrated as effective techniques [10-20] to manipulate or transport bio-entities. The flow-driven approach utilizes hydrodynamic forces to manipulate bacteria and particles. However, the laminar stream required to induce the displacement of bacteria and particles needs to be accurately controlled. This requires the fabrication of complex microchannel networks [18]. Optical methods depend on accurate beam focusing and alignment between the targeted particles and require complicated optical instruments [19]. DEP and MP are the most widely adopted particle and cell transportation techniques. DEP based transportation is achieved by the use of an

inhomogeneous electric field [10, 11, 13], while MP uses a magnetic field gradient to cause particle migration [20]. Both methods encounter limitations in their applications. First, in order to generate large enough electric/magnetic field gradients, electrodes or magnets have to be patterned in channels or chambers where the particles are carried. The generated force is relatively strong in the vicinity of the electrodes, but decreases with the distance from the electrode's plane. In order to maintain enough force on particles or bacteria to combat the hydrodynamic drag force, a high density of electrodes near the desired transportation paths is required, which limits the effective transportation distance. Moreover, in order to realize two or three dimensional transportation of particles, fairly complicated implementations of electrodes/magnets is needed [16, 12]. Second, in order to move the desired particles and bacteria, relatively high frequencies and voltage amplitudes are required to induce a sufficient DEP force, which may break down the bacteria's membrane and affect the viability of target bacteria. Additionally, for the transportation of bio-entities, the high voltage on the electrodes or electro-magnets induces joule heating, which may also cause damage on cells [17]. Third, DEP and MP both depend on the properties of the entities being manipulated and the medium containing them. Thus, unwanted entities with similar dielectric or magnetic properties to the targeted entities can be selected and controlled, which causes significant difficulties when trying to achieve high selectivity.

Through this brief introduction of conventional and current approaches, we conclude that there are at least four major challenges for rapid, specific, low-volume bacteria detection. 1. An extremely sensitive detection method is needed to identify single bacterium. 2. An efficient way to bring the targeted bacteria to the sensing area is needed. 3. The biosensor should be low cost, field deployable, and functioning in an automatic manner. 4. Those specifications should be achieved without sacrificing the viability of the target samples. In this research, we are trying to address the first three challenges by combining the conventional microelectronic technology with recent advances in microfluidic/lab-on-chip technology. The specificity of the single bacterium detection assisted by magnetotactic bacteria is also evaluated.

1.2 Overview of the thesis

The objective of the thesis is to contribute to the development of a microfluidic/CMOS hybrid system aimed at rapid single bacterium detection. The single bacterium detection is realized by impedance measurement through an array of vertical, face to face microelectrodes which is implemented onto a CMOS chip by stacking the metal and via layers together. Each microchannel created using post-processing procedures, goes through a CMOS die, forcing bacterium to pass between a pair of microelectrodes constructed using layers of a conventional CMOS process. With medium flow, bacteria are allowed to pass through the microchannels, where impedance variations are measured using a microelectrode pair on the wall, which is connected to on-chip sensing circuits. The through substrate microchannels allow high throughput and real-time detection for single bacterium to be achieved in a continuous manner. Two CMOS post-processing procedures, including Focused Ion Beam (FIB) for rapid prototyping and Deep Reactive Ion Etching (DRIE) for batch fabrication, are evaluated. A specific packaging method for encapsulating the whole system is also presented. The fabrication and testing results confirm that a high density of vertical microelectrodes can be constructed on a CMOS chip with a relatively simple post-processing procedure. The embedded sensing circuit can greatly improve the detection sensitivity. Preliminary tests show that a 2% electrical impedance change due to conductivity variations between a pair of microelectrodes can be distinguished by the proposed system. In this thesis, the feasibility of using MC-1 magnetotactic bacteria as a bio-carrier to accelerate the screening speed and achieve specificity is also explored.

1.3 Contribution of this research

1) Proposed and implemented face to face microelectrode arrays using CMOS technology. In this research, we first proposed a face to face microelectrode constructed by stacking metal layers using a CMOS technology. The idea was initially published in 2007 as :

   Z. Lu, R. Denomme, and S. Martel,"Micro/Nanoparticle Detection: An impedimetric microsensor based on CMOS technology", 7th IEEE International Conference on Nanotechnology (IEEE-NANO), Hong Kong, China, Aug. 2-5, 2007

R. Denomme, Z Lu., and S. Martel, "An integrated biosensor for the detection of bio-entities using magnetotactic bacteria and CMOS technology", 29th Annual International Conference of the IEEE Engineering in Medicine and Biology Society (EMBS), Lyon, France, Aug. 23-26, 2007.

The latest results are presented in the paper submitted to Journal Biomicrofluidics with the title of "*A novel vertical microelectrode array based on CMOS technology, design, microfabrication, and test".*

2) This research explored the feasibility of using focused ion beam (FIB) technology and conventional deep reactive ion etching (DRIE) to achieve through substrate microchannels(Vias) generally called TSV in 3D IC technology. Part of the results was published on IEEE Mixed-Signal Test Workshop (IMS3TW) 2008 with the title: *"A hybrid bacteria and microparticle detection platform on a CMOS chip: design, simulation and testing considerations".*

3) This research also proposed a novel impedimetric biosensor based on CMOS technology for single bacterium detection and analysis. The proposed sensing mechanism and circuit are novel, very sensitive, and impose no need for complex signal processing circuitry. The idea and results were published at IMS3TW 2008 with the title: *"A hybrid bacteria and microparticle detection platform on a CMOS chip: design, simulation and testing considerations".*

4) This research also explored the feasibility of using magnetotactic bacteria as a bio-carrier in the proposed system to enhance the detection specificity. The idea, prototype, and some experimental results were published in several papers.

Z. Lu, J. El-Fouladi, Y. Savaria, and S. Martel, "A hybrid bacteria and microparticle detection platform on a CMOS chip," The 11th International Conference on Miniaturized Systems for Chemistry and Life Sciences (μTAS), Paris, France, Oct. 7-11, 2007.

R. Denomme, Z. Lu, and S. Martel, "A microsensor for the detection of a single pathogenic bacterium using magnetotactic bacteria-based bio-carriers: simulations and preliminary experiments", 29th Annual International Conference of the IEEE Engineering in Medicine and Biology Society (EMBS), Lyon, France, Aug. 23-26, 2007.

J. El Fouladi, Z. Lu, Y. Savaria, and S. Martel, "An integrated biosensor for the detection of bio-entities using magnetotactic bacteria and CMOS technology", 29th Annual International Conference of the IEEE Engineering in Medicine and Biology Society (EMBS), Lyon, France, Aug. 23-26, 2007.

Z. Lu. and S. Martel., "Controlled bio-carriers based on magnetotactic bacteria", The 14th International Conference on Solid-state Sensors, Actuators, and Microsystems (Transducers 2007), Lyon, France, June 10-14, 2007.

Z. Lu, O. D. Truong, W. André. and S. Martel, "Preliminary design of a biosensor based on MC-1 magnetotactic bacteria," The 9th World Congress on Biosensors (Biosensors 2006), Toronto, Canada, May 10-12, 2006.

Z. Lu. and S. Martel, "Preliminary investigation of bio-carriers using magnetotactic bacteria," Proceedings of the 28th IEEE-EMBS Annual International Conference of the Engineering in Medicine and Biology Society, pp. 3415-3418, New York, Aug. 30 – Sept. 3, 2006.

Z. Lu and S. Martel, "Microfluidic system for assessing the controllability of MC-1 magnetotactic bacteria as carriers in micro-channels," The Nanotechnology Conference and Trade Show (NSTI) Nanotech, Boston, MA, USA, May 7-11, 2006.

1.4 Structure of the thesis

This thesis describes the systematic development of a microfluidic/microelectronic system based on CMOS technology and CMOS post-processing, covering topics such as bacteria detection, microfabrication, and microsystem integration. It is divided into seven chapters. The topic of each chapter is described as follows.

Chapter 1 presents the background, motivation, objective, and major contributions of the research.

Chapter 2 reviews the literature and development of technologies used in this research, including the single bacterium sensing technology, impedemetric biosensor, CMOS-based lab-on-chip system and CMOS post processing fabrication technology. The strengths and weaknesses of conventional technologies are

presented. The advantages and challenges of CMOS based biosensor are discussed as well.

Chapter3 defines the system architecture including a novel microelectrode structure based on a standard CMOS technology, sensing mechanism, on-chip microelectronic sensing circuit, system packaging methods. Design considerations such as biocompatibility, robustness and reliability are also discussed in this chapter, and finally, the feasibility of utilizing magnetotactic bacteria as bio-carriers to achieve specificity and high screening speed is also presented.

Chapter 4 focuses on optimizing dimensions of microelectrodes and microchannels using finite element modeling (FEM) simulations. The detailed circuit simulations provide design specifications for sensing circuits. Finally, the layouts of a prototype device based on the MicraGEM technology and a lab-on-chip based on a standard CMOS process are given.

Chapter 5 mainly focuses on some CMOS post-processing procedure for releasing the microelectrode array and forming through substrate microchannels. Two microfabrication technologies, FIB and DRIE, are discussed and compared, illustrated with microfabrication results. The MicraGEM technology used to fabricate prototype chips is also presented. The system packaging steps are finally described.

Chapter 6 presents the experimental results obtained with the proposed system. The test results are discussed and interpreted. The system deficiencies and possible remedies are presented. Preliminary experimental results related to utilizing the MC-1 magnetotactic bacteria to obtain bacterium specific detection are also presented.

Chapter 7 summarizes the thesis and points towards future directions to optimize the proposed systems.

CHAPTER 2 LITERATURE REVIEW

2.1 Introduction

As briefly introduced in Chapter 1, rapid and effective detection of single pathogenic bacterium is extremely important in diagnosis, disease control and prevention, biomedical and recent fight against bioterrorism. As an example, around 81 million persons in the USA are affected by food-borne diseases each year, with a cost of $8 to $10 billion per year [21-24]. Recently, outbreaks of food and air-borne pandemic diseases caused by *E-coli:O157*, Salmonella, and *H1N1* indicated that, with the change of human living style and highly centralized and integrated food processing, an ultrasensitive and rapid biosensor is urgently required both for early accurate diagnosis and disease prevention. This chapter aims to give an overview of pathogen bacteria detection methods. Since the literature of bacteria detection is vast, we will focus on three main topics: a) conventional methods for pathogenic bacteria detection, b) impedimetric detection methods and c) micro-nanotechnology and microelectronic technology based detection methods. The generic advantages and limitations for each method are also given. Based on the research literature, breakthroughs such as adoptions of magnetic beads, nanoparticles and integrated microelectronic-microfluidic hybrid microsystem will be highlighted.

2.2 Conventional individual bacteria detection methods

Polymerase chain reaction (PCR), culture and colony counting methods, as well as immunology-based methods are the most widely used methods for pathogen detection. They involve DNA sample amplification and analysis, bacteria culturing, amplification and identification, and antigen–antibody interactions, in sequence. In spite of weaknesses such as the long turnover time for the analysis, the complexity of the procedure and requirement for highly skilled staff, they still represent the most reliable and accurate detection methods among available technologies. These methods are often combined together to yield more robust results. The strengths and weaknesses of each technology are discussed below.

2.2.1 Plating, culturing, and counting method

The plating, culturing, and counting method was developed 100 years ago. As a standard procedure, it is still widely adopted in clinical laboratories all over the world [25]. Fig. 2.1 illustrates a typical protocol for identifying pathogenic bacteria from samples. Generally, the process starts with pre-enrichment, in which samples are incubated in a nutritious medium to allow amplification of the targeted bacteria [26~28]. Pre-enriched samples are then transferred into a specially formulated medium for selective enrichment, where the targeted bacteria are allowed to grow, while the growth of other bacteria is suppressed. After that, culture-enriched samples are plated onto selective and differential media, normally in a Petri dish, where different bacterial types are presumptively recognized on the basis of distinguishing colony characteristics. Finally, the results need to be verified by biochemical identification or serotyping procedure. Typical processing times range from 4 to 9 days for initial identification and 14 to 16 days for verification [29].

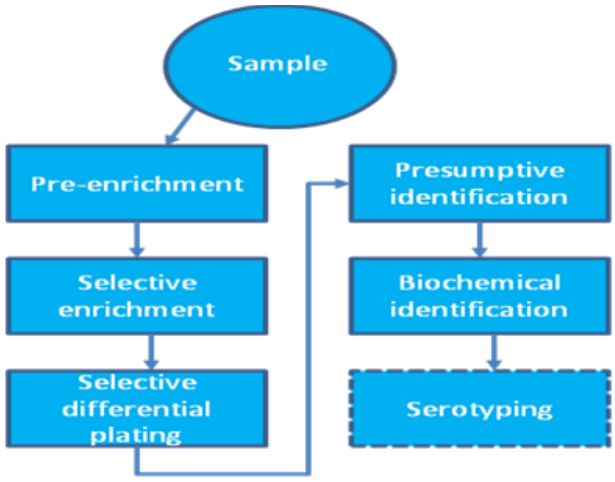

Fig 2.1: Flow chart showing the procedure for the isolation and identification of pathogenic bacteria from samples (Adapted from [25]).

As a result, this conventional method is inadequate for making real-time detection and identification. The situation gets even worst if the initial concentration of the pathogenic bacteria is very low, for example, the infectious dose of *E. coli* O157:H7 is around 10–100 cells, and the presence of even a single bacterium in food may pose a serious health risk [30, 31].

2.2.2 Polymerase chain reaction (PCR)

PCR is a nucleic acid amplification technology, which was developed in the mid 80s [32] and is very widely used in pathogenic bacteria detection. Firstly, DNA is extracted and purified from a sample, such as saliva, blood or water. Then, the DNA samples go through several thermal cycling illustrated in Fig 2.2, consisting of cycles of repeated heating and cooling, including denaturing, annealing, extension and polymerization procedure, to cause DNA melting and enzymatic replication of the DNA. Primers (short DNA fragments) containing sequences complementary to the target region along with a DNA polymerase are key components to enable selective and repeated amplification. As PCR progresses, the DNA replicates itself in the fashion of a chain reaction in which the DNA template is exponentially amplified. Within hours, a single or a few copies of a piece of targeted DNA generate thousands to millions of copies of a particular DNA sequence [33, 34]. The presence of the amplified sequence is subsequently detected by gel electrophoresis [35].

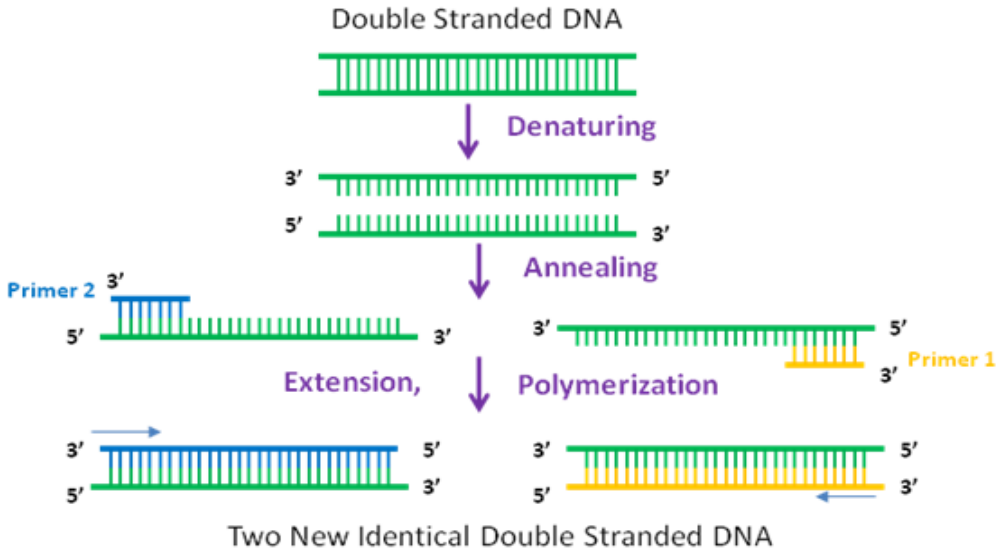

Fig2.2: Schematic of one PCR cycle taking place in a thermocycle [32].

There are various PCR methods developed for bacterial detection: for example, a) real-time PCR [36], b) multiplex PCR [37], and c) reverse transcriptase PCR (RT-PCR) [38]. There are also methods that couple PCR to other techniques such as, for example, surface acoustic wave (SAW)

sensor [39]or evanescent wave biosensors [40]. PCR is a lot less time-consuming than the culturing and plating method introduced above. Without considering the sample preparation and pre-enrichment steps, generally, it takes from 5 to 24 hours to reach the detectable threshold with PCR.

It is worth mentioning that the multiplex PCR method is very useful as it allows the simultaneous detection of several organisms by introducing different primers to amplify DNA regions coding for specific genes of each bacterial strain targeted [41].

The main advantage of real-time PCR is that the results can be achieved quickly without too much manipulation. This technique bases its detection in the fluorescent emission by a specific dye when it bonds itself to the targeted amplification. Since the fluorescence intensity is proportional to the amount of amplified product [42], it is possible to follow the amplification in real time, thus eliminating laborious post-amplification processing steps such as gel electrophoresis. Different alternative probes, deriving from this principle, have been developed recently [43].

One of the major limitations of PCR techniques is that the user cannot discriminate between viable and non-viable bacteria because DNA is always present independent of the viability of the bacterium.

2.3 Optical methods of single bacterium detection

Optical detection methods are probably the most popular tools in bioanalysis and have received considerable interest for rapid detection of contaminants [44, 45], toxins or drugs [46], and bacterial pathogens due to their sensitivity and selectivity. Optical-based detection offers large number of subclasses based on absorption, reflection, refraction, dispersion, infrared, Raman spectroscopy, chemiluminescence, fluorescence, and phosphorescence. However, all the above subclasses require a suitable spectrometer to record the spectrochemical properties of the analyte. The surface fluorescence and Surface Plasmon Resonance (SPR) are the most sensitive optical detection technology.

2.3.1 Fluorescence detection

Fluorescence occurs when a valence electron is excited from its ground state to an excited singlet state. The excitation produced by the absorption of light of sufficient energy usually through a laser source is called laser induced fluorescence (LIF). When the electron returns to its original ground state it emits a photon at lower energy, leading to light emission with a longer wavelength than the absorbed light since some of the energy is lost due to vibrations. The light emission takes place shortly after absorption, usually within 10ns. One of the typical applications of this phenomenon is the flow cytometry[47].

Flow cytometry is a widely adopted method for high throughput analysis of suspended particles, bacteria and other microorganisms. A typical flow cytometer with sorting function works as illustrated in Fig2.3. First, the sample flow containing microparticles is focused by a hydrodynamic flow focusing method by using the surrounding sheath flows. Then, the sample flow passes through an optical detection region formed by the intersection of the flow with laser beams, and detectors use the scattered light from the cell or bacteria samples to analyze the types and sizes of the cells/bacteria. The fluorescence labelling method can also be used to collect induced fluorescent signals from the fluorescence-labelled cells/bacteria. The fluorescence emitted from the cells/bacteria through several optical components is then collected by a digital camera or photomultiplier tubes (PMTs) and then recorded by a computer for image or signal processing. Finally, pairs of electrodes are used to sort different cell samples [48].

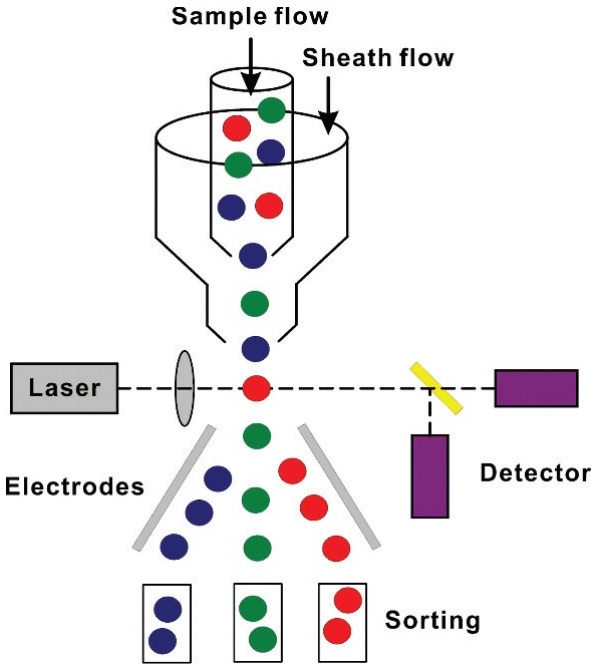

Fig 2.3: Schematic view of the operation principle of a flow cytometer for cell counting and sorting [49].

Not only can flow cytometer be used for single bacterium detection and identification, it has also been demonstrated for measurement and analysis of various cell properties, including surface antigen, intracellular antigen, transgenic expression, and immunoassay. However, delicate and complex optical components including focused laser beams, various optical detecting/filtering devices and complicated control circuits make the system relatively expensive. The calibration process is also relatively complicated, which usually requires an experienced, skilled staff to operate.

2.3.2 Surface plasmon resonance (SPR)

SPR biosensors [50] measure changes in refractive index caused by structural alterations on the surface of a thin film metal (typically Gold or Silver). In SPR biosensors, a surface plasmon is excited on a thin metal film to the surface of which a bio-recognition element is attached, for example, antibody or biotin. The binding of a bacterium or other bio-entities in solution to the bio-recognition element on the SPR sensor surface produces a local increase in the refractive index. The refractive index change gives rise to a change in the propagation constant of the

surface plasmon, which is subsequently measured as a change in the coupling angle of incidence (SPR sensors with angular modulation) or in the coupling wavelength (SPR sensors with wavelength modulation). A schematic view of the working principle of a SPR is illustrated as Fig 2.4.

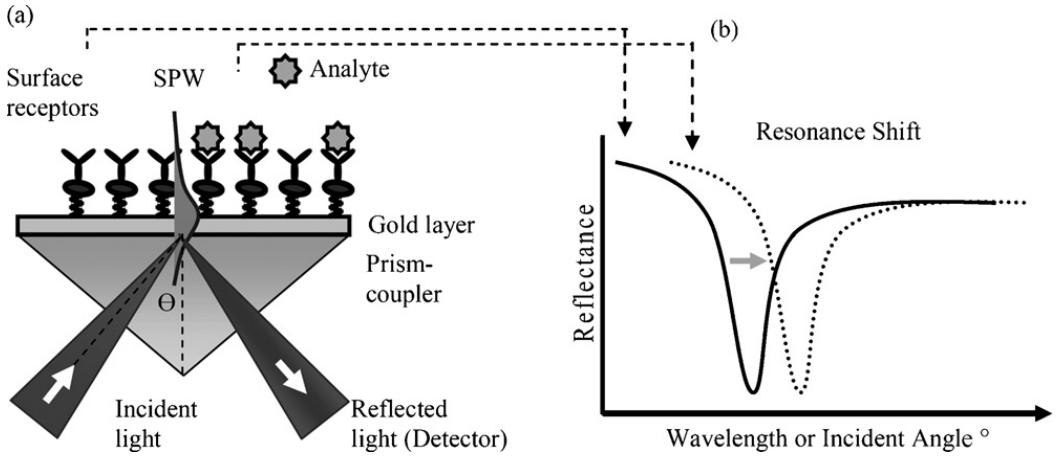

Fig 2.4: Schematic view of the working principle of SPR (a) prism-coupled configuration and (b) resonance shift in the reflected light spectrum [51]

SPR is a label free, highly selective, and fast (when the bacterium is bound on the surface of the SPR sensor) detection technology. Another major advantage of using SPR technology is that SPR sensors can detect bacteria, particles, and analytes in complex samples (e.g., blood, urine, stool extract, fruit juices, and food extracts) with limited or no sample preparation, purification or pre-amplification, SPR has successfully been applied to the detection of pathogen bacteria by means of immunoreactions[52,53]. The main disadvantages of this powerful technique lay in its complexity, demand for specialised staff, expensive equipment and relatively large size of desktop or bench top instruments implementing it. Since most of the microorganisms, e.g. bacteria are not mobile, diffusion is the only way for bacteria to migrate to the sensor surface. The total detection time with a SPR sensor is typically dominated by the ability of the target bacterium to reach the surface and bind to an immobilized antibody or biotin. As diffusion tends to be an extremely slow process, it limits the sensor response time significantly.

2.3.3 Immunology-based methods

The field of immunology-based methods for bacteria detection provides very powerful analytical tools for a wide range of targets. The enzyme-linked immunosorbent assay (ELISA) [54] test is the most established technique nowadays as well as the source of inspiration for many biosensor applications. ELISAs combine the specificity of antibodies and the sensitivity of simple enzyme assays by using antibodies or antigens coupled to an easily assayed enzyme. Fig. 2.5 illustrates the principle of a typical "sandwich ELISA"[55], which is the most common kind.

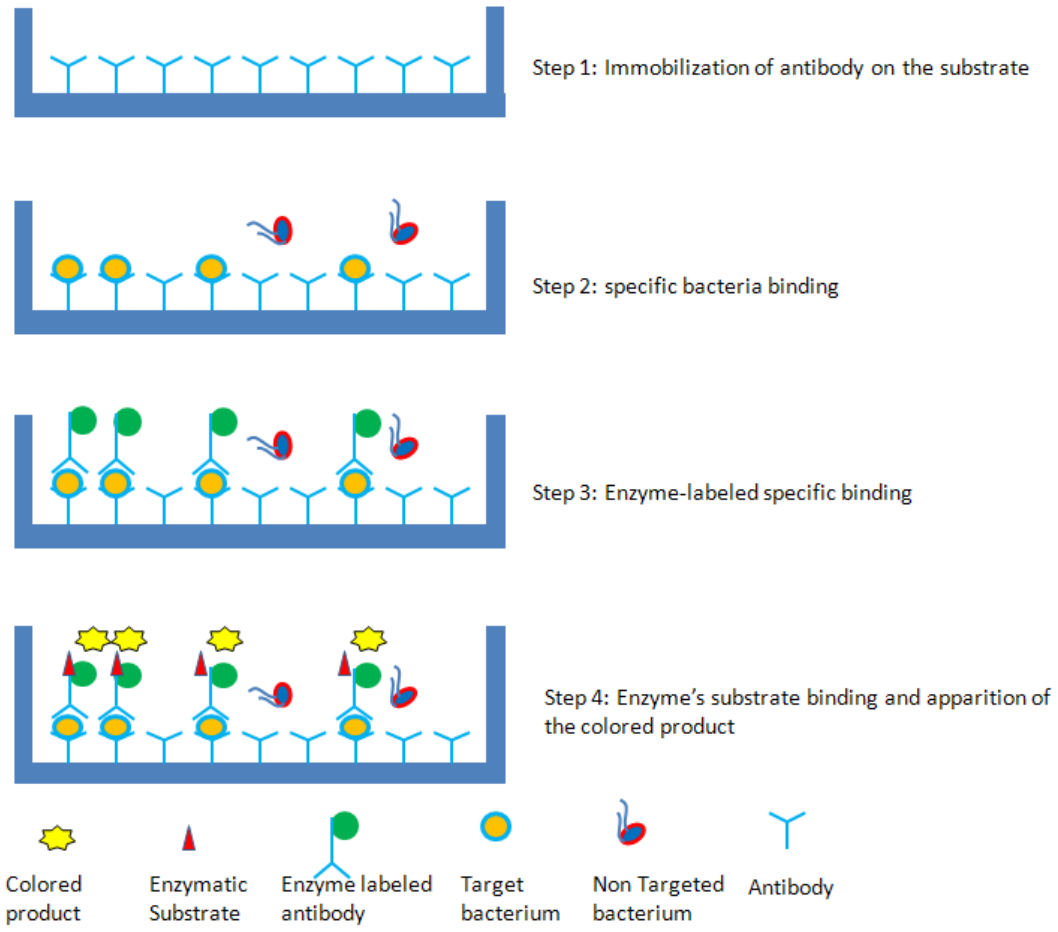

Fig 2.5: Schematic view of the sandwich-ELISA protocol [54].

Another important application of the immunology-based is immunomagnetic separation (IMS) [56], which extracts and captures targeted pathogens from a medium by introducing functionalized magnetic microbeads usually coated with specific antibody[57~60]. Off-the-shelf functional magnetic microbeads are available from a number of suppliers. Beads of widely

ranging sizes (from several nano-meters up to a few tens of micron meters) are available depending on the application.

Generally, functional magnetic beads are mixed with the medium containing targeted bacteria, after a suitable mixing procedure, targeted bacteria are supposed to attach to the surface of magnetic beads, then the mixed medium flows through a fluidic channel, where electromagnets or permanent magnets are used to capture the magnetic beads on the wall of the channel, thus separating the targeted bacteria from the medium and other bio-entities to realize the purification process. By removing the local external magnetic field, magnetic beads attached with targeted bacteria are released for further investigation. IMS can be combined with almost any other detection method, such as, optical, magnetic force microscopy, magnetoresistance [61] and Hall Effect [62] for further quantification and identification of the bacteria. The working principle is illustrated as Fig 2.6

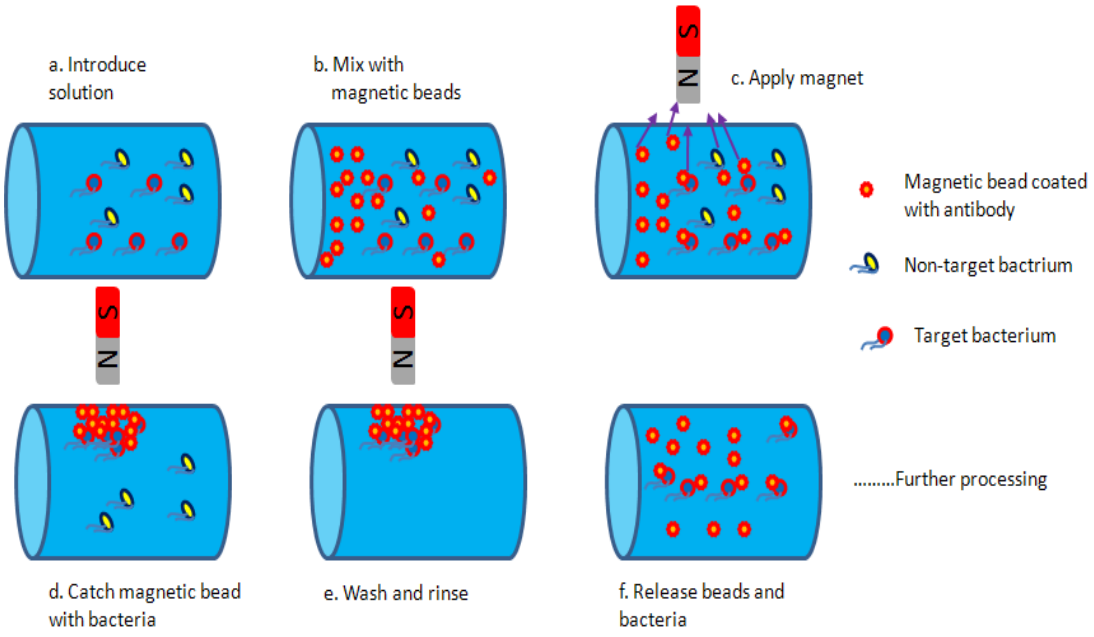

Fig 2.6: Schematic depiction of a typical magnetic separation procedure [56]

2.4 Electrochemical biosensors

These devices are mainly based on the observation of electric current or potential changes due to interactions occurring at the sensor-sample interface. Techniques are generally classified

according to the observed parameter: current (amperometric), potential (potentiometric), or impedance (impedimetric), but they all use electrodes or electrode array to produce or collect signals from medium containing target analyte, bacterial or other bio-entities. Compared to other methods, illustrated in Table 2.1-2.5 [63] below, electrochemistry allows the analyst to work with turbid samples. The main advantages of this kind of sensor include short response time, ease of integration, high reliability and much lower cost of equipment compared with conventional methods. On the other hand, in general, compared with their counterparts such as optical or culturing and counting methods, electrochemical methods present slightly less selectivity. Fig 2.7 compares the sizes of the various components of an electrochemical biosensor [63]. In this section, the amperometric and potentiometric methods are reviewed briefly. The impedimetric technology is discussed in detail in the next section.

Table 2.1: Detection of *E.coli*[63]

Detection technique	Sample type	Time of analysis	Working range (CFU* mL−1)	Detection limit (CFU mL−1)
ELISA	Ground beef	Next day	103–104	1.2 × 103
PCR-ELISA	Milk	5 h	100–104	100
PCR-electrophoresis		2 h	101–104	1000
Real-time PCR	Culture medium Ground beef	5 h 20 min 3 h 20 min	5–5 × 104cells	5 cells 1.3 × 104 cells/g
RT-PCR coupled to fluorescence	Drinking water	30 min	1–106	102
Fiber optic immunosensor	Culture	10 h	Tested up to 6.5 × 104	2.9 × 103
SPR biosensor	Culture	NA	102–109	102
QCM Immunosensor	Culture/water	170 min	103–108	103
Amperometry	Culture	30 min	100–600	
Conductimetric biosensor	Mixed culture containing up to five different microorganisms Water	10 min	10–105	79
	Vegetable wash water	6 min	10–106	81
Impedimetric immunosensors	Culture/water	10 min	104–107	104 in culture and 107 in water.

Table 2.2: Detection of *Legionella pneumophila*[63]

Detection technique	Sample type	Time of analysis	Working range (CFU/ mL)	Detection limit (CFU/ mL)
Colony count	Water	5–14 days	2.5–994	1
PCR		1–2 h	0.015–150	1–10
Sandwich hybridization assay (SHA)	Water	1–2 h		1.8 × 103 cells
SPR	Culture	2 h 20 min	102–109	102

Table 2.3: Detection of *Campylobacter jejuni*[63]

Detection technique	Sample type	Time of analysis	Working range (CFU/mL)	Detection limit (CFU/mL)
ELISA	Bovine vaginal mucus and prenuptial washing	5 days	105–107	105–106
Real-time PCR-IMS	Chicken fecal suspension	4 h		100–150
Total internal reflection	Culture	Over 2 h		ca. 103
Amperometric biosensor	Culture and chicken carcass, wash water	2–3 h	103–107	2.1 × 104

Table 2.4: Detection of *Salmonellae*[63]

Detection technique	Sample type	Time of analysis	Working range (CFU mL−1)	Detection limit (CFU mL−1)
IMS-plating	Raw chicken	Next day		1–10
IMS-ELISA		Next day	106–109	106
Electrochemical sandwich ELISA	Meat	Same day	Unknown	1–10 cells/25 g
PCR-ELISA	Milk	Next day	1–108	103
QCM	Phosphate buffer	60 min	105–5 × 108	104
Amperometric biosensor	Culture and water	1–2 h	Not specified	5 × 104

Table 2.5: Detection of *Listeria monocitogenes*[63]

Detection technique	Sample type	Time of analysis	Working range (CFU /mL)	Detection limit(CFU/mL)
PCR	Beef simple	Next day		1000 cfu/g
Real-time PCR	Fresh product (salad)	Same day	100–1000	1000
Magnetic DNA isolation-PCR	Milk	7 h	1–105	10
Amperometry	Phosphate buffer and milk	3–4 h	103–106	9 × 102
Amperometric immunosensor	Culture	> 2 h	104–107	

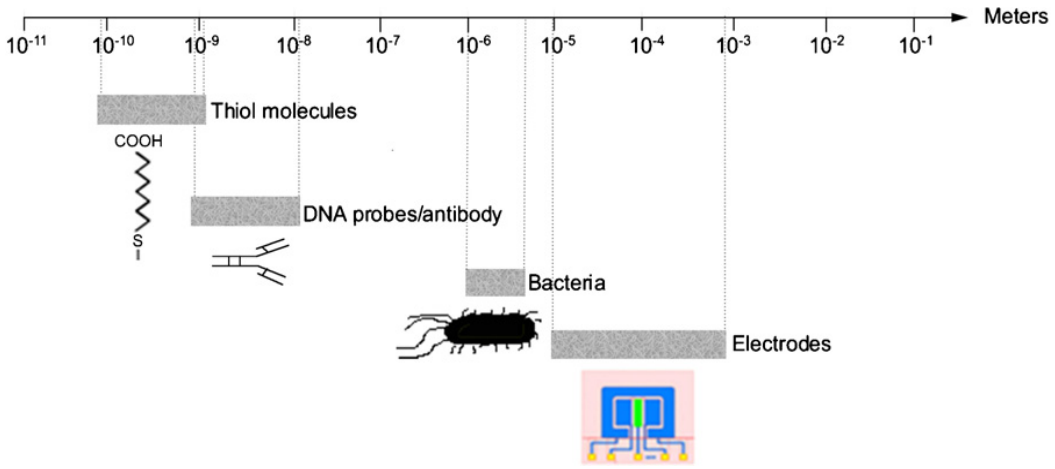

Fig2.7: Diagram ofthe comparative sizes of the parts integrating a biosensor [43]

2.4.1 Amperometric methods

This is perhaps the most common electrochemical detection method used in biosensors. Its working mechanism is based on the assumption that the relationship between the concentration of analyte and the measured current from a sensor is linear, compared with a logarithmic relationship in potentiometric systems. This makes amperometric biosensors well suited for bacterial assay. Amperometric biosensors have the advantage of being highly sensitive, rapid, and inexpensive. Generally, the sensor potential is set at a value where the analyte, directly or indirectly, produces a current at the electrode. However, there are some biosensors which cannot allow direct electron exchange between the electrode and either the analyte or the biomolecule. In those cases, redox mediators are required [64](Redox mediators are small size compounds able to reversibly exchange electrons between both the sensor and the enzyme of choice (e.g.,

ferricyanide, osmium or ruthenium complexes, dyes, etc.)). Many different combinations and strategies to build biosensors are possible. The actual choice depends on constraints imposed by sample matrix, analyte, or usability [65]. Bacterial biosensors that do not differ much from more conventional biosensors are found in [66]. In this work, E. coli is detected in 30 min and between 100 and 600 cells/mL using a flow-through immunofiltration method coupled to amperometry. Fig.2.8 shows how this disposable amperometric immunofiltration sensor works.

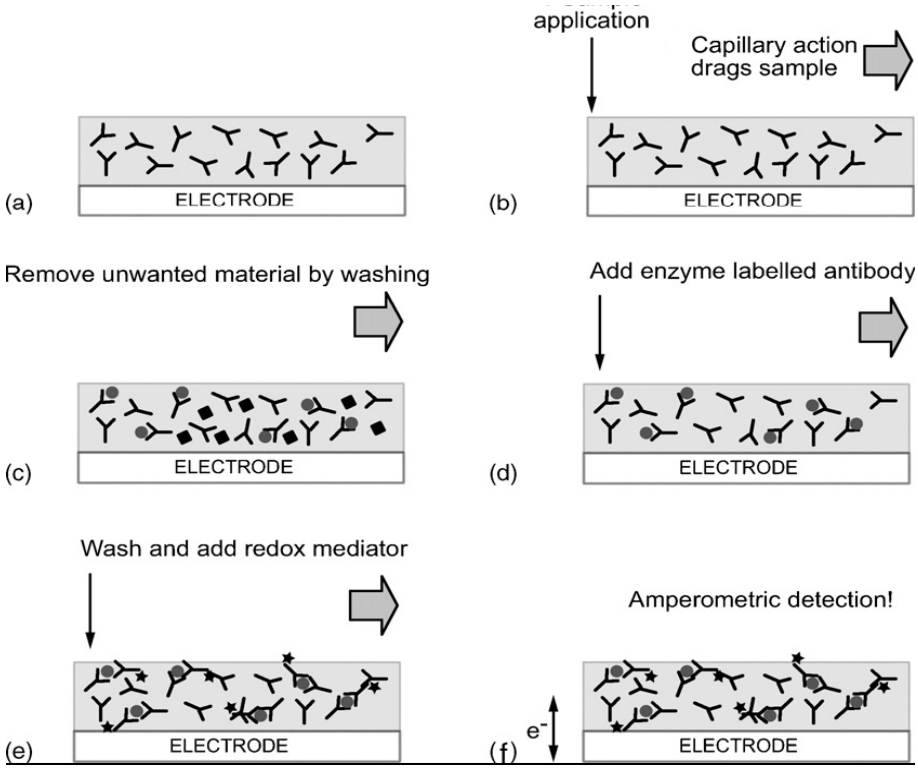

Fig 2.8 Diagram of how an amperometric immunofiltration biosensor works [63]

2.4.2 Potentiometric methods

The potentiometric sensor has characteristics that are different from amperometric sensors in several aspects: a). The measured species, usually concentration of ions (such as H+, NH4+, etc.) are not consumed. b). The sensor measures the activity (for dilute solutions, molar concentration can be used), of a specific ion in reference to its predefined threshold. c). The ion specificity comes entirely from the membrane. For example, there are all kinds of ion selective membranes,

for example, specific to H+, NH4+, or Ca++, etc. d). The output of a potentiometric sensor is in voltage proportional to the natural log of ion concentration and independent of the sensor size.

Since potentiometry yields a logarithmic concentration response, the technique enables the detection of extremely small concentration changes. One of the most successful applications of this approach is called ion selective field effect transistors (ISFETs) [67] which utilize the semiconductor field-effect to detect biological recognition events. ISFETs use an electric field to create regions of excess charge in a semiconductor substrate in order to enhance or decrease local conductivity. They consist of a p-type silicon substrate with two n-doped regions known as source and drain, separated by a short distance (gate) covered by a layer of insulator. The gate insulator is typically SiO_2 and it is covered by an ion selective membrane which is selectively permeable to a certain ion, e.g., K+, Ca2+, F−, as described in [68]. More details on the functioning of ISFETs are reviewed in [69]. The application of these devices in the area of biosensors is constrained due to following issues: a) most bio-molecular immobilization methods are not compatible with the ISEFT fabrication technology b) it offers poor detection limits, linear range, and reproducibility, and c) it has inadequate device stability.

The potentiometric detection may be applicable to a wide range of bacteria. However, similarly toamperometric methods, the response times highly rely upon microorganisms' growth, thus potentiometric biosensor cannot provide a real-time analysis and pre-enrichment steps are required.

2.5 Electrochemical impedance spectroscopy (EIS)

Impedance spectroscopy is a powerful method used to characterize the chemical and physical properties of solid, liquid, and gas phase conductive materials. In the last two decades, this technique has gained widespread adoption in developing biosensors for monitoring the catalyzed reaction of enzymes; the bio-molecular recognition events of specific proteins, nucleic acids, whole cells, antibodies or antibody-related substances; presence of bacterial cells in the aqueous medium or growth of bacterial cells.

In this technology, generally, a small amplitude sinusoidal excitation signal is applied to a transducer, and resulting current is used to calculate the impedance at each of the frequencies

probed [70]. The amplitude of the current and voltage signals and the resulting phase difference between voltage and current, which depends on the resistive and capacitive properties of the system under study, reflect the system impedance. The equivalent circuit models can be used for interpreting the impedance spectra, and it can also be used in analysis tool investigating electrode kinetics for the characterisation of conducting polymers, animal and plant tissues, and general materials. Meanwhile, a variety of bio-molecular have been used as basic detection elements of AC impedimetric biosensors with different degrees of success. For instance, enzymes, antibodies, nucleic acids, cells and other micro-organims have been successfully immobilized onto the surface of electrodes to construct impedimetric biosensors.

As impedance has a real and an imaginary component, the signal processing and mathematical treatments are quite difficult and cumbersome. Equivalent circuits are often used to interpret the results over ranges of frequencies and amplitudes [71-73]. The equivalent circuits are made up of a combination of capacitors and resistors. Although this methodology is widely accepted because of its ease of use, caution must be taken to ensure that the equivalent circuit obtained represent the real physical scenario. In fact, the same impedance data may well be fit by several different circuits. Researchers have to decide which circuit fits best. Generally, if several parameters need to be determined, measuring the impedance at several frequencies can be very helpful. The selectivity or sensing specificity of EIS technology is often achieved with functionalized electrode arrays using for example antibody binding or DNA probe immobilization [74, 75].

Among the reported EIS based biosensor, the highest sensitivity achieved so far was obtained by Alocilja et al. [76] His group reported a conductimetric method using polyclonal antibodies against E. coli [76, 77]. This was applied in a single-use system operating in 4 steps, as shown in Fig2.9., the authors reported a detection limit of 83 CFU/mL for this system and that the signal decreases beyond 10^5 CFU/mL.

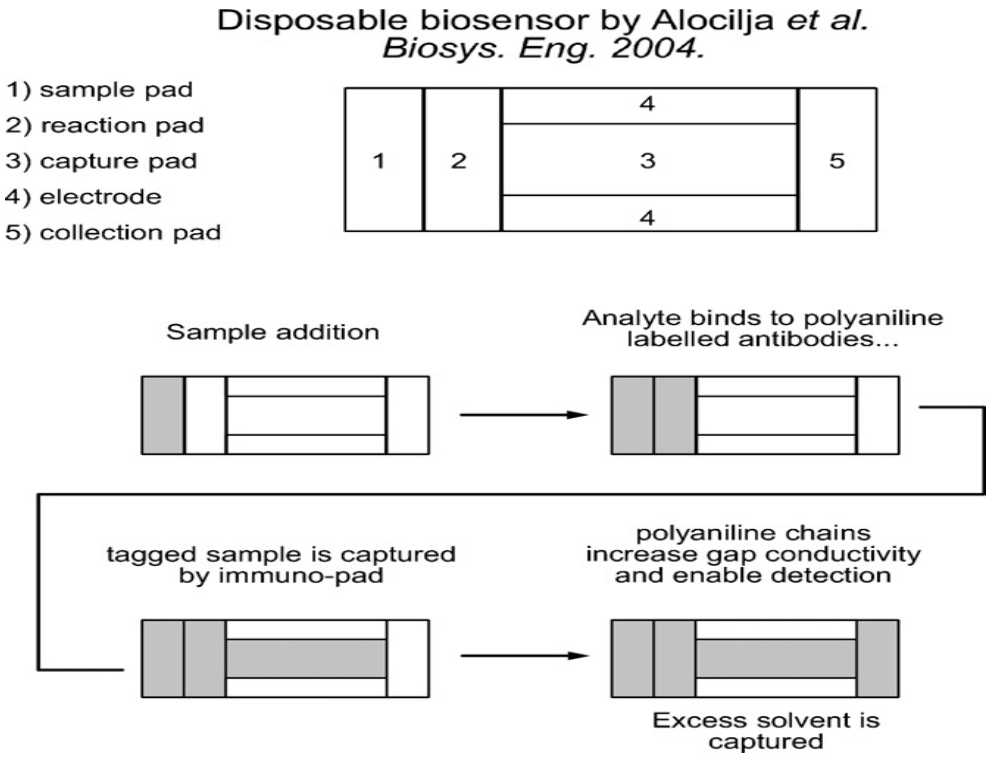

Fig2.9: Simplified representation of a disposable conductimetric biosensor[76]

In order to extract or recover the sensing signal from the background noise, bulk desktop instruments are required such as LCR-meters, impedance analyzers, lock-in amplifiers and frequency response analyzers (FRA). The last two instruments are the most widely used but bring both inherent advantages and disadvantages. Impedance systems based on lock-in amplifiers are very sensitive. They can effectively remove background noise and minimize harmonic distortions. On the other hand, it is difficult to use them for stand-alone measurements which are generally slow, and they cannot be used over a wide frequency range. By contrast, impedance measurement systems based on FRA provide fast analysis over a wide frequency range, remove harmonic distortions and dc components and can easily be fully automated. However, limited sensitivity and background removal requirements as well as their relatively high cost are disadvantages associated with FRA based measuring systems.

Last, impedance measurements also enable remote sensing, as described by [78], where passive RLC sensors enclosed within the sample may be used to monitor temperature, permittivity, conductivity, or pressure changes non-invasively. Because sensors may be easily and cheaply

incorporated in compact packages, this approach would enable rapid and automated quality control in the food industry.

Impedimetric techniques exhibit impressive detection capabilities. However, they could not provide detection sensitivity as good as traditional methods [79] such as fluorescent labelling and optical detection techniques. Compared with amperometry and potentionetry technology, one advantage of EIS is that it is a label free sensing approach, thus significantly simplifying sensor and sample preparation. However, deeper fundamental understanding of the phenomena involved in this type biosensors must be developed. For instance, studies of optimized electrode size and separation distance are not available.

2.6 Micro-, Nanotechnology based Biosensor

The combination of micro- and nano-fabrication techniques with biosensors holds great promise. In the last decade, different applications are beginning to crop up [80~82]. The miniaturization or scaling down of conventional biosensors offers the following advantages: a) dramatic reduction of required sample and reagent volume, thus bringing down the cost; b) microfluidics or lab on chip improve mixing rates and mass transport efficiency, which leads to much faster analysis; c) the possibility of mass production and reduced unit costs; d) multiple analysis and synthesis are enabled in the same device, which also shorten analysis time; e) potential for mass fabrication, which could also bring down unit cost; f) because the volumes of sample and reagent consumed are very small, usually, in the range of nanoliters, these devices are more environmentally friendly; g) since the actuator and sensors are so tiny, power required is extremely low and the contamination associated to waste material is easier to control, which make these biosensors very suitable for the applications demanding high screen throughput and real-time, on site analysis.

To the best of the authors' knowledge, Bashir and co-workers were the first to report bacterial detection microsystems in 2001[83]. Their work presents a microsystem capable of detecting *listeria* using impedance spectroscopy. Another pioneer effort at adopting microsystemswas made by Woo and coworkers [84].They reported the selective amperometric detection of *E. coli* in a very short time (40 min). Other examples combining pathogen detection and miniaturization can be found in the literature [85, 86]. It is interesting to see that all the conventional detection methods introduced above can be miniaturized and their performance would tend to improve

accordingly. There are several papers reviewing microsystems based on conventional detection technologies, such as PCR, immune-biosensors and florescent detection[87~90].Among those micro and nanotechnology based biosensor, the hybrid or monolithic integration of the powerful microelectronic circuits with Microfluidic functionalities may revolutionize the traditional biosensing method. Some pioneer work has been done by Gawad et al. at EPFL, who first demonstrated clear differentiation of microbeads, erythrocytes and ghost cells [91]. The principle of single-cell impedance analysis and microfluidic device in the papers is illustrated in Fig 2.10.

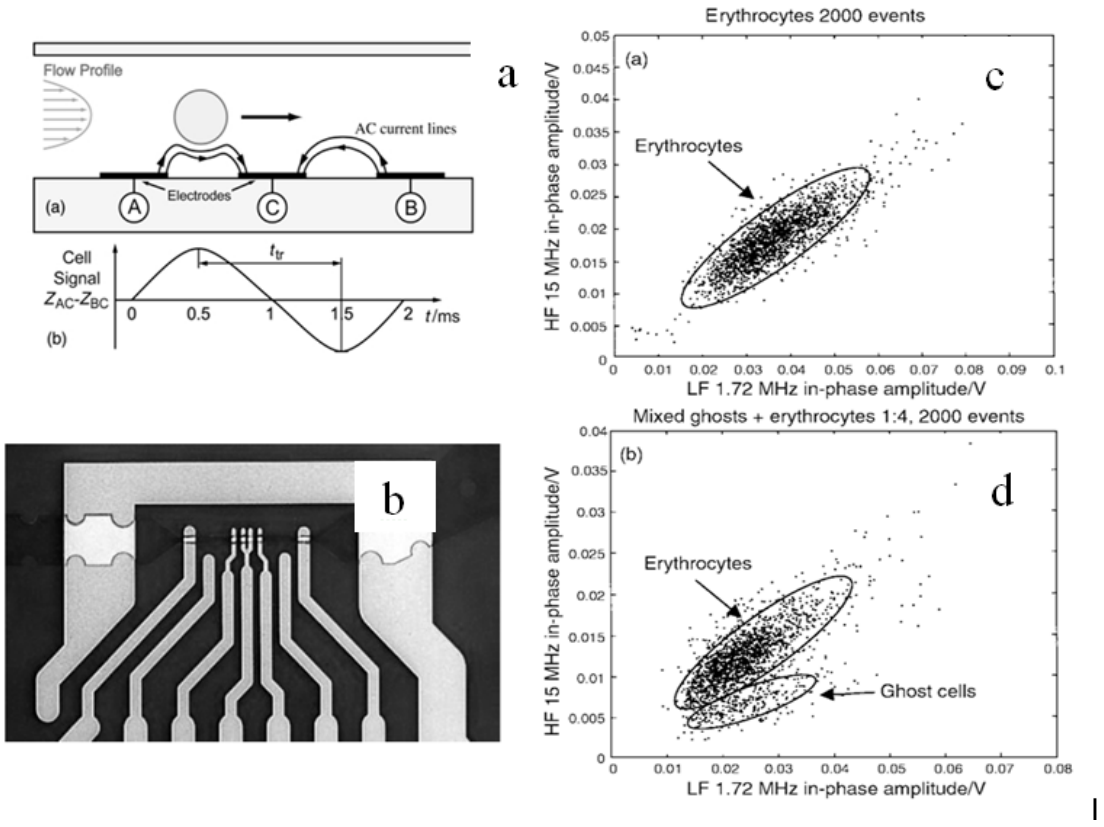

Fig2.10: a) Schematic diagram showing a particle flowing over a three microelectrode impedance chip, and a typical impedance signal for a single particle. b) Microscopy image of the microelectrodes within the microchannel. c) Impedance scatter plots for particles flowing through the device. [91]

Similar microelectrode design was adapted for signal particle/cell impedance sensing and countering by many other researchers [92-95], however the non-homogeneous electric field distribution caused by planar electrodes has a major influence on the variation in the impedance signal amplitude. Those research also demonstrated that the control of particle/cell's position is more significant for the planar microelectrode design than for the parallel, face to face microelectrode configuration because the electric field distribution in the latter design is more uniform.

Chueng et al. [96] adopted parallel, face to face microelectrodes to measure the dielectric properties of red blood cells (RBC). They compared the difference between ghosts and RBCs in a microchannel with dimensions in the range of 20-30μm. The results showed that the opacity of RBCs with fixed cell membranes was significantly different from normal RBSs. It also showed that cells can be accurately detected at around 500 kHz. An example of the use of high frequency measurements for cell identification and analysis was reported by Kutel, et al [97], who proposed a sensing method using an input signal at 8.7 MHz. They demonstrated the differentiation of parasitized RBC from uninfected RBC. Very recently, Ferrier et al. [98] reported a microwave interferometric microsystem, which can detect capacitance changes from a single cell at a frequency of 1.6GHz. However, all the reported integrated microelectronic and microfluidic system still required fairly complicated desktop instruments either for signal conditioning or processing.

2.7 Conclusion

Traditional pathogen detection methods, although sensitive enough, are often too slow to be of any use. Therefore, new methods are needed that exceed their performance. Over the recent years, a lot of effort has gone into the study and development of biosensors of the most diverse natures, but their performance is irregular and still needs improvement. In the near future, pathogen detection will undoubtedly benefit from the integration of biosensors into micro-devices. Although, barring selectivity, performance will lie in a necessary compromise between time and sensitivity. Optical techniques perhaps provide better sensitivity than electrochemical ones, but their cost and complexity makes them unattractive to most end users. Electrochemical techniques, on the other hand, are much easier to use but when it comes to detecting pathogens, their

performance is still far from adequate. In order to become attractive, biosensors first need to show that they are capable of reaching at least the same detection levels as traditional techniques (between 10 and 100 CFU/mL). Next, they need to do so in a fraction of the time without overlooking cost.

Though conventional pathogen detection methods are sensitive, they lag behind the analytical methods by detection time. However, analytical techniques like optical and electrochemical detection have some disadvantages as well, considering sensitivity and cost. Therefore, new rapid methods are considered necessary for better performance. Optical techniques possibly provide better sensitivity relative to electrochemical detection, but they are expensive and complicated. In contrast, electrochemical techniques involve much simpler procedures but for the detection of pathogens, it requires enhanced performance. Though, numerous research efforts have been made during the past decades and in recent years for food-borne pathogen detection, in spite of everything it needs further improvement. Since food-borne pathogens are mostly present in very low numbers (100 CFU/g) in the middle of millions of other bacteria, it is very difficult to detect them. So there are more chances that these microorganisms may remain undetected.

Therefore, a detection technique which is reliable, rapid, accurate, simple, sensitive, selective and cost effective has to be developed. In addition, it should be able to detect pathogens in very low concentrations of the samples and must be suitable for in situ real-time monitoring as well. Such a technique of detecting pathogens could offer a great commercial advantage to food processing and food manufacturing sector. High throughput microfluidics based single-cell impedance metrology is an important and promising area. The fast growing micro-, nanotechnology and matured microelectronic technology enable faster and more accurate detection. Further innovations are required to obtain better sensing circuitry, efficient method of capturing target bacteria and automatic differentiation signal process.

CHAPTER 3 SYSTEM ARCHITECTURE AND ANALYSIS

3.1 Introduction

The previous chapter reviewed the existing literature relating to means of detecting single bacterium or single micrometer size particles. We notably focused on so-called impedimetric measurement methods. This demands very precise and complex sensing circuits, usually associated with desktop instrumentation such as an impedance analyzer, which makes the miniaturization of the whole system into a Lab-on -Chip a very challenging task.

The ultimate goal of this research is to develop a portable and disposable Lab-on-Chip microsystem, which can detect single bacterial cells in real time. This kind of system should be able to handle liquid samples containing targeted bacteria in a very low concentration. How to realize high screening speed and specificity should be considered when designing such systems. CMOS is an ideal technology for integration of highly sensitive, multiple channel, and extendable sensing circuits. Such circuits can comprise high density electrode arrays, signal conditioning and processing, convenient interface to external computers and very low fabrication cost in mass volume.

This research is an effort to address five main issues: 1) investigate a suitable microelectronic circuit with sensitivity high enough to achieve single cell detection without amplification, 2) investigate the optimized structure and geometry of microelectrodes to measure the variations induced by single cells, 3) explore a reliable process to fabricate large electrode arrays using CMOS technology, 4) develop a suitable and cost effective packaging for integration of microfluidic components with a CMOS chip, and 5) develop a magnetotactic bacteria based transportation method to accelerate the screening speed and achieve sensing specificity.

In this chapter, a novel architecture of a Lab-on-Chip system based on CMOS technology is introduced. The major advantage of adopting CMOS technology is that the sensing circuits and microelectrode array can be implemented onto the same substrate. Thanks to the well developed semiconductor fabrication process, the signal-to-noise level of the microelectronic circuits can be greatly improved, compared with the conventional approach of using isolated components

interconnected with a PCB board. The volume and power consumption of an integrated CMOS based sensors can also bring down the cost and make it more suitable for point of care usage.

Meanwhile, there are also some challenges that have to be addressed when building the microelectrode array and microelectronic circuits on the same CMOS chip, as outlined below.

1. Compatibility of the required post-processing with CMOS technology

Generally, the CMOS fabrication processes are composed of a series of strictly defined standard procedures [99], which cannot be changed to accommodate custom requirements, for instance, to implement cavity or channel structures into a CMOS chip. Thus, additional fabrication steps are required to build specific microfluidic structures after the original CMOS chips are fabricated by the foundry. Those subsequent fabrication steps are denoted as the CMOS post-processing procedure [100]. As the unpackaged CMOS die, which is a few square millimetres, is very sensitive to the environmental conditions, such as temperature, pressure, dust, chemicals and humidity, the post-processing should be fully compatible with CMOS technology to avoid any kind of damage or contamination leading to degradation of the performance of microelectronic circuits on the CMOS chips. After the CMOS post processing procedure, in most cases, a dedicated package needs to be developed for isolating the circuitry, bonding pads and wires from the samples, usually an aqueous medium, and also providing access to the sensing area.

2. Compatibility of the CMOS chip with bio-entities

Biocompatibility is also a very important issue that needs to be considered. The most frequently used materials in a standard CMOS process are aluminum, tungsten and copper, which cannot be used directly as electrode material, as they show poor electrochemical stability in physiological solutions and are toxic for most biological cells [101]. Therefore, typically, inert conductors such as gold or platinum are patterned on the top of CMOS chips as microelectrodes [102~104].

3. Microelectronic circuits

The embedded microelectronic sensing circuits should be sensitive enough to detect the impedance variations caused by a single bacterium. However, in order to achieve a high screening rate, a high density electrode array should be used, which not only shrinks the area left for the sensing circuits and interconnections, but also introduces cross-talk and interference

among microelectrodes. Furthermore, considering the very precise measurements conducted on the chip, the mismatch of transistors, the layout of interconnecting wires and temperature distribution also requires great attention when designing and implementing the sensing circuits.

To address these issues, a novel chip design is presented, which combines on-chip microelectronics, microfluidic components, and a microelectrode array on a single CMOS chip, aimed at high throughput and real-time single bacterium detection.

3.2 System architecture and design

The proposed system comprises a microelectrode array, an on-chip sensing circuit, a microchamber, through substrate microchannels, and fluidic access ports. Fig 3.1 shows how these components could be assembled to implement the proposed system onto the CMOS chip. To the best of our knowledge, this is the first time that a vertical face to face microelectrode array on a CMOS chip is proposed. Previously, only planar microelectrodes have been proposed. We are also the first to construct the microelectrodes by utilizing the metal and via metal provided by the CMOS technology, to avoid having to deposit and pattern additional metallic material for microelectrodes on top of CMOS chip.

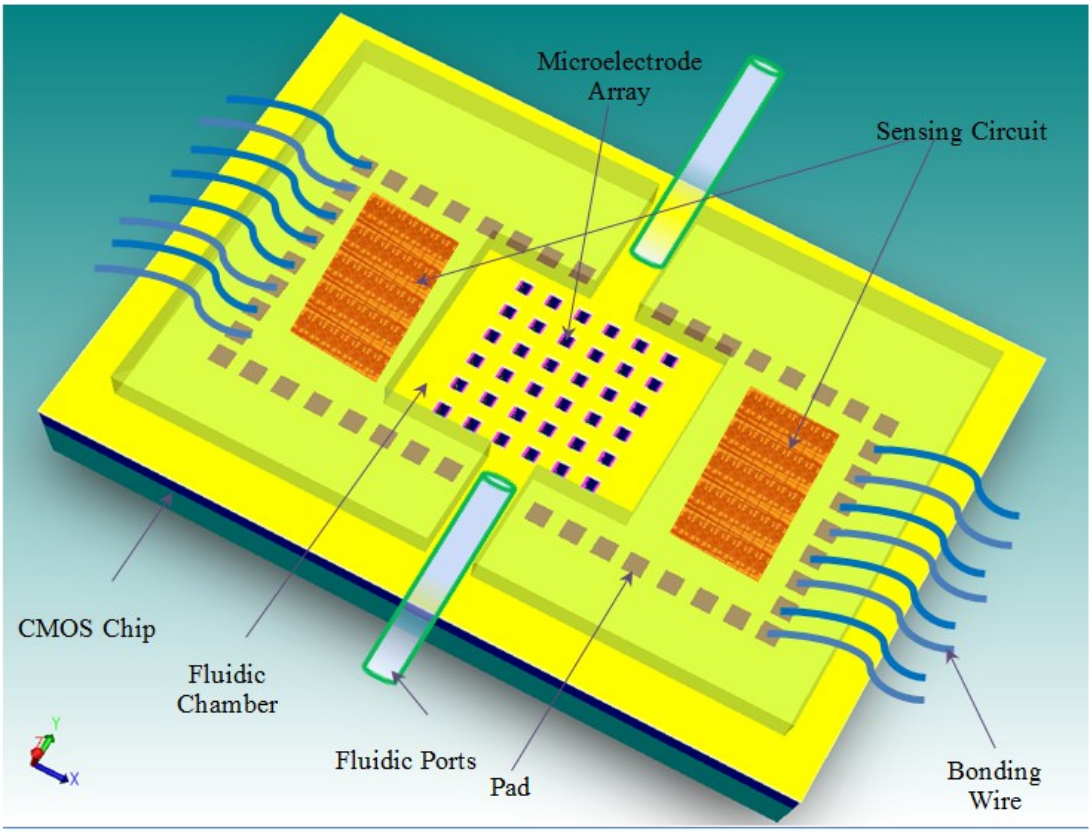

Fig 3.1: Schematic of the Lab-on-Chip system based on a CMOS technology

3.2.1 Structure of the microelectrodes

To mitigate costs and avoid complicated post processing procedures while taking full advantage of the CMOS technology, several features of standard CMOS technologies were investigated. A cross-sectional view of a standard 0.18µm process is illustrated in Fig3.2. The thickness of each metal layer varies from 0.5 µm to 1 µm.

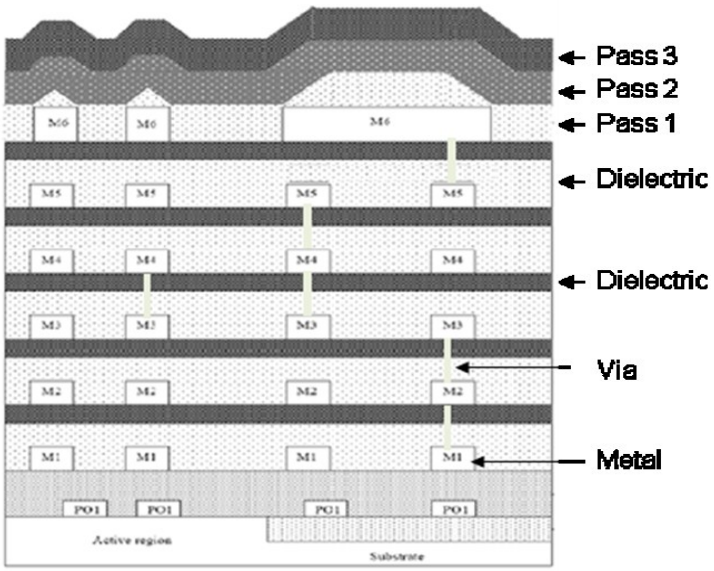

Fig3.2: Crosssection view of a standard 0.18 μm CMOS process

The via layer is typically used to realize interconnections between two metal layers. In total, in the chosen CMOS process, there are 6 metal layers and 5 via layers. If all the metal and via layers are stacked together, the height from the top metal layer to the bottom metal layer is around 8μm, which is an ideal height for implementing microelectrodes considering that the normal size of a bacterium is around several micrometers. Also, the thickness of each passivation layer (pass 3 to pass 1 in Fig 3.2) on the top metal layer is around 1.75μm, and is composed of silicon dioxide, silicon nitride and polyimide [105]. These layers can be used as a protection or mask layer for the subsequent CMOS post-processing procedures. After detailed investigation of the CMOS fabrication procedure and design rules for several technologies, it was found to be generally possible to construct vertical, face to face microelectrodes by stacking the available metal and via layers together instead of depositing additional metal layers on the top. The whole microelectrode array can be implemented by the standard CMOS foundry and released through a post-processing procedure. The number and size of microelectrode pairs can be defined by the designer according to the design rules of the CMOS process as well as specific applications. The height of the microelectrodes can also be varied by choosing the number of stacked metal and via layers.

According to the fabrication procedure of the CMOS chip, there is no cavity allowed between a pair of microelectrodes [106]. So, when the chip is fabricated at the foundry, the space between a

pair of microelectrodes is filled with silicon oxide. That oxide has a thickness equal to the height of the microelectrodes (around 8µm when all metal layers are used in TSMC 0.18µm Technology). A suitable CMOS post-process is required to release the microelectrode array. Fig 3.3 illustrates a schematic 3D view of the proposed microelectrode structure.

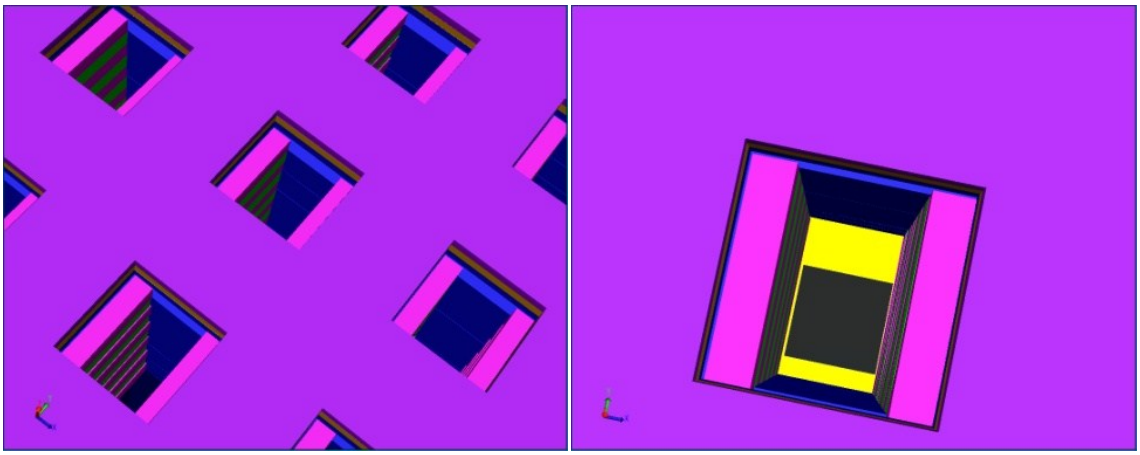

Fig 3.3: 3Dschematicview of the microelectrode array

As this experimental system is designed to prove concepts, despite a great deal of uncertainty, the first prototype is designed so that it can adapt to multiple applications. Thus, different sizes of microelectrodes are implemented. Specifically, the sizes 5µm x 5µm, 6µm x 6µm, 8µm x 8µm, 10µm x 10µm, 12µm x 12µm, 16µm x 16µm, and 20µm x 20µm (microelectrode length x microchannel width) are chosen for this design. The height of the microelectrodes was also varied by changing the number of the stacked metal and via layers. This was invaluable for evaluating the performance of the sensing circuit and to aid in the selection of the best parameters that will allow the device to meet the requirements of different applications.

3.2.2 Throughsubstrate microchannel

A through substrate microchannel structure is proposed, as depicted in Fig3.4. With this structure, a small pressure difference between the top and bottom of the CMOS chip forces the liquid medium to flow between the microelectrodes through the microchannel, with the targeted bio-entities included. In comparison with reported architectures using planar microelectrode arrays, which mainly rely on the diffusion of the targeted bio-entities, this structure allows a continuous impedance measurement, which will greatly increase the screening throughput of the system.

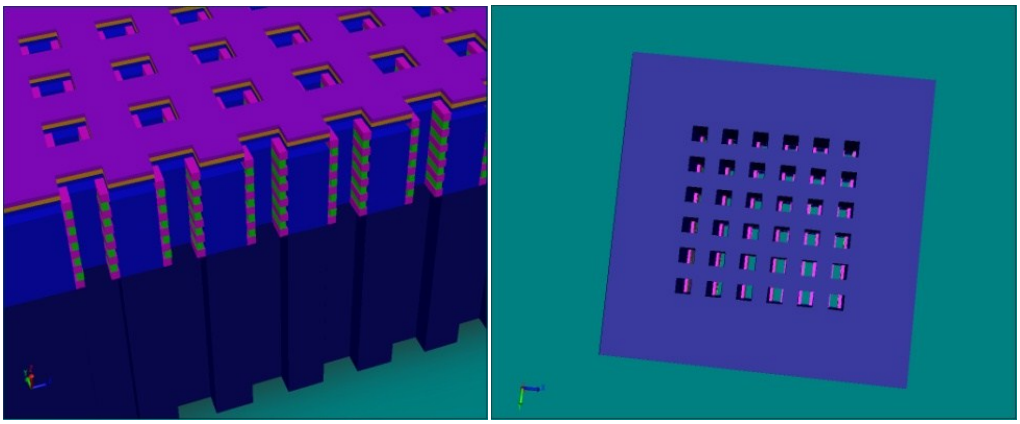

(a)

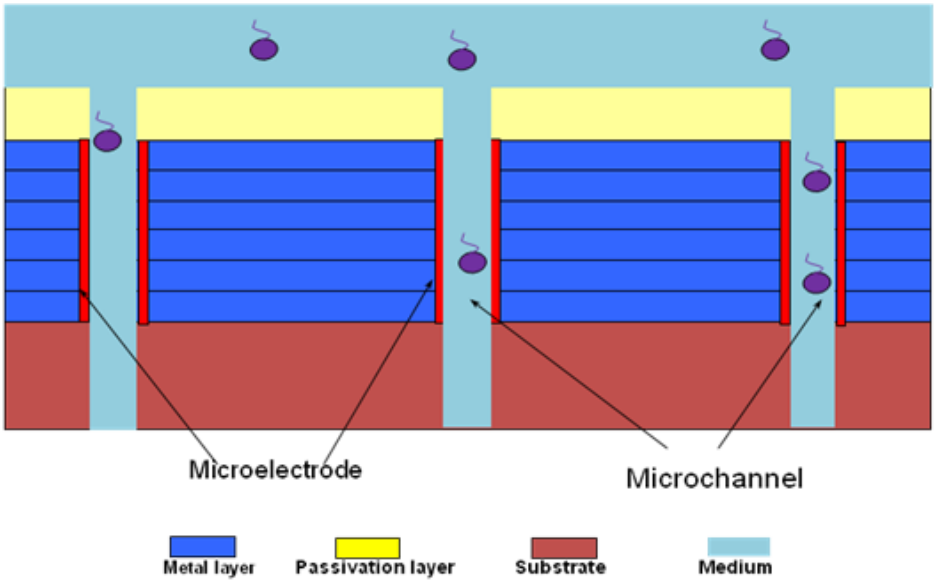

(b)

Fig 3.4: (a)3D structure of the microchannel (crosssection view in upper left and bottom view in upper right) and (b) cross-section view of the through substrate microchannel.

3.2.3 Sensing circuit

The sensing microelectronic circuit is designed to be flexible to meet various potential applications related to the proposed Lab-on-Chip system. The sensitivity of the circuitry must be high enough to identify a single bacterium. Meanwhile, it must be robust in order to minimize the impact of parametric variations due to various steps of the CMOS post processing procedure.

Considering that the Lab-on-Chip system works in a continuous manner, the induced temperature variations on the chip should not affect the viability of the targeted bacteria. Thus, a design with low power consumption and heat dissipation is expected. Moreover, the ultimate goal of systems embedding the proposed chip is to be used as point of care hand-held instruments. Instant screening reports should be generated and accessible to users without the need for additional desktop instruments, such as an impedance analyzer.

The design and simulation of the sensing circuit is based on two assumptions. The first assumption is that the liquid medium containing the target bacteria is an electrolyte having a conductivity ranging from 0.2 to 5 S/m. The second assumption is that the bacteria to be detected are floating in the electrolyte and they are considered essentially non-conducting [107~109], with a conductivity value typically around 0.1pS/m, which is much lower than that of the electrolyte.

To simplify the implementation, as compared to conventional sophisticated impedance sensing circuits, usually composed of amplifiers, filters and other signal processing components, we need to develop a novel impedance analysis circuit. The optimized design specification should be based on various studies with finite element models (FEM) of the physical structure, combined with detailed circuit simulations; the preferred solution isolates the microelectrodes from the fluid media with thin dielectric layers. To form these layers, the microelectrodes are coated with a thin layer of Parylene [110], which results in the formation of a relatively high value capacitance at the interface between each microelectrode and the electrolyte. According to material properties, microelectrode dimensions, and the dielectric thickness, the value of this interface capacitance ranges from 2pF to 15pF.

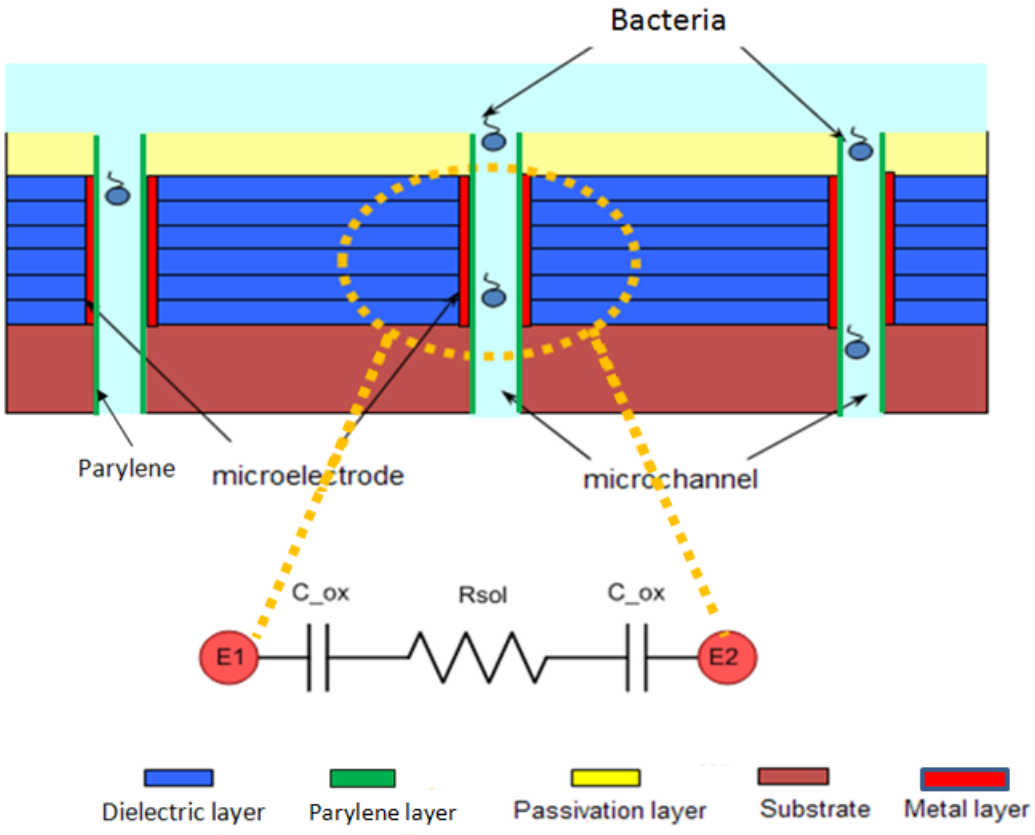

Fig 3.5: Electrical model for each microelectrode pair

The simplified electrical model for each microelectrode pair is shown in Fig 3.5. The resistance R_{sol} represents the finite conductivity of the electrolyte. The value of R_{sol} is greater when a non-conductive bacterium/microparticle is passing through the microchannel between the microelectrodes. The C_{ox} capacitors are due to the thin dielectric layers on the surface of the microelectrodes. For a given microelectrode pair, both capacitance values should be fairly equal, as their geometry is the same and the means of coating the dielectric is equivalent. However, some slight variations on these values should be considered, which can be caused by directional asymmetry or variations in the process used to coat the microelectrodes.

To design the sensing circuit, the presence of the relatively large capacitance C_{ox} is used to integrate a DC current. The resulting circuit can be reduced to Fig 3.6, for which Equations (3.1), (3.2) and (3.3) apply.

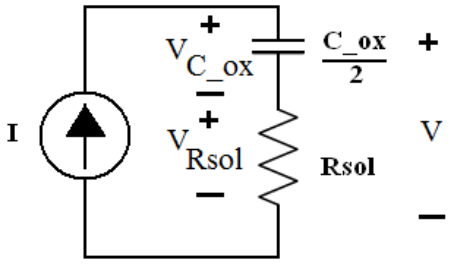

$$V = V_{Rsol} + V_{C\_ox} \tag{3.1}$$

$$V = R_{sol} I + \int \frac{2*I*dt}{C\_ox} \tag{3.2}$$

$$V = R_{sol} I + \frac{2*I*t}{C\_ox} + V_0 \tag{3.3}$$

Fig 3.6: The equivalent circuit to model the injection of a DC current into a microelectrode pair

Shown in Fig 3.7, if a reference current "I" is injected, the voltage across a microelectrode pair is given by equation (3). It is a linear relationship with a slope inversely proportional to C_{ox}, and a value at origin directly proportional to R_{sol}. If, for instance, C_{ox} is a constant, a change in R_{sol} resultsin a vertical translation of the voltage across an electrode pair. Recall that a change occurs when a non-conductive bacterium/microparticle is present between an electrode pair.

Therefore, the conceptual diagram of Fig 3.7 is proposed to model the sensing mechanism associated with each electrode pair.

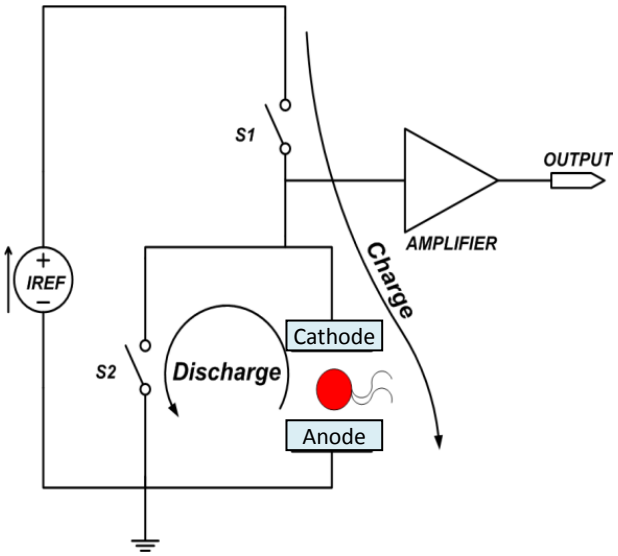

Fig 3.7: Conceptual diagram of the sensing mechanism.

When the switch (S1) controlling the capacitor charging process is on, the switch (S2) controlling the capacitor discharging process is forced off (mutually exclusive control) and the reference current is injected in the upper microelectrode, generating a voltage modeled by equation (3.3). This voltage is built up on the input of a buffer with a threshold voltage set as $V_{dd}/2$, where V_{dd} is the supply voltage. After a certain time, the Charging switch is turned off and the Discharging switch is turned on. The input of the buffer is then grounded, and both capacitors are gradually discharged. After a suitable time, this process can be repeated. As a result, a pulse train is created at the output of the circuit and the width of the pulses composing this train is related to the value of R_{sol}. The greater the R_{sol}, the wider the pulse. Hence by analyzing this waveform, the system can automatically determine when a bacterium or micro-particle passes by.

Note that the proposed sensing circuit is totally self-referenced. The presence of a target bio-entity can be determined by comparing the width of adjacent pulses generated on the same microelectrodes pair. Thus, the impact of mismatch due to the CMOS fabrication, post-CMOS process and other sources of parametric variations can be greatly minimized. As a result, no extra reference microelectrodes are required in this system.

3.3 Biocompatibility, robustness, and reliability

As discussed before, the metal material used in the CMOS process can threaten the viability of the bacteria. Meanwhile, the CMOS chip can be contaminated, leading to the degradation and failure of the sensing circuits, due to the alkaline ions contained in the aqueous mediums that are used in the chip [111,112]. In order to expand the life-time and sustain the reliability of the Lab-on-Chip system, a specific package is demanded to protect the CMOS chip from the possible corrosion/erosion caused by the medium sample. The most commonly used technique is to coat the CMOS chip with some biocompatible material, such as polymer, silicon nitride or silicon dioxide, as used in the chosen CMOS technology.

Parylene, which is an excellent dielectric and biocompatible material [113], is chosen to protect metal pads and bonding wire, and avoid corrosion on the surface of the microelectrodes. This family of polymers, including Parylene C, N, and D, is generated from derivatives of diparaxylylene (DPX). A solid material at room temperature, DPX can be melted at temperatures above 80° C. When this vapour is passed through a high-temperature zone (>680° C), the DPX dimer decomposes to a monomer. Upon depositing on a surface at a temperature below 95° C, the monomer spontaneously polymerizes forming a uniform, conformal coating over all exposed surfaces [114]. Parylene C, which has been used here, has good mechanical properties, high dielectric strength (2.2MV/cm), high volume resistivity (8.8×10^{16} ohm-cm), excellent chemical resistance, and biocompatibility [115,116]. Parylene C can be deposited in thickness ranging from a few angstroms to 50mm or even more.

3.4 Specificity of the lab-on-chip system

As described in Chapter 2, the specificity of this kind of biosensor is often achieved by surface modification on the microelectrode array. Antibody-antigen binding is the most frequently adopted approach to achieve specificity of this kind of lab-on-chip [117~120]. However, when a specific antibody is immobilized on the surface of the microelectrode array, the lab-on-chip system is constrained to detect only one type of bacteria at a time. In the meantime, if the concentration of the targeted pathogenic bacteria is very low, it will take quite a long time, usually several hours to days, for the bacteria migrating nearby to attach to an antibody on a microelectrode array.

In this research, we introduce a new method of using magnetotactic bacteria (MTB) as bio-carriers to achieve specificity and accelerate the bacteria-antibody binding process [121~123].

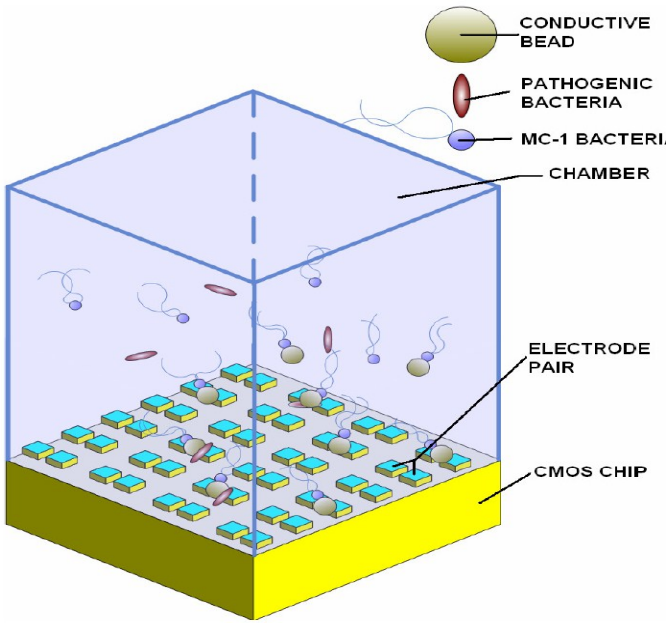

Fig 3.8: Schematic view of the MTB assisted Lab-on-Chip microsystem.

The proposed method, as depicted in Fig 3.8, is innovative in several ways.MTB are used to capture and transport targeted bacteria into the sensing area. A special species of bacteria, called MC-1, is used in this research. MC-1 MTB responds to the magnetic field through magnetotaxis, where the swimming direction of the MTB can be controlled by setting the direction of the magnetic field. In some typical conditions, the MC-1 bacteria swim at an average speed of approximately 200μm/s, which makes the sensing time very small for reasonable size microchambers.

To capture the pathogenic bacteria, MC-1 bacteria are attached to conductive microbeads where some specific antibodies are immobilized. Antibody specific to the targeted bacteria are also immobilized on the same bead. When the MC-1 bacteria swim in the sample and encounter a bacterium, the antibody should attach the latter and stick to it. A group of MTB can sweep the whole sample area in a very short time for targeted bacterial cells, and then, controlled by the magnetic field generated by external permanent magnets or on-chip electro-magnets [124, 125],

the MTB are guided to migrate toward the sensing area where impedance measurement can begin [121].

3.5 System packaging

A specific packaging is developed to hold the processed CMOS die and provide enough mechanical support as well as dielectric isolation for bonding wires and pads. The packaging scheme adopted for the implemented prototype is illustrated in Fig 3.9(a). On a standard microscope glass cover (size of 1.8cm x 1.8cm), a through hole of the size of the microelectrode array, is drilled manually using a diamond bit. (b)The CMOS die is attached to the glass cover using epoxy. All four of the edges are sealed with epoxy to ensure that there is no gap between the CMOS die and the glass cover. Then,(c) in the middle of a chip carrier (DIP 64, Spectrum Semi, CA, USA), a through package cavity (0.9 cm by 0.9 cm) is formed by an excimer laser (PulseMaster 848, GSI Lumonics On, Canada). Finally, (d) The glass cover with the CMOS die is installed from the back side of the chip carrier and ready for wire bonding.

In order to construct a microchamber on top of the microelectrode array and to protect the bonding wires and pads, the CMOS die, bonding wires, and pads on the chip carrier are encapsulated in a dielectric biocompatible epoxy. Thus, only the microelectrode array area is opened for liquid sample injection, which allows the sample medium to flow through the CMOS chip and chip carrier. Shown in Fig 3.10(b), a block of PDMS is temporally bonded on the area of the microelectrode array on the CMOS die. A small pressure can ensure there is no air bubble trapped in between. A liquid, transparent, and biocompatible epoxy (EP302-3M, EPOTEK, MA, USA) is poured on the surface of the CMOS chip to cover it completely, including pads and bonding wires. After the liquid epoxy is fully cured, the PDMS block is removed to leave a microchamber on top of the microelectrode array.

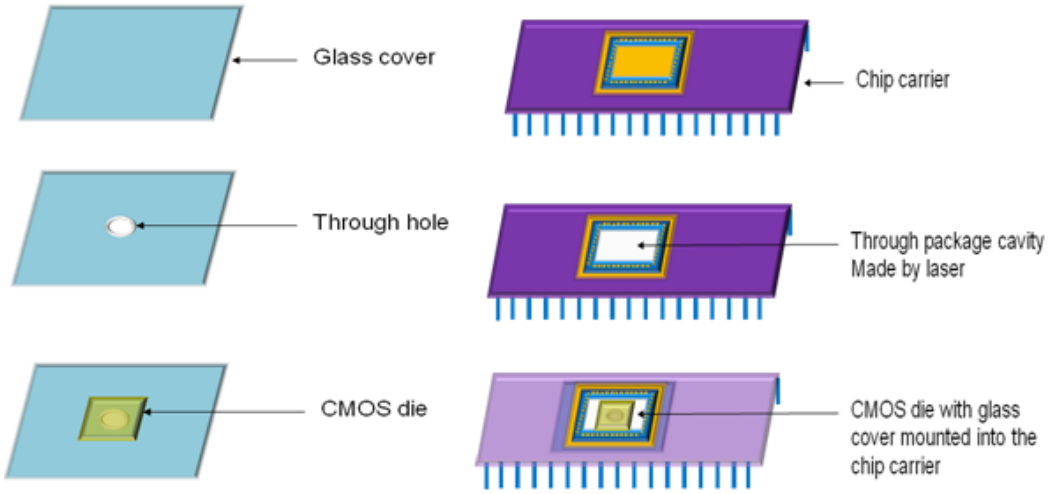

(a)

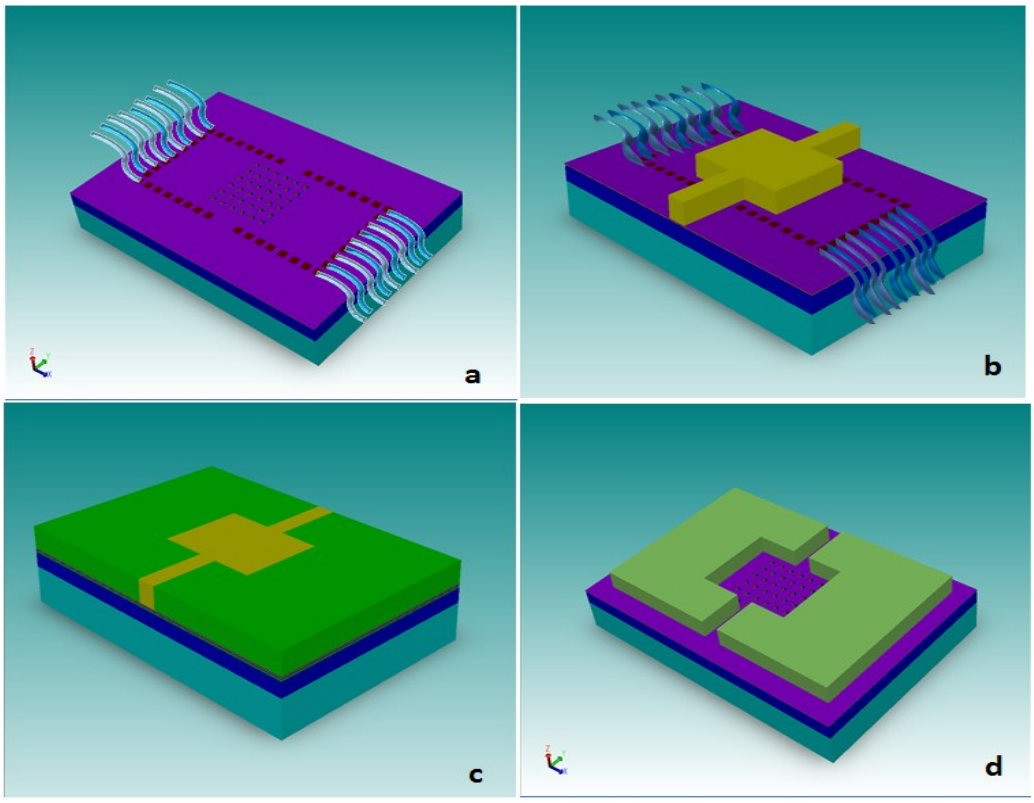

(b)

Fig 3.9:Packaging scheme

3.6 Conclusion

The system architecture of a novel lab-on-chip microsystem is presented. A conventional standard CMOS technology is adopted in this research to validate the idea of monolithic integration of a face to face microelectrode array and sensing microelectronic circuits on a CMOS chip. By adopting a standard CMOS technology, the task of fabricating a high density array of face to face microelectrodes can be achieved relatively easily, and the proposed on-chip sensing circuit also greatly increases the signal-to-noise ratio. With assistance of magnetotactic bacteria, it is expected that the throughput of the proposed lab-on-chip microsystem can be increased significantly and the system specificity could also be achieved by introducing functional microbeads pushed by MTB.

As it is a first prototype for validating the concept, evaluating the performance of the circuit, and the feasibility of the microfabrication process, the parameters are chosen for better understanding of the challenges. Theses parameters can changed over a wide range, thus leaving room for further adjustment to meet the requirements of different applications.

In order to achieve higher screening speed and throughput, higher microelectrodes density is needed. This could increase the background noise and cross-talk of various circuits, thus reducing the performance of the system. Following the concepts of design-for-test, this first prototype aims at developing a uniform platform for validating the performance of the circuits and microelectrodes under different conditions and providing data for further optimization studies.

CHAPTER 4 SIMULATION, ANALYSIS, DESIGN AND LAYOUT

4.1 Introduction

As discussed in chapter 3, this thesis has five goals: a. Investigating how to obtain a suitable microelectronic circuit with sensitivity high enough to achieve single cell detection without amplification; b. Investigating the optimum structure and geometry of microelectrodes to measure the impedance variations induced by a single bacterial cell; c. Exploring a reliable process to fabricate large electrode arrays using CMOS technology; d. Developing a suitable and cost effective packaging for integration of microfluidic components with a CMOS chip; And finally e. Developing a magnetotatic bacteria based transportation method to accelerate the screening speed and achieve high specificity.

In this chapter, we address the first two goals by simulation and rapid prototyping. The working mechanism of the system is established by physical and electrical models through simulations. The advantages of a proposed vertical, face to face structure over the conventional planar microelectrodes are verified using finite element modeling (FEM). The FEM simulations also provide guidelines to determine the optimum dimensions of the face to face microelectrodes, and the impact of the sensing volume, of the dimension of the microchannel between a pair of microelectrodes, of the detectable size of the targeted bacterium, of the effect of the position of the bacterium in the sensing volume. These simulations not only validate the system architecture, but they also provide guidance for detailed design of the Lab-on-Chip microsystem.

The simulation and models are validated by two designs. In one design, a microfluidic device consisting of an in-channel planar microelectrode array is fabricated using a standard microfabrication technology. The performance of the planar microelectrodes is evaluated and compared with the simulation results. Through this prototype, the controllability of MTB as bio-carriers in a micrometer size environment is also investigated. In the second design, a hybrid Lab-on-Chip system with an array of face to face microelectrodes and on-chip sensing circuitry is implemented into a CMOS chip to realize the architecture presented in Chapter 3.

4.2 FEM simulation: bacterium in microchannel

The FEM simulation [126~128] is the most widely used simulation tool to provide guidance for defining the parameters of the Lab-On-Chip system. It allows characterizing the sensitivity of the microelectrodesas a function of orientation , and of size, geometry, sensing volume, and material. It allows characterizing the signal to noise level required for on-chip sensing circuits[129~132].

A complex FEM simulation is developed to model the working mechanism of the proposed Lab-on-Chip system. The FEM simulations are used to compare expected and experimental results, and to optimize the design of the sensor in order to achieve the required sensitivity to detect a single bacterium. Multiple parameters, such as microchannel size, electrode geometry, sensing volume, bacterial size and bacterial relative position between a pair of microelectrodes are investigated to determine their effects on the system's sensitivity. Fig. 4.1 shows the equivalent circuit model of a bacterium in between a pair of microelectrodes.

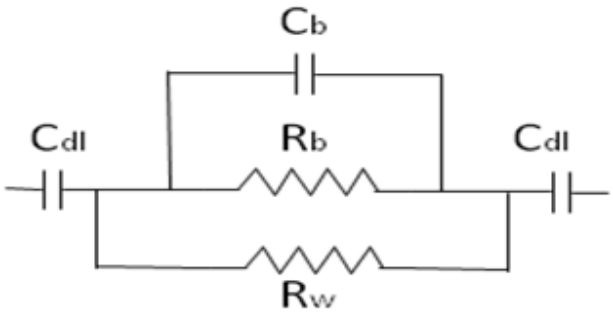

Fig4.1: Equivalent circuit of a bacterium in between a pair of microelectrodes. (C_{dl}: double layer capacitor, R_b: resistance of bacterium, R_w: resistance of medium, C_b, capacitance of bacterium)

4.2.1 Model definition: lab-on-chip and microbeads

The software chosen for the simulations is Comsol Multiphysics [133~135]. The 3D Electrostatics module of Comsol Multiphysics is chosen. It solves the following differential equation using the specified boundary conditions and subdomain settings:

$$-\nabla(\sigma + j\omega\varepsilon_r\varepsilon_0)\nabla V = 0 \ , \tag{4.1}$$

where ε_r is the relative permittivity of the domain, ε_0 is the permittivity of a vacuum (8.854e-12 F/m), σ is the conductivity of the domain, j is the imaginary number, V is the voltage (dependent variable), and ω is the angular frequency given by 2πf, where f is the frequency of the applied signal in Hertz (Hz).

In a first considered structure, the sensors' microchannel is modeled as a box with dimensions 20 μm x 20 μm x 85 μm (W x H x L). The Electrodes are embedded into the walls of the channel and are modeled as perfect conductors with a finite thickness, and with dimensions of 20 μm x 20 μm (W x L). These parameters are chosen according to the specification of a standard microfabrication process [136] used to fabricate a rapid prototyping microfluidic device, which is introduced in following sections. In order to simplify the initial simulation model, polymer dielectric sphere microbeads are used to model bacterium, assuming bacterial cells are made of dielectric material. The position and radius (R) of these microbeads are varied as described in the subsequent sections. All microchannel walls are given insulating boundary conditions. In each simulation, the microbead is given continuous boundary conditions. The source electrode is given a potential of V = 0.5 V and is stimulated with a sinusoidal waveform of 1 MHz frequency in most cases. The other electrode is grounded (V = 0). The parameters for the input signal were selected to minimize the effects of the double layer capacitance and to keep the viability of the targeted bacteria.[137 ~139].

The microchannel and microbead subdomains are modeled using the complex forms of the permittivity and conductivity to take into account their frequency dependence. The equations for the complex conductivity and permittivity are given below, respectively:

$$\bar{\sigma}_R = \sigma_R + j\omega \in_0 \in_R \tag{4.2}$$

$$\bar{\in}_R = \in_R + \sigma_R /(j\omega \in_0), \tag{4.3}$$

where $\in_R$ and σ_R are the real (static) permittivity and conductivity of the subdomain [140]. The microchannel subdomain is modeled as a solution of the same permittivity and conductivity as the one where the magnetotactic bacteria live(similar to sea water). The static conductivity of that media was measured to be 2.99 S/m (using a Thermo Scientific, Orion 5 Star Multimeter)

and the relative permittivity was found to be approximately 85 for sea water from the literature [141]. The polymer microbeads are modeled as insulating spheres, with a static conductivity of 10^{-15} S/m and a relative permittivity of 2.5, both representative of polymers such as polystyrene [142].

The numerical simulation results are computed using an AC signal with a logarithmic sweep of 30 points from 100 Hz to 100 MHz. A custom tetrahedral mesh is defined in order to obtain adequate accuracy in reasonable computation times. After solving for each frequency point, the result is exported to MATLAB for post processing. The normal current density is integrated over the source electrode using MATLAB coding to obtain the average current flux normal to the electrode surface for each measurement point. The impedance magnitude is then calculated using the following classical equation:

$$Z = V / I , \tag{4.4}$$

where V is the voltage applied over the electrode (0.5V) and I is the current outflow normal to the surface for each frequency point.

In order to investigate sensitivity changes between different modeling cases, the results are compared using relative impedance changes from a reference. This is calculated using the equation below:

$$\Delta Z = \frac{(Z_{bead} - Z_{ref})}{Z_{ref}} \times 100\% , \tag{4.5}$$

where Z_{bead} is the impedance with a polymer bead present and Z_{ref} is the impedance with no bead present. By using the relative impedance change, comparisons can be made between different modeling cases by using a normalized sensitivity value. The model given above describes the general simulation parameters that were used to define the microfluidic device. Described below are the specific modeling cases that investigate the changes in sensitivity when specific microfluidic device design and conditions are changed. Any changes made to the model are described in each section.

4.2.2 Microelectrode: planar or face to face orientation

The orientation of the microelectrodes will affect the detection sensitivity [143 ~ 145]. The microelectrodes are modeled in two different orientations: planar and face to face. The planar electrodes are placed side by side on the bottom of the microchannel, with a center to center separation of 35µm. For the face to face electrodes, one is placed on top of the channel and the other on the bottom of the channel (separation of 20µm). Polymer microbeads with diameters from 2µm to 15µm are placed in the center of the sensing region for both electrode orientations to investigate the difference in sensitivity over a range of microbead sizes. Shown in Fig 4.2 and Fig4.3 are images from the FEM simulation showing the face to face and planar electrode models. Results of the relative impedance change as a function of the microbead diameter are shown in Fig 4.4.

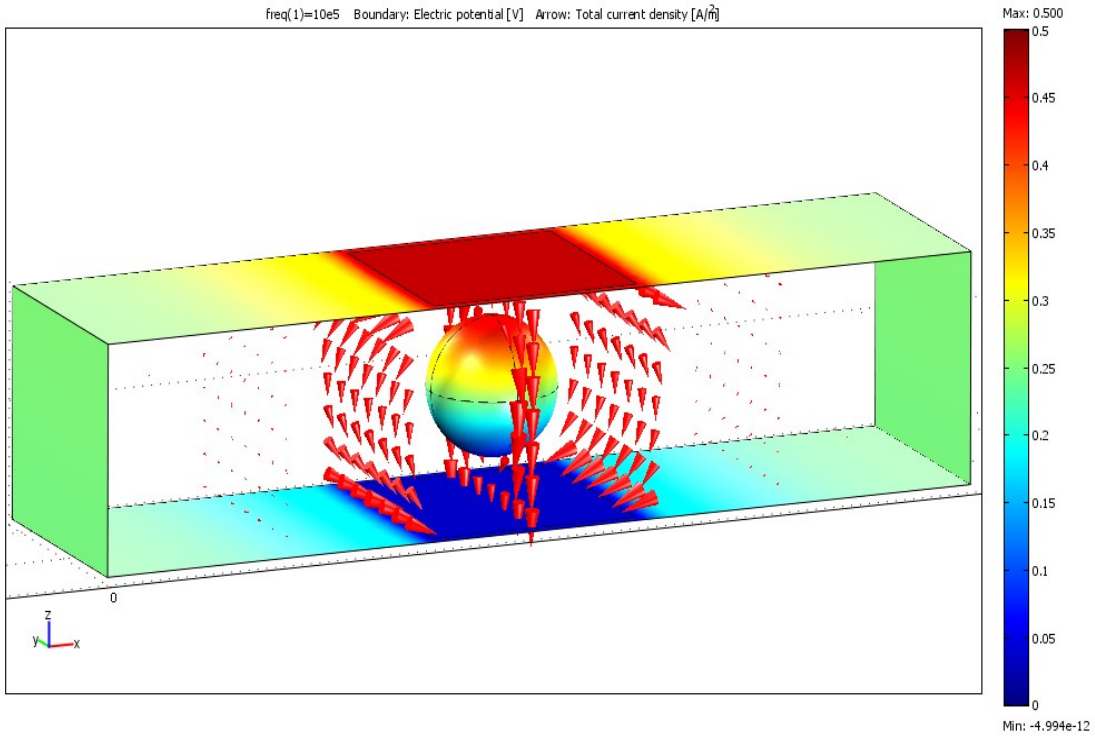

Fig4.2: FEM simulation image of the microchannel with face to face electrodes and a 12 µm polymer bead situated in the center of the sensing region. The applied potential is a 0.5V sine wave of 1MHz frequency. The arrows in the figure indicate the direction of current flow and its density.

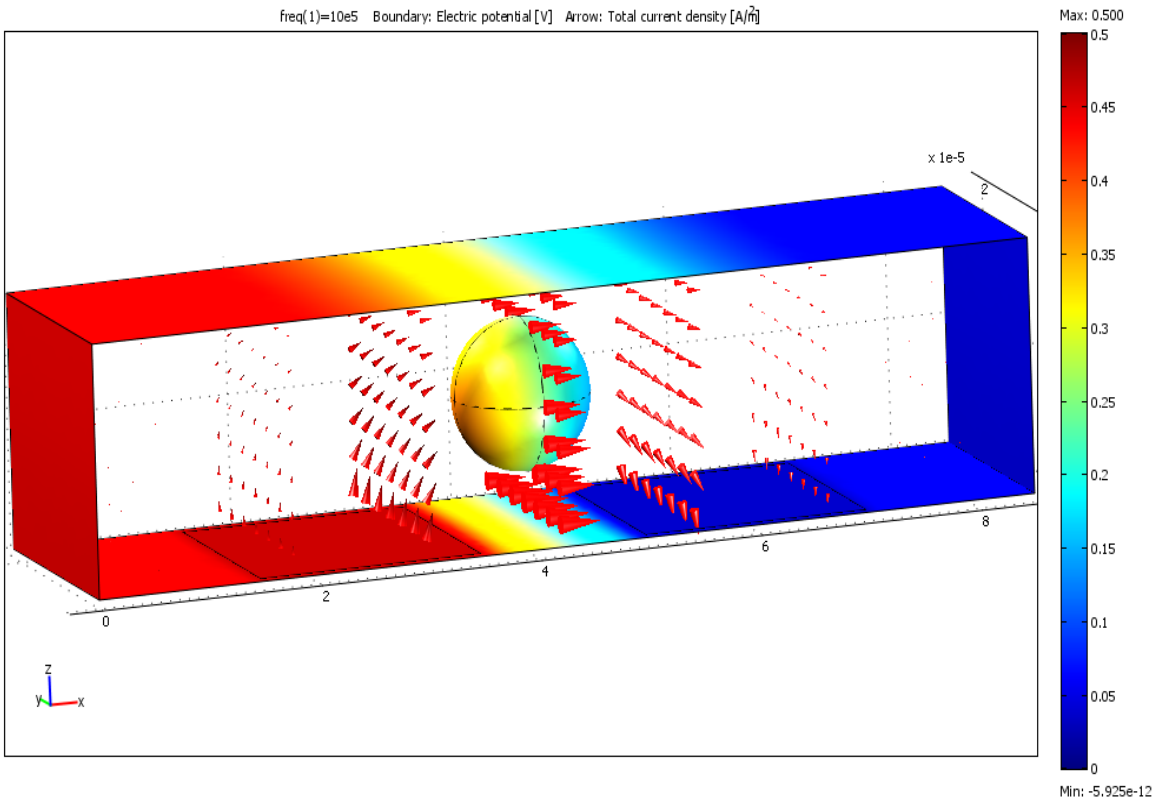

Fig4.3: FEM simulation image of the microchannel with planar electrodes and an 12µm polymer microbead situated in the center of the sensing region. The applied potential is a 0.5V sine wave of 1MHz frequency.

It is clear that the orientation of the microelectrodes have important effects on the detection sensitivity of the proposed Lab-on-Chip. As shown in Fig 4.4, higher sensitivity can be achieved when the electrodes are in face to face orientation rather than planar orientation, which is true for all sizes of microbeads investigated. With face to face electrode, the average sensitivity increases up to 30% when compared with planar electrodes of the same size. The center to center separation distance between the face to face electrodes can be made much smaller than the center to center separation for planar electrodes. This is because planar electrodes that are close together suffer high stray capacitance effects [146, 147] if their edges are very close to each other. Having the electrodes as close as possible with minimal stray capacitance allows greater sensitivity to be achieved, and so face to face electrodes will achieve higher sensitivity, as shown in the results.

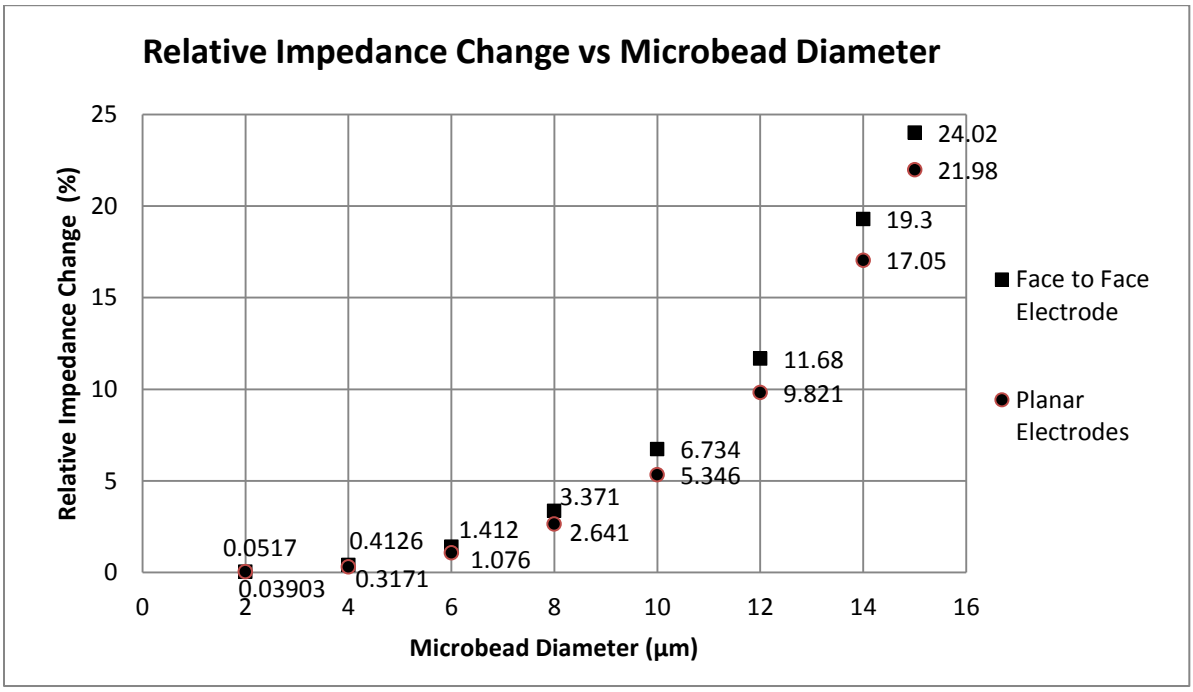

Fig4.4: Graph of the relative impedance change at 1MHz for microbeads of various diameters using microelectrodes in face to face and planar orientation.

4.2.3 Microbead size

The ability of a Lab-on-Chip to detect very small objects, such as pathogenic bacteria, and its ability to differentiate between objects of similar size is very important. This was investigated simultaneously with the effect of microelectrode orientation given in Fig4.4. Using both orientations, beads with diameters from 2µm to 15µm were placed into the channel and the relative impedance change was calculated to determine the sensors ability to detect small objects and objects of similar sizes. Note that when the size of the object is close to the size of the microchannel and of the microelectrode, higher resolution is expected.

4.2.4 Sensing region volume

The volume of the sensing region directly affects the detection threshold of the device. The sensing region volume is the volume of space in between the electrodes. In order to investigate the effect of the size of this volume, the channel depth is reduced while using face to face

electrodes. The simulation is performed with channel depths from 5µm to 20µm in 2.5µm increments. A polymer microbead of 4µm in diameter is placed at the center of the sensing region and the relative impedance change calculated for each different depth.

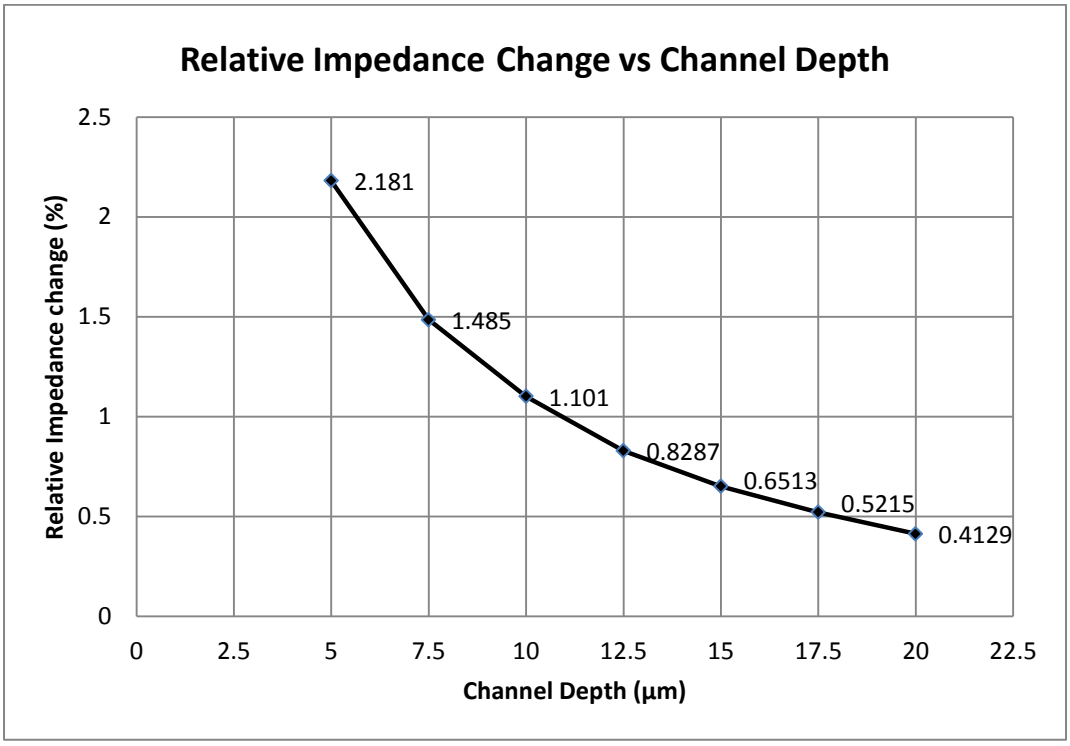

Fig4.5: Graph of the relative impedance change at 1 MHz for a 4 µm microbead with numerous different channel depths. Electrodes are in the face to face orientation.

As shown in Fig.4.5, decreasing the depth of the channel causes a large increase in the detection sensitivity. Each time the volume is halved, the sensitivity approximately doubles. This is because having a larger channel increases the volume of liquid between the electrodes. When a small bead enters this region, it displaces some of the liquid and causes an increase in impedance as it is less conductive than the liquid it has displaced. The relative increase in impedance depends upon the ratio of the volume displaced (bead size) to the volume of the sensing region. Therefore, having a larger sensing volume reduces this ratio and so reduces the relative change in impedance. Since the object size will be more or less fixed by the size of the target bacterium, the sensitivity can be significantly increased by shrinking the sensing region volume.

4.2.5 Microbead position

The horizontal and vertical position of the microbead within the channel is investigated using face to face electrodes and an 8μm polymer bead. For the vertical position, the bead is initially located 0.5 μm below the source electrode and is moved to 0.5μm above the ground electrode in 2.5μm increments. For the horizontal position, only the x-direction must be investigated, as the electric field is approximately constant in the y-direction. Here, the x-direction refers to a vector along the length of the channel and the y-direction is a vector along the width of the channel. Since the electrodes basically take up the entire width of the channel, the y-position of the bead should not affect the impedance change because the electric field is symmetric. To investigate the effect of the x-position of the bead, only half of the electrode is considered because of the symmetry of the electric field. The bead is centered in the sensing region and moved out along the x-direction in 5μm increments until its center is 20 μm from the center of the sensing region.

As shown in Fig4.6, for the vertical position, a greater sensitivity is achieved when the microbead is closest to the sensing electrode, and decreases greatly as it moves to the ground electrode. The current density is highest close to the source electrode, so the closer the bead is to the source electrode the higher the change in impedance. The horizontal position of the bead also has a large effect on the detection sensitivity. As the bead moves away from the center of the sensing region and is no longer in between the electrodes, the impedance change becomes virtually undetectable for a bead as large as 8 μm, as shown in Fig4.7. This demonstrates that in order to detect a single bacterium that is being moved very quickly by the flow through the detection region, the rate of impedance measurements over time must be high so that measurements will be made while the bacterium is in the center of the sensing region. Alternatively, the flow could be slowed down as the target bacterium enters the sensing region to allow impedance measurement to be recorded while the bacterium is in the optimum position.

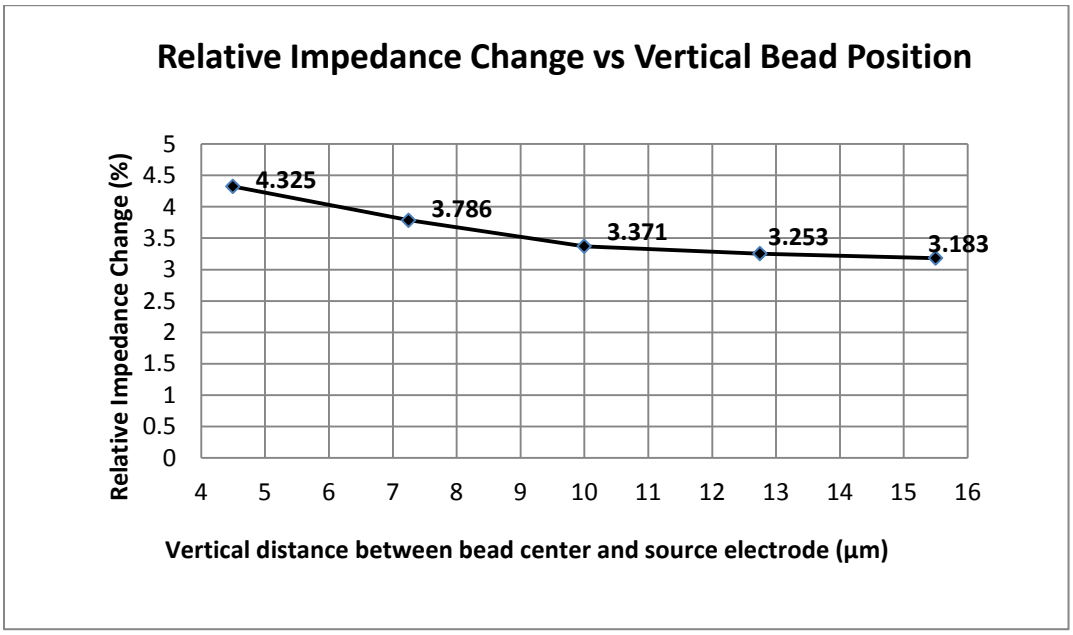

Fig4.6: Graph of the relative impedance change for an 8 µm bead at numerous different vertical positions within the sensing region. Microelectrodes are in face to face orientation and results are obtained for a signal at 1 MHz frequency. Size of the microchannel is 20µm by 20µm (H x W).

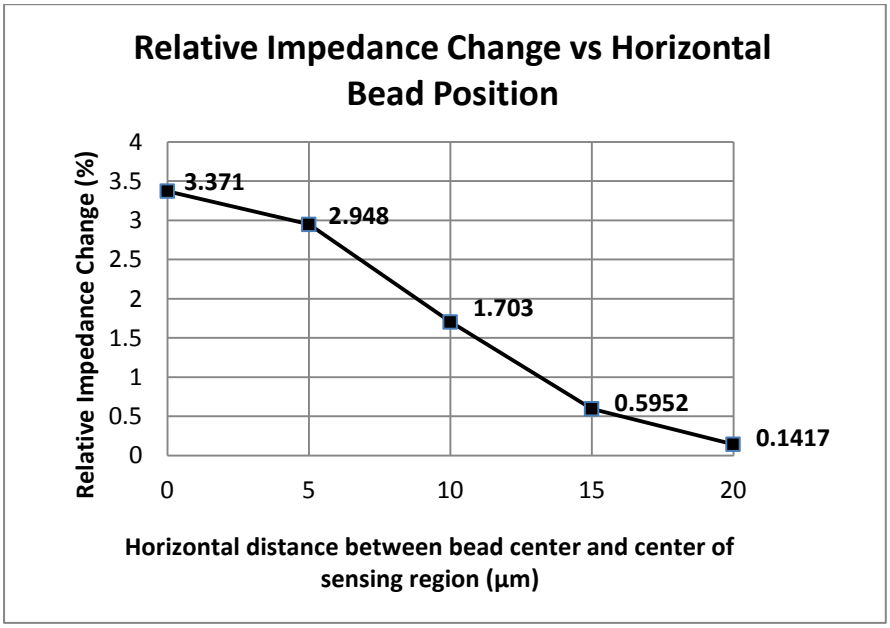

Fig 4.7: Graph of the relative impedance change for an 8 µm bead in numerous different horizontal positions within the sensing region. Size of the microchannel is 20µm by 20µm (H x W). Electrode orientation is face to face and results are obtained for a signal at 1 MHz frequency.

4.2.6 Size of microelectrodes

Another important parameter of the Lab-on-Chip system is the size of the microelectrodes, which is not only directly related to the sensitivity of the sensor, but also defines the cost and complexity of the microfabrication procedure. Illustrated in Fig4.8, a microbead, 2 μm in diameter is placed at the center of a pair of face to face microelectrodes. According to the different size of microelectrode pairs, the relative impedance change is calculated. The size of the microchannel in between is the same as the size of the microelectrodes. As illustrated in Fig4.8, when the size of the electrode is comparable to the size of the microbead, higher resolution is expected.

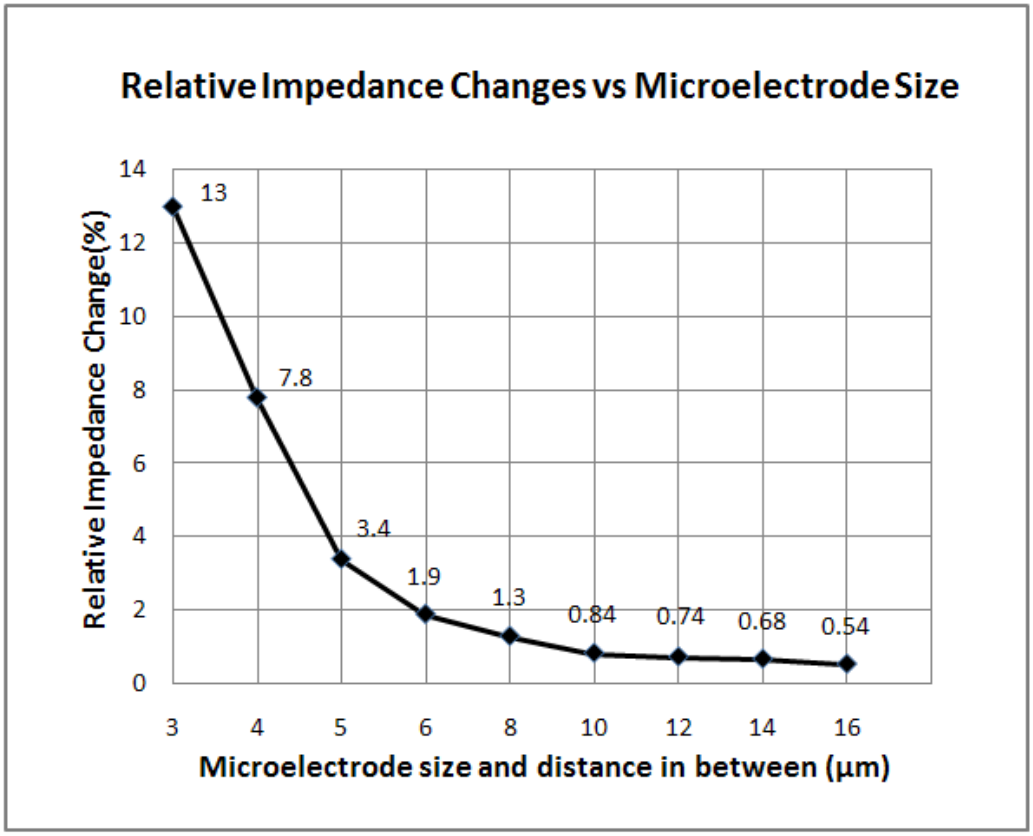

Fig 4.8: Graph of the relative impedance change at 1 MHz for a microbead (2 μm in diameter) at the center of the microchannel between a pair of microelectrodes of various size in the face to face orientation.

4.3 FEMsimulations: magnetotactic bacteria assisted lab-on-chip system

This section describes the FEM model used to simulate the Magnetotactic Bacteria bio-carrier with *E. coli* as the target pathogenic bacterium. It is assumed here that a MTB is used to propel a microbead coated with specific antibody searching for targeted bacteria. The complex is then brought to the sensing area, a microelectrode array measuring impedance changes. Since the movement of a MTB can be controlled by an external magnetic field, the manipulation can be achieved relatively easily by controlling the direction of local electrical magnetic field generated by an on-chip coil array or just a permanent magnet. Due to its fast swimming speed, up to 250 μm/second, a group of MTB can push functional microbeads sweeping the whole sample area in a very short time, in order to capture the targeted bacterium.

4.3.1 Model definition: MTB bio-carrier with target bacterium *E. coli*

The model used here is similar to the one used in the previous section to optimize the design parameters of the device. However, advanced modeling techniques are required in order to adequately model the impedance of biological cells such as the MTB and the *E. coli* bacteria. Biological entities are complex structures that contain many layers [148], each with different electrical properties. The MTB and the *E. coli* both contain numerous thin layers surrounding their cytoplasm [149]. Fig 4.9 shows the equivalent circuit model of the MTB carrier system.

To simplify the model, only the cell membrane surrounding the cytoplasm is considered. The cell membrane is a thin non conductive layer that surrounds the bacterium and acts as a capacitor. The cytoplasm is a large conductive region that holds all the organelles, and that acts as a resistance, as shown in Fig4.9. The membrane capacitance of biological cells, 1 $\mu F/cm^2$, is used to approximate the *E. coli* and MTB membrane capacitance [150]. The static conductivity and relative permittivity of the cytoplasm of the MTB and of the *E. coli* are given the approximate values for common biological cells, which is 0.5 S/m and 60, respectively [151]. Modeling the thin membrane layer using COMSOL is very difficult because of the large difference in size between the layer (being on the order of nanometres) and the rest of the model (several micrometers). Many elements are required to accurately resolve such a thin layer, which leads to memory problems and extremely long solution times. In order to avoid this problem, an alternate method is used to effectively model the thin layer of the bacteria membranes.

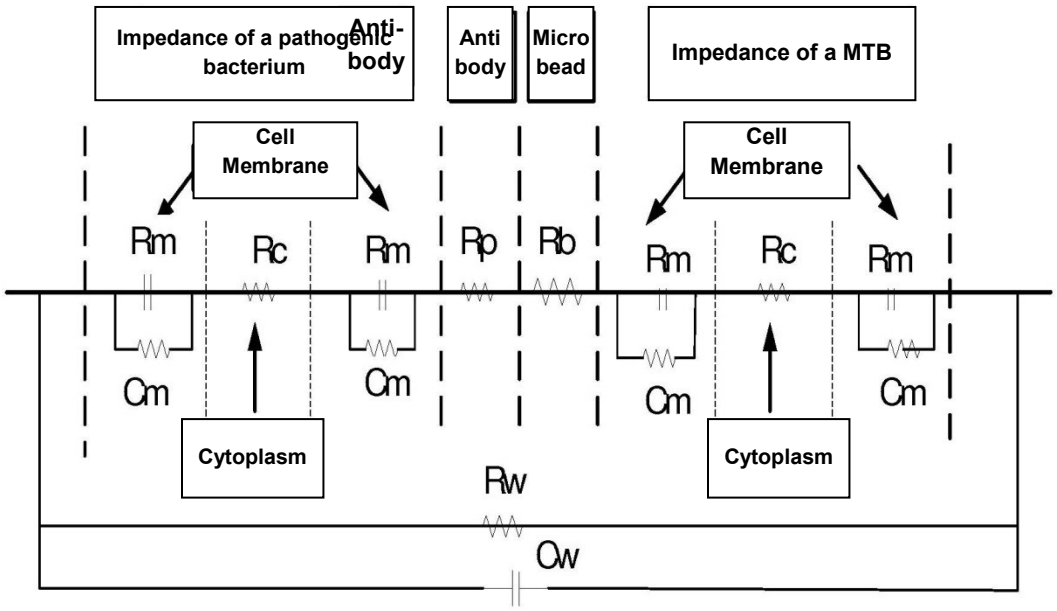

Fig 4.9: Equivalent circuit model of the MTB bio-carrier system pushing an attached pathogenic bacterium in between a pair of face to face microelectrodes. R_m, R_c ,R_p, R_b, and R_w represent the resistance of the bacteria membranes, cytoplasm, the antibody, the microbead, and the medium, respectively. C_m and C_w represent the capacitance of the bacteria membranes and the medium between the electrodes, respectively.

In order to model the thin membrane of the bacteria, Jones' equivalent complex permittivity for shelled spheres is used [150]. This model calculates an equivalent complex permittivity for the cytoplasm of the cell based on the capacitance of the membrane layer. Using this model, the membrane capacitance can be considered without having to construct the thin layer in the FEM simulation. The use of the equivalent permittivity to model the thin membrane layer is illustrated below in Fig 4.10.

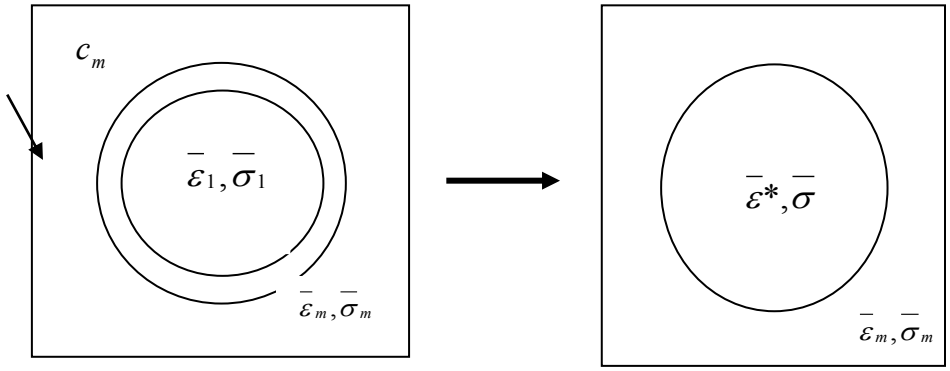

(a) **(b)**

Fig 4.10 (a) The thin shell structure of a bacterium membrane surrounding its cytoplasm in an external medium. (b) The equivalent shell model of the bacteria after applying equation (4.6).

In left side of the above diagram, c_m represents the capacitance of the membrane shell, $\bar{\varepsilon}_1, \bar{\sigma}_1$ represents the complex permittivity and conductivity of the cytoplasm, and $\bar{\varepsilon}_m, \bar{\sigma}_m$ represents the complex permittivity and conductivity of the medium (in this case, the bacteria medium). Applying Jones' equation for the equivalent permittivity of shelled spheres (4.6) gives the right side of the diagram, in which $\bar{\varepsilon}^*, \bar{\sigma}$ represents the equivalent complex permittivity and conductivity of the biological cell.

$$\bar{\varepsilon}^* = (c_m \times R \times \bar{\varepsilon}_1) / (c_m \times R + \bar{\varepsilon}_1) \tag{4.6}$$

In Jones' equation above, c_m is the capacitance of the cell membrane, R is the radius of the cell, and $\bar{\varepsilon}_1$ is the complex permittivity of the cytoplasm as defined by (4.3) [150]. The complex conductivity of the cytoplasm is simply given by equation (4.2). Using this method, the membrane capacitance of the MTB and *E. coli* bacterium are taken into account in the FEM simulation.

The MTB is defined as a sphere of 2 μm in diameter with continuous boundary conditions (with electrical properties defined above) and is placed behind a polymer microbead of 3 μm in diameter. This represents the MTB bio-carrier. The *E. coli* is modeled as an ellipsoid of dimensions 3 μm x 1 μm x 1 μm and with the electrical properties as defined above. Since the *E. coli* is ellipsoid shaped and equation (4.6) is meant for shells, the radius (R) used in equation (4.6)

for the *E. coli* is approximated by using a radius that yields a sphere of the same volume of the ellipsoid. The *E. coli* is given continuous boundary conditions and is situated on the opposite side of the microbead. The impedance change from reference is calculated for 3 different cases: the single MTB, the MTB with an attached microbead and the MTB with an attached microbead and *E. coli* bacterium. The model uses face to face electrodes in a channel with a depth of 20 µm. The model is shown in Fig 4.11. Results are shown in Fig 4.12.

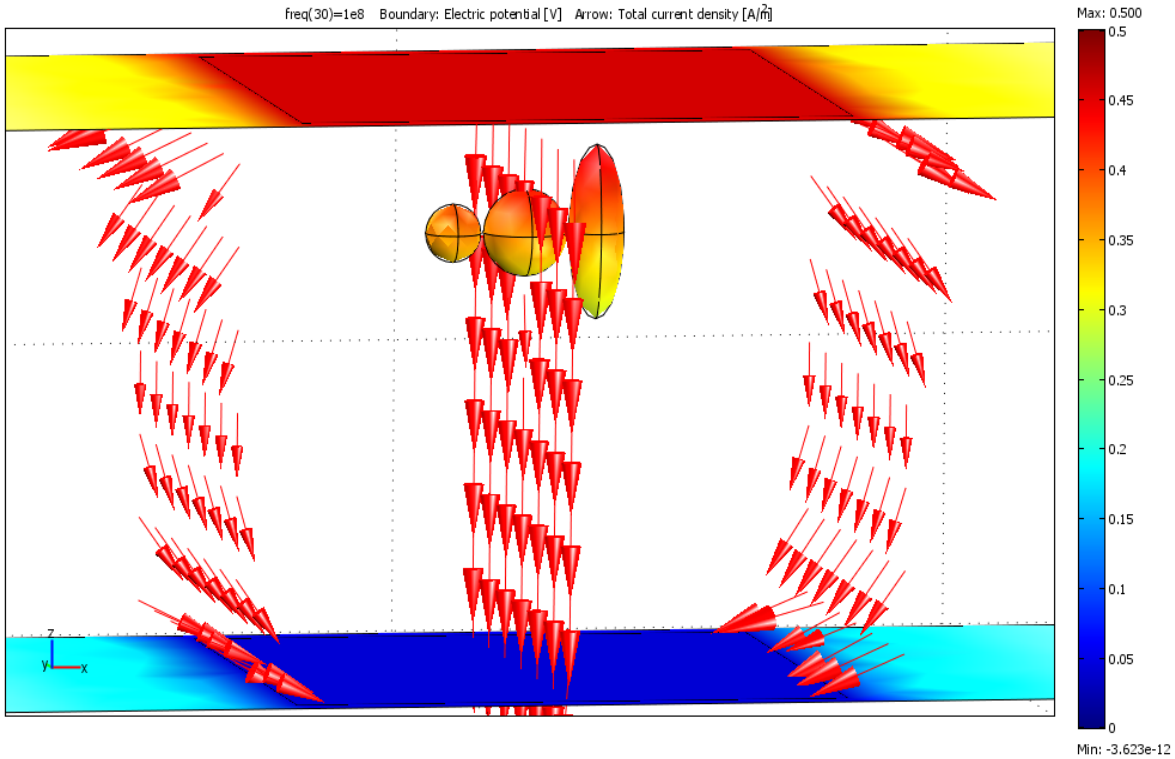

Fig 4.11: FEM image of the MTB bio-carrier system with an E. coli bacterium attached placed between face to face electrodes. The MTB is located on the left, the anti-body coated microbead in the middle, and the *E. coli* bacterium on the right. The applied potential is a 0.5 V sine wave of 1 MHz frequency.

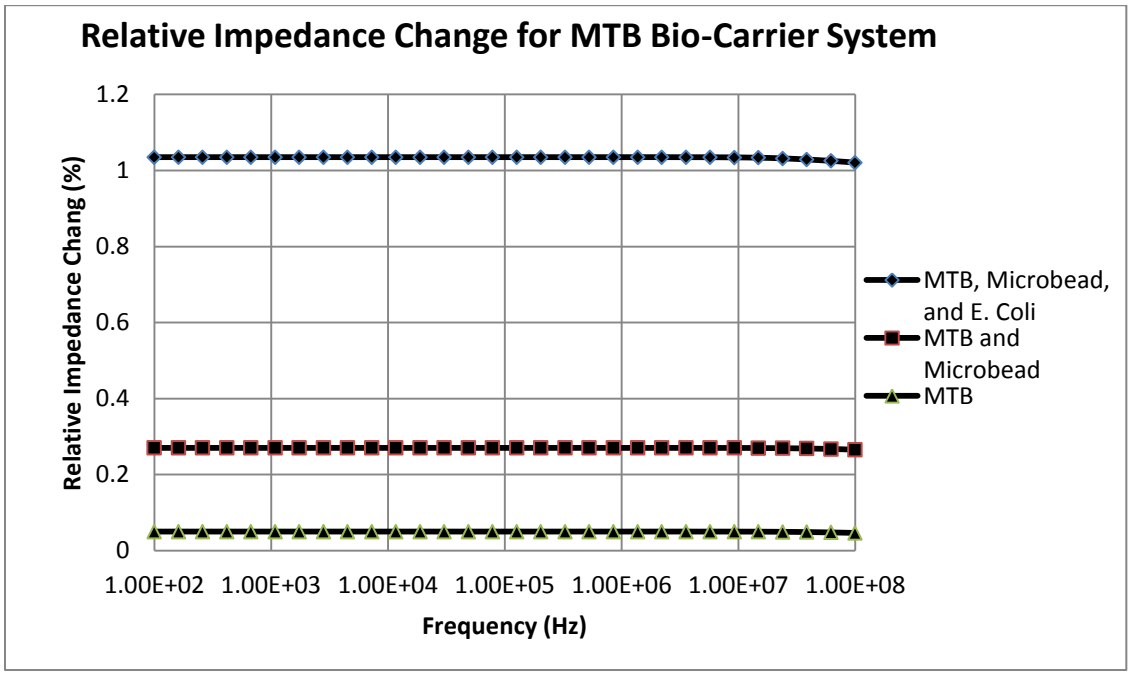

Fig4.12: Graph of the relative impedance change over a frequency from 100 Hz to 100 MHz for the 3 considered cases of the MTB bio-carrier system. Microelectrodes are in face to face orientation. A relatively large increase in impedance is seen when the *E. coli* bacterium becomes attached to the bio-carrier.

4.3.2 Analysis

In order to investigate the signal produced by a pathogenic bacterium, such as *E.coli*, when attached to the MTB bio-carrier, a second simulation was developed. The results of this simulation, as shown in Fig 4.12, indicate that with the sensor design used in this simulation, it would be possible to detect the presence of the *E. coli* bacterium (assuming 1% noise) attached with a microbead and a MTB. Since the size of *E. coli* bacterium is generally larger that a MTB, the induced impedance change is larger than the background noise, which makes the detecting and counting the number of target bacterium feasible. However, many types of bacteria are smaller than the *E. coli* investigated here, and equivalent electrical noise may be higher than the 1% fluctuation assumed here. Also, the impedance analyzer is very sensitive to the variation of the external environment, which makes it difficult to achieve repeatable experimental results. Therefore, a biosensor with higher sensitivity is expected to detection single bacterium with

small size. Based on the FEM simulation results previously discussed, the design of the Lab-on-Chip can be further optimized to increase its sensitivity. One of the approaches is to minimize the sensing volume. For instance, by shrinking the channel height by half, reducing the electrode separation to 10 μm, an additional increase in impedance change could be above 2%, which make the detection more feasible for a single pathogenic bacterium.

In order to validate the simulation results described in previous sections, two rapid prototyping designs were implemented. One adopted a standard microfabrication process, on which planar microelectrode pairs were implemented into a microchannel. Medium containing microbeads were injected into the microchannel. The impedance changes caused by the presence of microbeads were measure by electrode pairs. The experimental results were compared with FEA simulation. The chip design and layout were introduced in section 4.4; the experimental results were presented in Chapter 5. Based on the results of the first prototype, a second design based on standard CMOS technology was proposed and optimized with face to face electrode array and on-chip signal condition and processing circuitry. The design, simulation and layout are introduced in section 4.5; detailed fabrication process was given in chapter 5 and experimented were presented and analyzed in Chapter 6.

4.4Rapid prototyping with MicraGEM technology: chip design and layout

A structure similar with the structure describedin Fig 4.3was fabricated using the MicraGEM process provided by Micralyne [151] through CMC Microsystems. MicraGEM uses Pyrex glass as its substrate material. Two different microchannel depths, 10 μm and 12 μm can be etched into the Pyrex glass layer. A single crystal silicon layer (10μm) is anodically bonded to the Pyrex substrate to form the structural layer. Metal can be deposited on the Pyrex glass and on top of the single crystal silicon layer, which allows the creation of electrodes and/or electronic connections. In this process, we implemented a microchamber (3mm × 3mm) and numerous microchannels (25μm × 10μm, W x H) on the Pyrex substrate. Microelectrodes (20μm × 20μm) for impedance measurement were patterned on the bottom of each microchannel. The single crystal silicon layer is used to seal the microchannels and the microchamber, and to form openings which provide inlets and outlets for sample injection. A metal microcoil array, used to generate the local magnetic field in the microchamber, is deposited on top of the single crystal silicon layer. The

local magnetic field generated by the microcoils can control the swimming direction of the MTB to realize the function of bacteria mixing and sorting. Since the MTB react to very small magnetic field, only small DC currents are required when coupled with an insulation layer with a thickness of 10μm. The layout of the whole system is presented in Fig 4.13. The fabricated microfluidic device is shown in Fig 4.14.

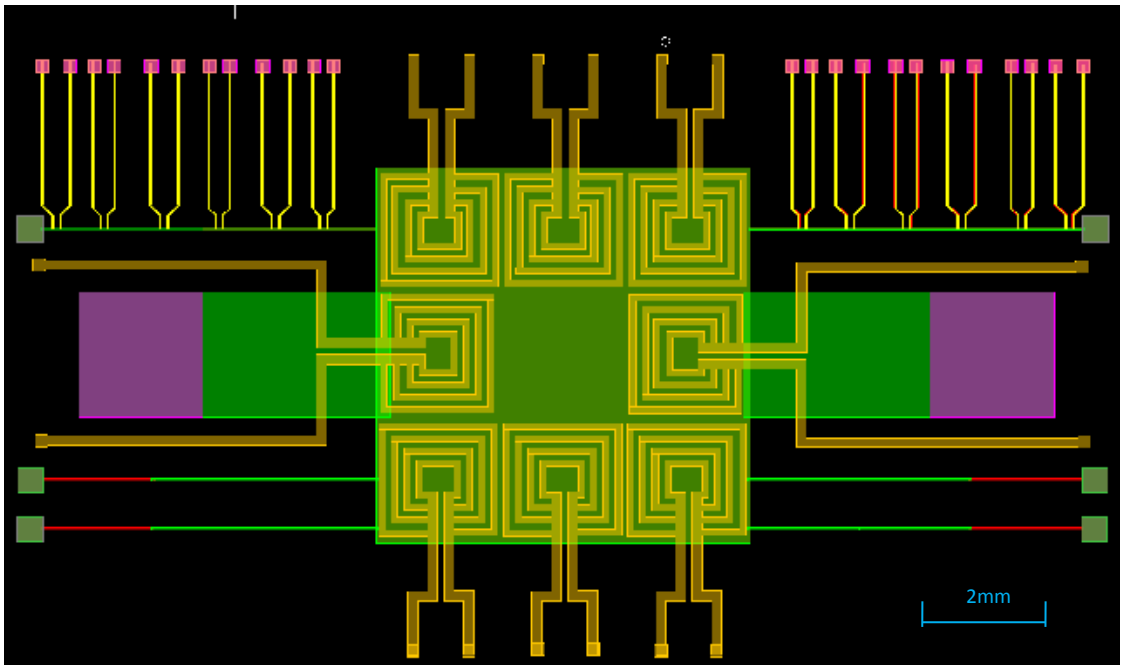

Fig 4.13: Schematics of the microchip system using the MicraGEM process

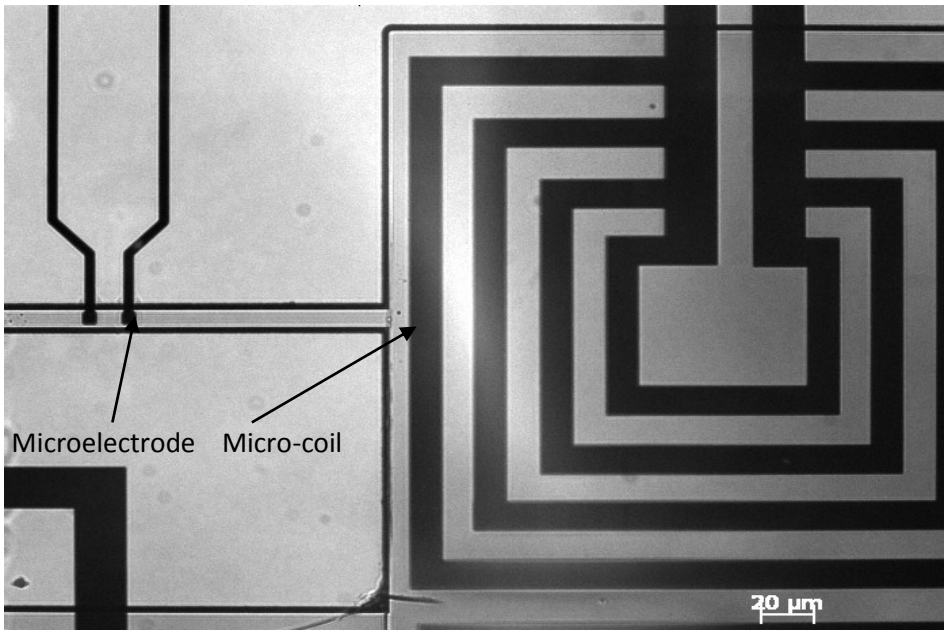

(a)

Fig 4.14: Microscopic image of fabricated microelectrodes, microchannel and a micro-coil(a)

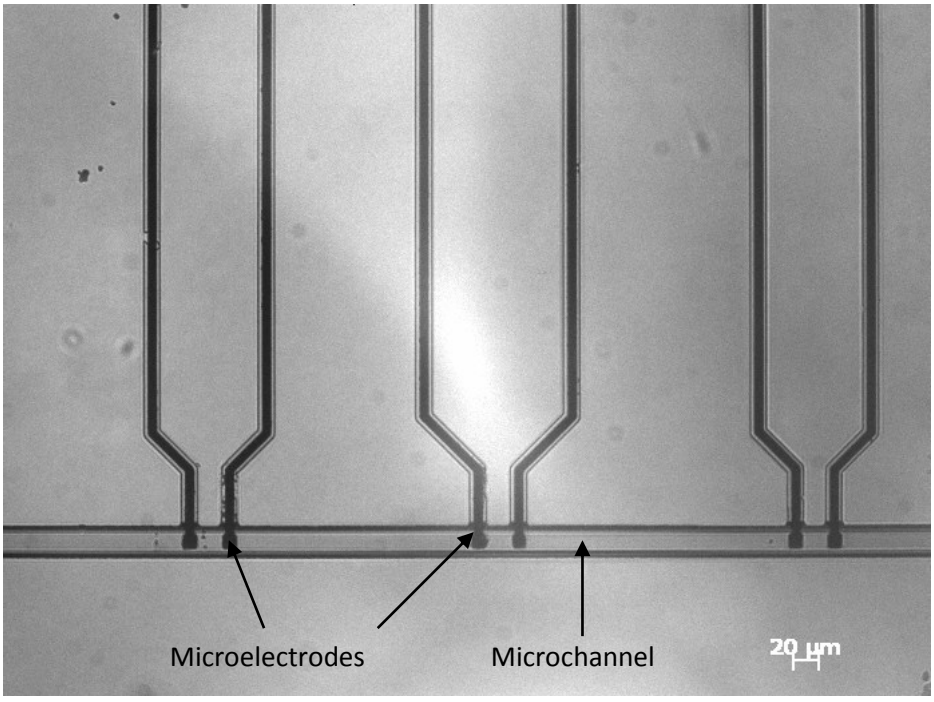

(b)

Fig 4.14: Microscopic images of fabricated microelectrodes, microchannel and a micro-coil(b)

4.5 Prototypingbased on a CMOS technology, chip design and layout

As indicated in section 4.2.2, the orientation of electrodes has big impact on the sensitivity of detection. Compared with planar electrodes, besides the 30% of increase of sensitivity in general, face to face orientation allows the electrodes to get closer to each other, which shrinks the sensing volume and makes the target particles/cells close to the surface of electrode, thus further increase the biosensor's sensitivity. However, there is no standard fabrication process accessible to fabricate such structure. As reviewed in section 2.6, several methods of fabricating face to face have been explored and the testing results were promising. In those pioneering works, complex fabrication process has been used to fabricate electrode, but a feasible and cost-effective method of fabricating a large scale face to face electrode array was still in investigation. Meanwhile, in most of the previous works, expensive desktop instruments, for instance, impedance analyzer and lock-in-amplifier had to be equipped in order to read-out and extrapolate the signal from the electrodes, which make the miniaturization of such functionalities into a Lab-on-Chip system a very challenging job.

To address these challenges, we proposed a novel structure based on a standard CMOS fabrication process. Within this structure, a scalable face to face electrode array were implemented by stacking the metal layers of CMOS process; signal conditioning and sensing circuitry were implemented on the same substrate as well. In this section, a sensing circuit is introduced first, followed by the design of microelectrode array and layout of the proposed CMOS chip.

4.5.1 Sensing circuit design

Instead of utilizing the conventional AC driven impedance measurement circuit, in this research, we proposed a novel design using DC current as stimuli and the sensing mechanism was realized through the integration of the current in the interfacing capacitor, which is in proportional with the size and electronic properties of medium and target particles/cells in between a pair of electrode. The detailed circuit design, analysis and simulation results were described below.

The circuit that implements the impedimetric detection for the system is shown in Fig 4.15. The reference current is provided from outside the microchip and it is injected into the detection

circuit using a simple current mirror. An externally generated current was adopted to alleviate uncertainties. This was necessary as the design of the required custom integrated circuit occurred in parallel with the development of the post-processing microfabrication steps, and the different possible applications were not known at design time. Obviously, different applications may require very different stimulation currents. Ultimately, in a fixed application, with well characterized post-processing steps targeting a low-cost system, the current source would be on-chip. At this stage, external control of the injected current is essential for characterization tests.

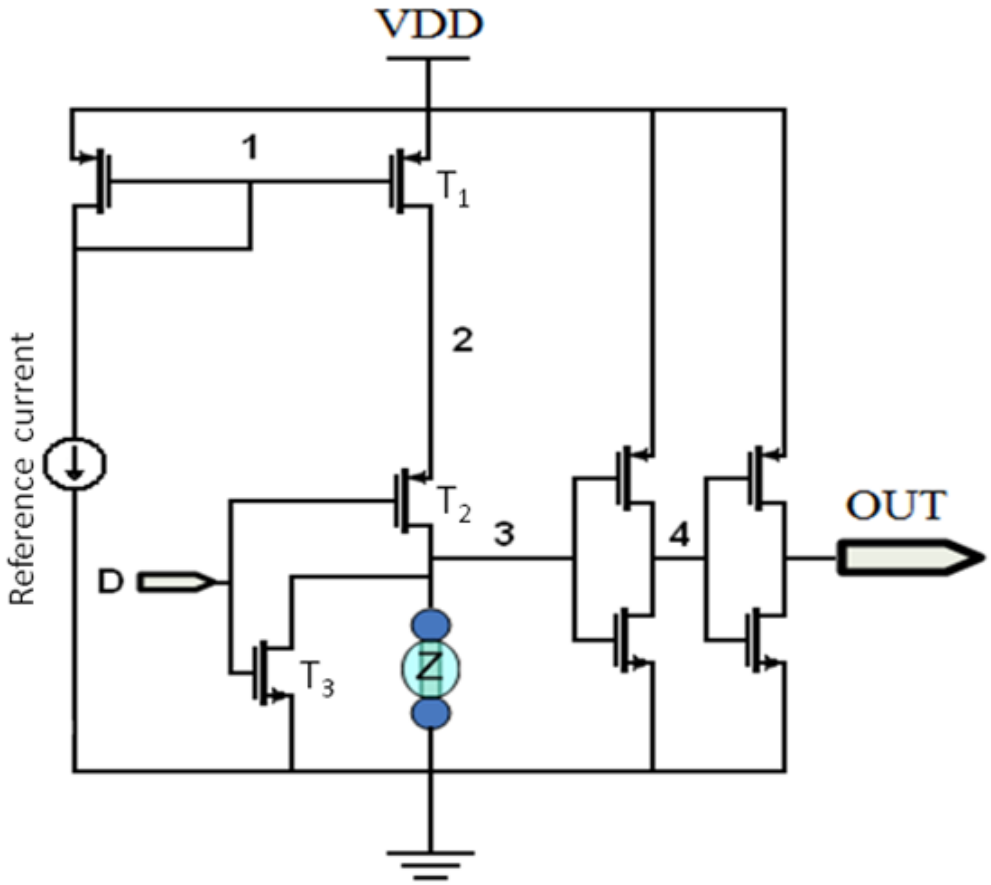

Fig4.15:CMOS stimulus generation and detection circuit.

The charge switch is implemented using a PMOS transistor (T_1)and the Discharge switch is implemented using a NMOS transistor (T_2). Thus, as a mutually exclusive conduction is desired, only one control signal is needed for both switches. The buffer is easily implemented with two simple CMOS inverters. One should note that the gate capacitances are also changing in the

charging phase. The C_{ox} capacitance should then be large enough to make the impact of the inverters negligible in the detection scheme.

In order to explore a reference design, the conductivity of the electrolyte is assumed to be 1S/m. Fig 4.8 presents impedance changes with various sizes of microelectrodes and microchannels based on these modeling assumptions. Although the simulation results were achieved using AC stimuli and here the DC stimulus was adopted, It is obvious that smaller microelectrodes with narrower channels provide better discrimination. When the channel is much larger than the microbead, more reference current flows around the microbead, thus reducing the sensitivity of the circuits. However, it is much more difficult to fabricate narrower channels due to microfabrication constraints.

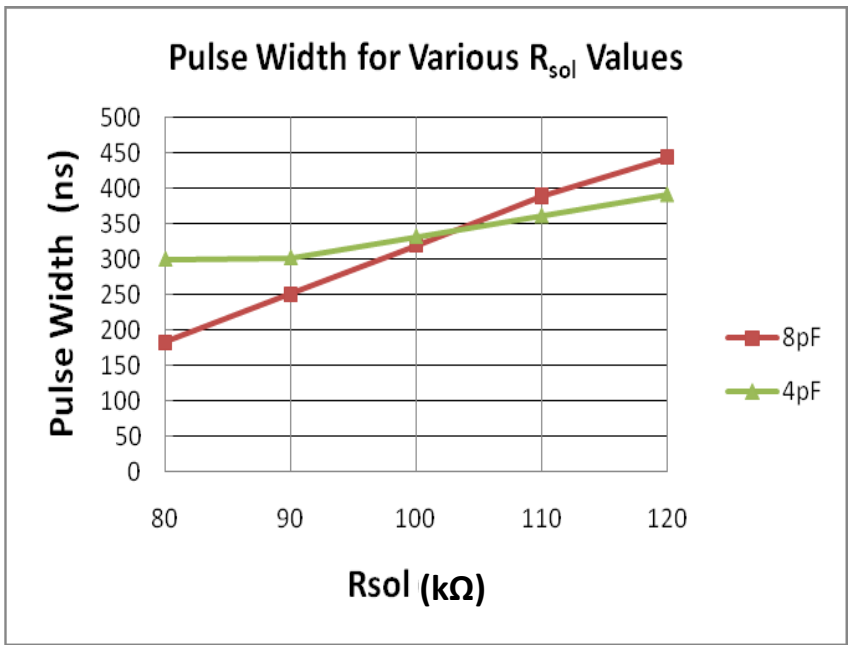

Fig4.16: Width of pulse for various R_{sol} values

In a typical simulation, the size of a pair of microelectrodes is defined as 10µm x 8µm x 2µm (L x H x W) with a 10µm square microchannel in between. C_{ox} is assumed to be 8pF (estimated based on the material's properties and geometry of the electrodes) and the charging and discharging time are set as 500ns with input current of 1.25 µA. Fig 4.16 indicates the linear relationship between R_{sol} and the pulse width. To characterize the impact of possible process

variations, we performed a set of simulations with the C_{ox} value halved to 4pF. As a result, the variation of the pulse width with R_{sol} decreased. In general, as the value of C_{ox} increases, the slope of the voltage generated at the input of the inverters is smaller. A longer time is then needed to reach the threshold of the inverters in the proposed microelectronic circuit.

The circuit simulation results given in Fig 4.17 also confirm the expected linear relationship described by equation (3.3) in Fig 3.6, which is referred to in the figure as the "Internal Analog Signal" (node 3 in Fig 4.15) as well as the pulse wave generated at the output of the sensing circuit. The controlling signal is also illustrated and shows when the circuit is in the charging or the discharging mode. Note that there is a small spike at 6 µs in the voltage of the internal analog signal caused by the S1 switch. However, its effect on the output is negligible. Moreover, the acquisition and analysis of the data from each output is done in such a manner that the circuit becomes self-referenced.

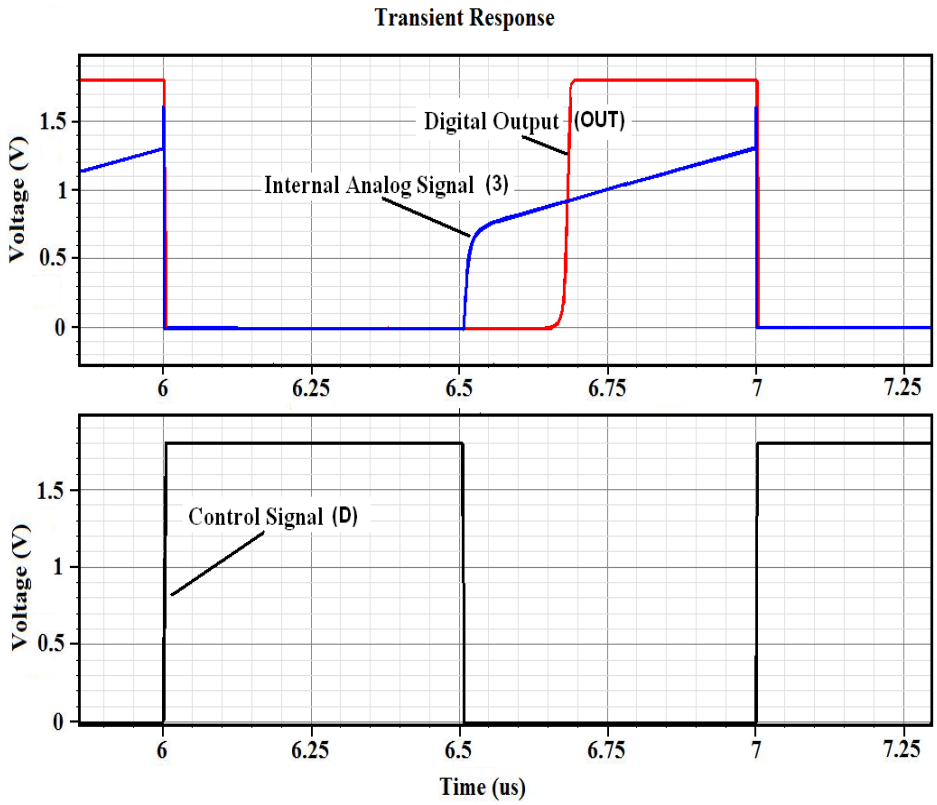

Fig.4.17: Simulation results of delay time according to the impedance variations between the microelectrodes

The circuit proposed was designed in a manner which makes it flexible in multiple ways. Firstly, one can control the amplitude of the injected current according to the values of the impedance to measure. It is then possible to vary the charging and discharging time for the capacitors C_{ox}. Note that the same circuit can be used for a wide range of C_{ox} and R_{sol}, making the circuit robust against inaccurate knowledge of the device parameters and variations of these values. Thirdly, the threshold of the inverters can also be adjusted to change the integration time (at node 3 in Fig.4.15).

4.5.2 Design and layout of microelectrode array

The fabrication of the CMOS chip was done through the services of CMC Microsystems [152] and MOSIS [153]. TSMC 0.18µm CMOS technology was employed to implement the system. The CMOS chip has a total area of around 2800µm x 2000µm (L x W). The area of the microelectrode array is 1000µm x 1200µm (L x W). This experimental system was designed to prove concepts, despite a great deal of uncertainty, as the first prototype was designed with the idea that it must adapt to multiple applications. Thus, different sizes of microelectrodes were implemented. Specifically, 5µm x 5µm, 6µm x 6µm, 8µm x 8µm, 10µm x 10µm, 12µm x 12µm, 16µm x 16µm and 20µm x 20µm (microelectrode length x microchannel width) were chosen for this design. This would be essential for evaluating the performance of the circuit and to aid in the selection of the optimal parameters for a variety of applications.

According to the design rules of TSMC 0.18µm technology, in a typical design, 10µm x 2µm (L x W) stacked metal rectangles are separated by 10µm. In order to minimize the potential cross-talk among pairs of microelectrodes, the distance between the microelectrode pairs is kept at 100µm in our first prototype. A total of 120 microelectrode pairs are implemented on the prototype. The microelectrode array is located at the center of the CMOS chip while the sensing circuits are in to the surrounding area. Only Metal 1 and Metal 2 are adopted as interconnection layers between the microelectrodes and the sensing circuits, and Metal 6 is used to cover all the sensing circuit area.

Those two arrangements are to take full advantage of the CMOS process itself, in order to provide protection for the microelectronic circuit during the subsequent post-CMOS processing

and to simplify the required post-processing procedure. In order to increase the robustness of the system, four independent sensing circuits are implemented on both sides of the central microelectrode array with isolated I/O ports. Each sensing module is responsible for 30 microelectrode pairs. The integrated multiplexers allow accessing the output of each pair of microelectrodes one at a time. The redundancy of the sensing circuits increases the reliability of the system and provides multi-functional capabilities for the system. Moreover, experimental data, obtained from microelectrodes with the same size in each module, can be used to calibrate the accuracy, repeatability and reliability of the system. Eight pairs of microelectrodes are also connected to the pads directly. Desk-top instruments, such as the impedance analyzer, can be connected to measure the impedance variations and then a comparison can be made with the results obtained from the on-chip circuits. This feature is very useful to validate, calibrate and evaluate the sensing circuits. The layout of the whole system is depicted in Fig 4.18 (a). The scheme of the microelectrode array is illustrated in Fig 4.18 (b).

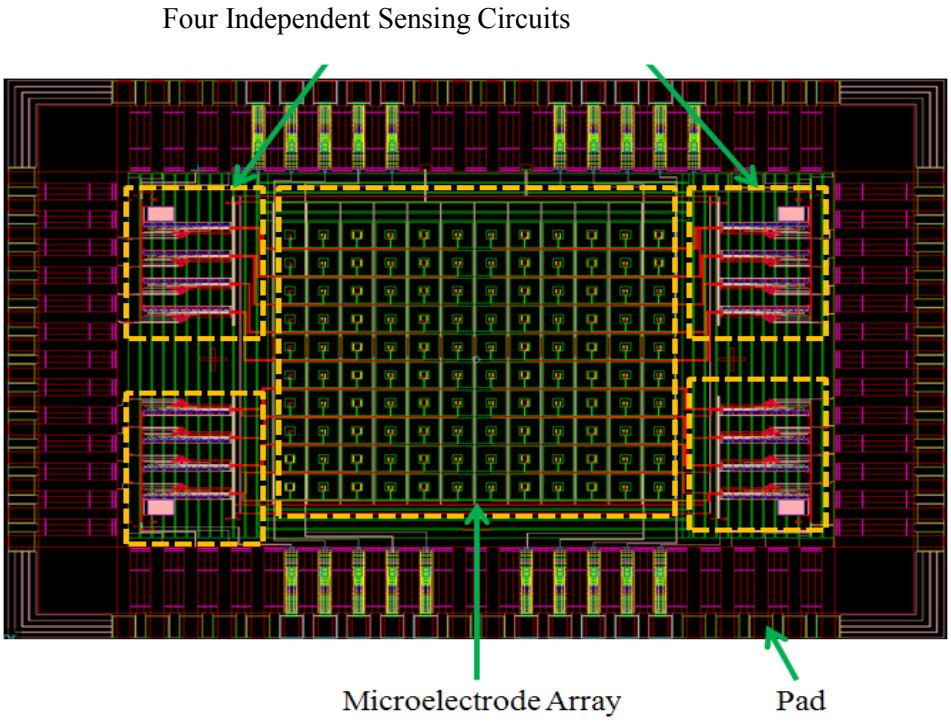

(a)

Fig4.18: (a) Layout of the microelectrode and sensing circuit

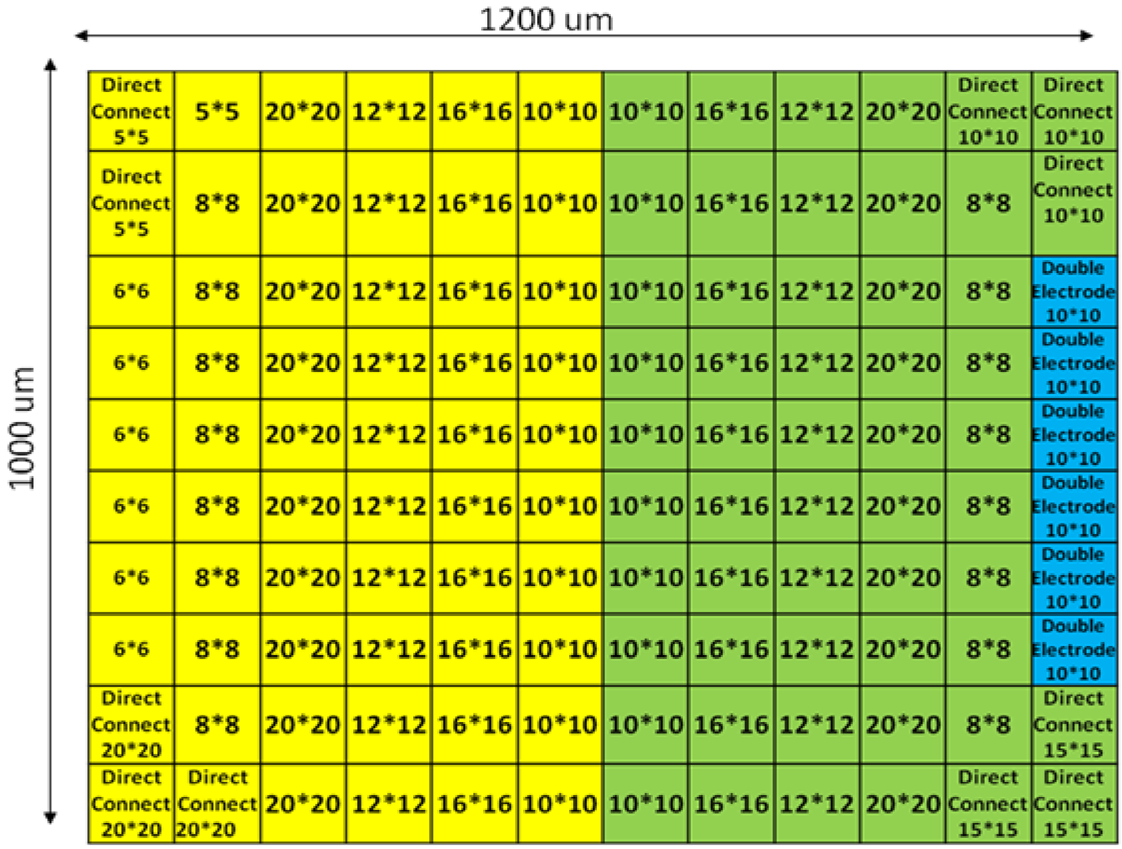

(b)

Fig4.18: (b) the size of each pair of microelectrodes on the chip.

4.6 Conclusion

In this chapter, by establishing the physical model and FEM based simulation, parameters for the proposed Lab-on-Chip microsystem were defined. The simulation results indicate that face to face microelectrodes offer better sensitivity, more than 30%, compared with planar microelectrodes. Other important parameters, such as sensing volume, relative position of the targeted bacterium between a pair of microelectrode, size of microelectrode, and size of bacterium were also investigated through FEM simulations and comparisons. Adopting MTB as bio-carrier for transporting targeted bacteria through functional microbeads was also simulated. A microfluidic chip with in-channel planar microelectrode pairs was developed to validate the simulation results, the performance of planar microelectrode and the controllability of MTB as

bio-carrier. The detailed design and layout of a proposed CMOS based hybrid Lab-on-Chip microsystem was presented. A novel sensing circuitry was developed to prove that single bacterium detection can be realized. As a proof of concept system, various sizes of microelectrodes were implemented on the CMOS chip. The purpose was to evaluate the performance of the sensing circuit and to provide optimal parameters for a variety of applications.

CHAPTER 5 MICROFABRICATION AND CMOS POST-PROCESSING

5.1 Introduction

The main purpose of the CMOS post-processing used in this research is to release the microelectrodes and construct substrate microchannels through the fabricated CMOS die needed to implement the system of Fig 4.18 (a) That post-processing procedure includes two steps, first to remove the silicon oxide between a pair of microelectrodes; Second, to etch through the silicon substrate to form a through substrate microchannel. Indeed, the different materials involved imply different post processing procedures and steps.

Generally, according to the technologies adopted, conventional CMOS post-processing procedures can be classified as either wet etching or dry etching. In a typical wet etching process, the CMOS die is immersed in a solvent to remove some selected material, in most cases, silicon or silicon oxide. Generally, an additional protection layer, for instance, photoresist, is required to cover circuitry and pads on the CMOS die, to avoid damage or contamination. The advantage of the wet etching process is that etching depth can be very well controlled by checking the results regularly, and the uniformity of the etching results can be also be very good. This method is utilized widely in surface micromachining when patterning planar microelectrodes on top of CMOS dies [154~156]. Compared with wet etching, dry etching uses gas instead of liquid to expose the target material to etchant. Usually, plasma of reactive gases, such as fluorocarbons, oxygen, or chlorine, bombards the surface of the target material to accelerate the chemical reaction [157]. The dry etching process typically etches directionally. This directional process is also called anisotropic etching. Thus, it is more suitable for etching high aspect ratio structures, and the dry etching process can be easily controlled in an automatic manner. The most frequently used dry etching processes are reactive ion etching (RIE), deep reactive ion etching (DRIE) and focused ion beam (FIB) etching.

Wet etching is a rather inexpensive processing method. Currently, only two silicon etchants are CMOS compatible (no alkali ions), which are TMAH (tetramethylammonium hydroxide)[158] and EDP (ethylene diamine pyrochatechol)[159].However, both of them are anisotropic etchants, which means that they etch much faster along a specific crystal orientation (100) than the other

crystal orientation (111). As shown in Fig 5.1, pyramidal profiles are formed. As we know, CMOS circuits have traditionally been fabricated on (100) silicon substrates due to its higher electron mobility and reduced interface trap density [160] when compared to other orientations. If the opened windows on the silicon substrate are very small (the smallest feature is 5 µm in our case), through substrate microchannels cannot be etched through without aggressively thinning the wafer. Therefore, the wet etching method cannot be used in this research. Dry etching becomes the only available technology to release the electrode array and etch through the silicon substrate.

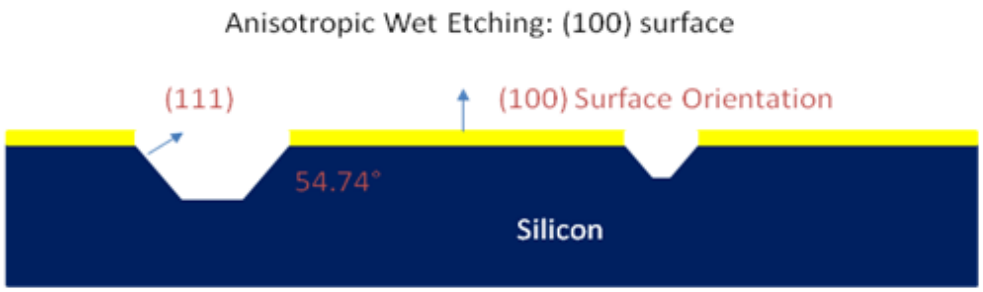

Fig 5.1: Illustration of anisotropic etchant on silicon substrate, adapted from [161]

As described in Chapter 4, in our design, various sizes of through substrate microchannels, from 5 µm to 20 µmwith square crosssection, are implemented on the CMOS die. The measured thickness of the CMOS substrate is approximately 325 µm. To etch through the CMOS die, the maximum required aspect ratio will be at least 65 considering a 5 µm square cross section. Considering the required aspect ratio, DRIE and FIB are the most suitable technologies for this task. Recall that there are two kinds of materials that need to be removed between a pair of microelectrode, silicon oxide first and then the silicon substrate. With DRIE, the gases used to etch those two materials are different. Generally, in order to avoid contamination in the high vacuum chamber, two different DRIE chambers are required to do the job. Meanwhile, a protection layer must be very well patterned and aligned with the opened windows on the CMOS chip. As an alternative choice, FIB is a direct milling maskless process that is very suitable for rapid prototyping.

In this chapter, the CMOS fabrication technology used in this research is introduced first, followed by a comparison of the advantages and disadvantages of DRIE and FIB processes. DRIE, as the process of choice for high aspect ratio structure, is widely adopted in surface and bulk micromachining on silicon, and it is becoming the mainstream technology to construct through silicon vias (TSVs) for 3D IC technologies. However, Constrained by the accessibility of the specific DRIE equipment, FIB is firstly used as rapid prototyping to evaluate the feasibility of the proposed structure and to minimize the fabrication steps and cost. In this research, due to some practical issues, the capabilities of DRIE on silicon dioxide and silicon etching was also evaluated but could not be fully investigated. The fabrication challenges we met and the solutions we have tried are summarized in the rest of this chapter. Some preliminary experimental results are also presented.

5.2CMOS fabrication process

The detailed steps used in a CMOS fabrication process can be found in many textbooks [162~164] and will not be discussed here. It should be emphasized that the CMOS process does not normally allow any kind of cavity in a chip. Silicon dioxide is generally used to fill all the space between the Metal and Via layers. Meanwhile, except for the pad area, the top surface of CMOS chips is conformably covered by passivation layers to protect the chip from dust, chemical erosion and moisture [164]. However, in order to pattern metal pads on the chip, windows, also called pad windows [165], are allowed on the passivation layer shown in Fig 5.2 (a). Pad windows are put in the places where the microchannels will be etched between pairs of microelectrodes.

In the proposed procedure, the passivation layer is removed to leave the silicon dioxide exposed for subsequent etching processes. The same method is used to make three alignment crossing marks for future processing, in case a photomask needs to be aligned in a standard photolithograph procedure. A pair of microelectrodes in an opened window on a CMOS die is shown in Fig 5.2(b).

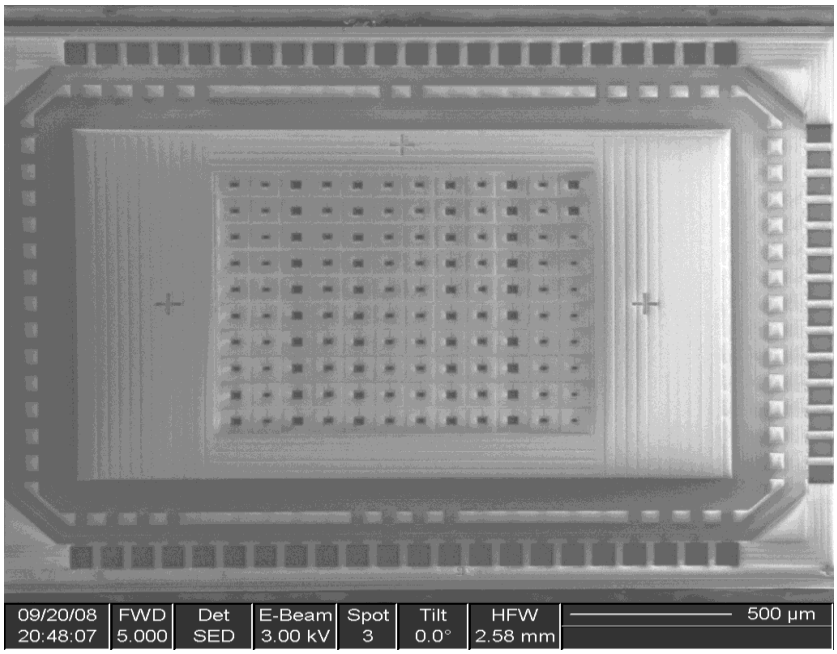

(a) A SEM Micrograph of the CMOS chip

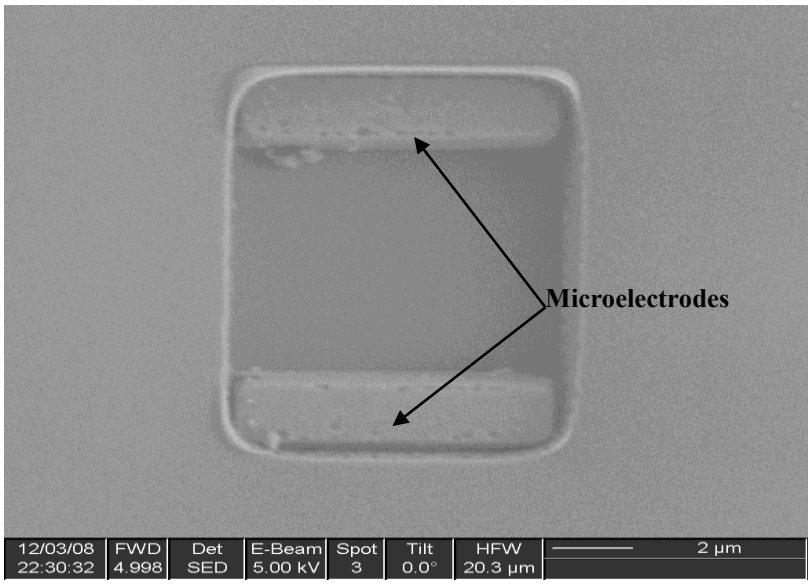

(b) A SEM micrograph a pair of microelectrode

Fig 5.2: SEM micrograph of a fabricated CMOS chip (a) and a close up view of one pair of microelectrodes (b)

Before post-processing, the geometry of the CMOS chip is verified by measuring some of its key dimensions, especially the thickness of the die with an optical microscope and a scanning

electron microscope (SEM). These measurements led us to observing two important differences as compared to the dimensions that were expected based on information provided by the foundry. Firstly, unlike the published data, as shown in Fig 5.3, the measured thickness of the die is 325µm +/- 10µm, much thicker than the expected 250µm. Secondly, in our design, the opened windows on the passivation layers should cover both microelectrodes and only leave the silicon oxide area in between. However, as shown in Fig 5.4, there is no passivation layer on the surface of the microelectrode. These two unexpected defects make the subsequent post-processing significantly more challenging.

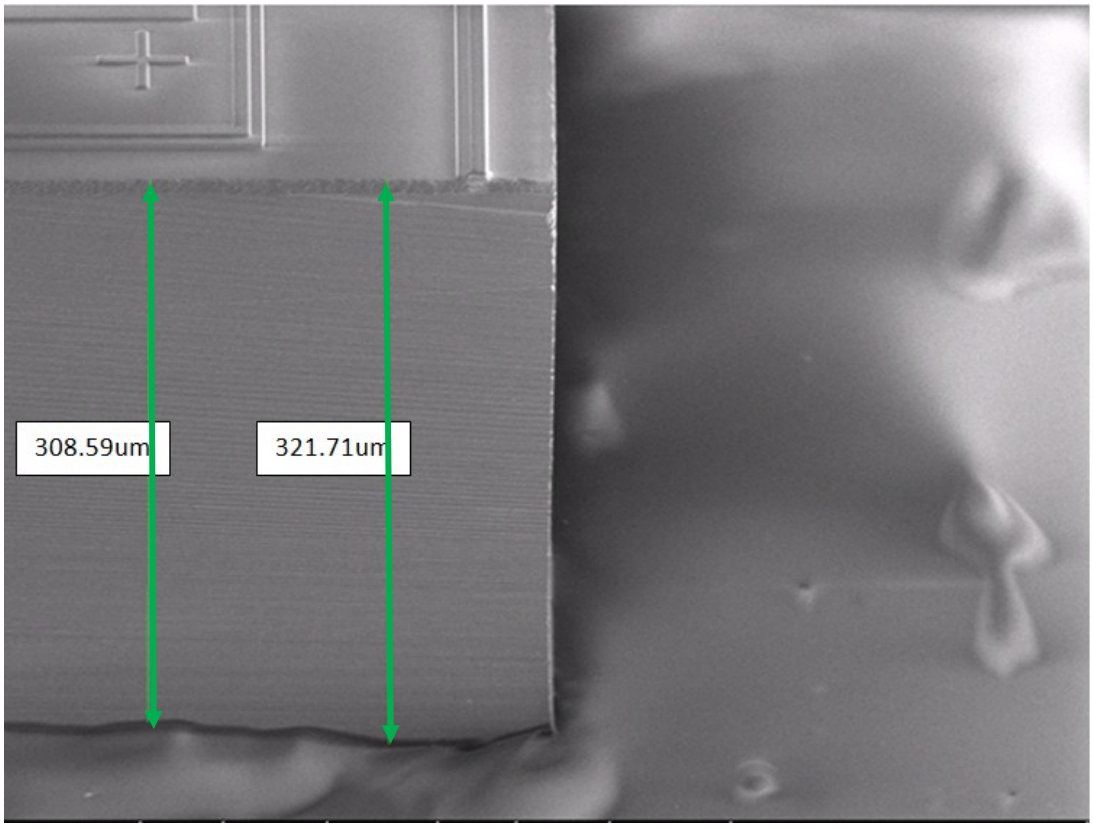

Fig 5.3: Side view of the fabricated CMOS die and its thickness measured using a SEM

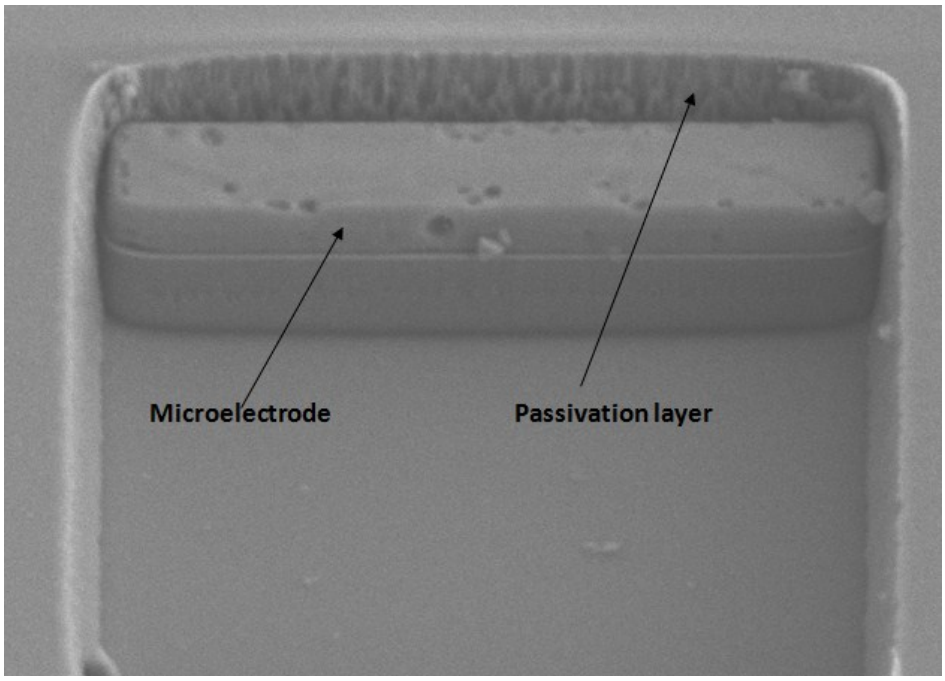

Fig 5.4: Microelectrode without passivation layer

5.3 Focused ion beam milling

As a one-step maskless process, FIB can mill directly on the CMOS chip with very high aspect ratio. The FIB used (xP DualBeam, FEI, USA) can achieve a 7nm diameter beam size [166]. By changing dwell time, adjusting beam aperture size and controlling the actual beam current and ion spot size, different milling results can be obtained. The FIB technique is widely used for TEM sample preparation and microelectronic circuit micro-surgery [167, 168].

5.3.1 Introduction of FIB system

The working principle of the FIB technology was introduced in Appendix 1. Here we introduced the features of a FIB system used in this research.

The FIB system used in this research is a dual-beam system from FEI (xP Dualbeam, FEI, USA). Shown in Fig 5.5 (a), this system has two guns; one generates a FIB and the other one makes the system behave as a SEM. The relative position of both columns is presented in Fig 5.5(b).

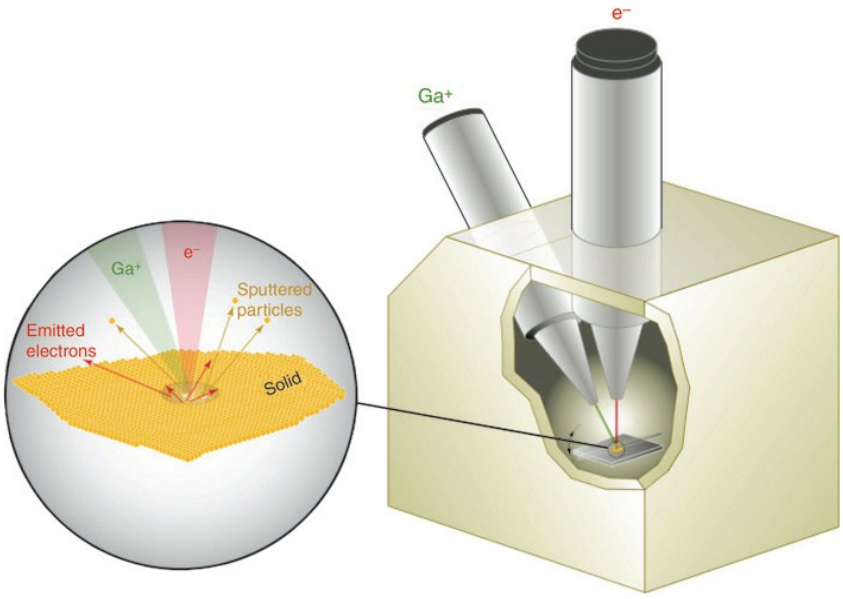

(a)

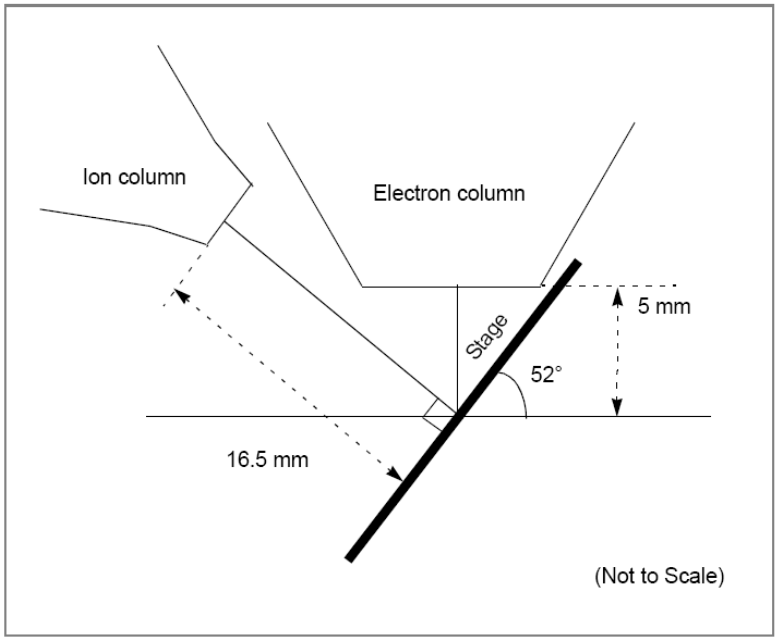

(b)

Fig 5.5: Illustration of the FEI FIB system used in this research. The system includes two guns, shown in (a). Ion gun for FIB and electron gun for SEM. Relative position of two guns is illustrated in (b) [169]

DualBeam systems provide an expanded range of capabilities not possible with separate FIB and SEM tools. For instance, they offer:

a) Real-time cross section images with the electron beam during FIB milling;

b) Focused electron beam charge neutralization during FIB milling;

c) Focused ion beam charge neutralization during SEM imaging;

d) High resolution elemental microanalysis of defect cross sections;

e) Image sample surface with the electron beam during navigation without erosion or gallium implantation from the ion beam;

f) TEM sample preparation with *in situ* conductive coating.

This system also offers choices of Gas Injection System (GIS): when a gas is introduced near the surface of the sample during milling, the sputtering yield can increase depending on the chemistry of interactions between the gas and the sample. This results in less re-deposition and more efficient milling.

This apparatus uses focused Ga+ ion beam with energy of 5-50keV, and a probe current of 1pA - 20nA. For the smallest beam current, the ion beam can be focused down to 7nm in diameter. By changing dwelling time, beam current and spot size, different drilling results can be obtained.

5.3.2 CMOS post-processing by FIB

Since no cavity is allowed in a standard CMOS fabrication process, silicon oxide is filled between a pair of microelectrodes in the fabricated CMOS dies. In order to construct a through substrate microchannel, the silicon dioxide is removed first, followed by milling through the silicon substrate underneath. In this research, no additional mask is patterned on top of the microelectrode array to protect the surface from the post processing; thus, the ion beam should be precisely and constantly aligned with the defined drilling windows between the microelectrodes to avoid damage on the wall of microelectrodes during the milling procedure. However, due to the nature of FIB working principle, two effects have significant impact on the milling speed, accuracy and maximum depth.

5.3.2.1 SEM, FIB charging effect

In a SEM or FIB system, electrons or ions emitted are accumulated on the surface of the sample gradually, which induces a local electric field working as a shield on the top of the object, leading to defocusing or shifting of the electron/ion beams. This phenomenon gets worse on the surface of dielectric materials, such as silicon oxide or dielectric polymers. Generally, when observing an object with a dielectric surface, a very thin layer of gold, several nanometers in thickness, is deposited on the surface to increase the conductivity. Through this thin metal layer, electrons or ions reaching the surface flow into the ground through the metal chip holder, thus prevent the build up of electrons or ions. However, this method is not applicable to a CMOS chip, where the top layers not only include the dielectric passivation layers, but also metal pads. Depositing a blanket layer of metal, even very thin, will cause an electrical short between pads. Several approaches to address this problem have been tried in this research.

In our experiment, a CMOS die is mounted on an aluminum sample carrier using a metal adhesive tape. The die should have a good contact with the metal tape and the sample carrier, which is grounded, to alleviate the charge build-up phenomena when adjusting SEM or FIB beam to focus on the CMOS die. The dielectric passivation layers on the top of the die enhance the charging effect, resulting in distortion of SEM and FIB images. As a result, the induced beam shift and image distortion will have a direct effect on FIB milling accuracy. The shift of the FIB beam during the milling procedure can also lead to damage to the microelectrode. Some observations with SEM and FIB drift effect are illustrated in Fig5.6

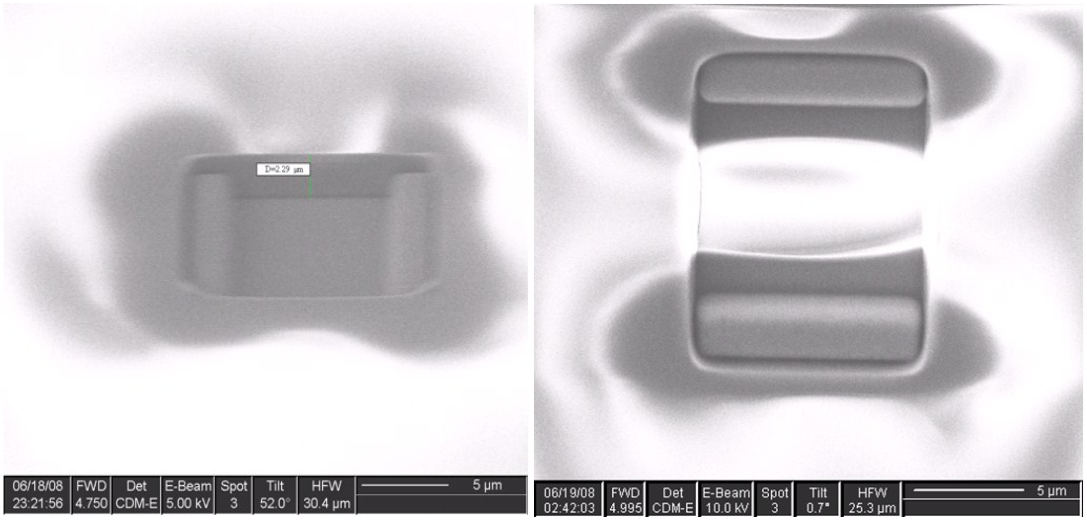

(a)

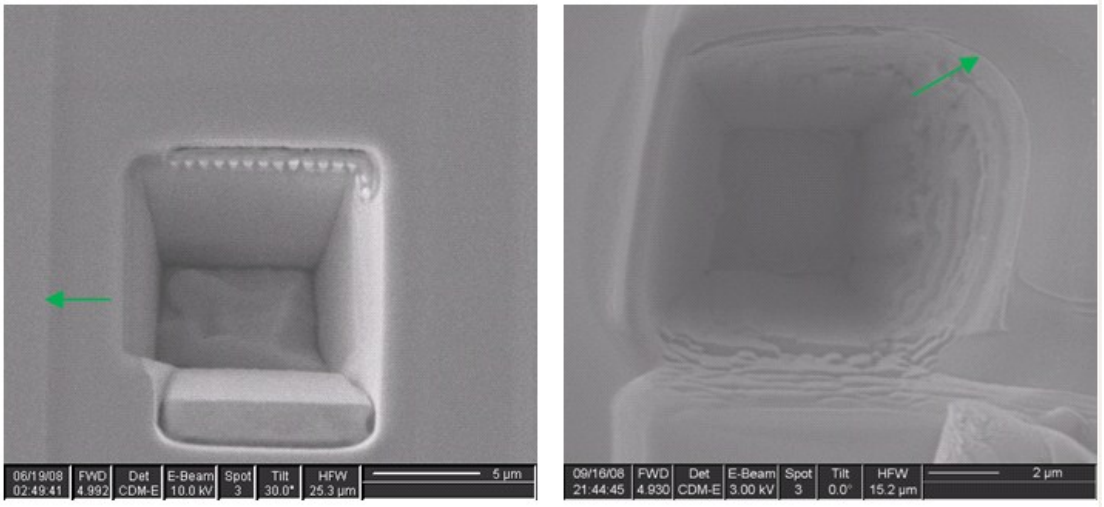

(b)

Fig 5.6: The charging effect on the SEM images and FIB milling process (a) Charging effect observed on an SEM image, (b) FIB beam shift during the milling procedure due to charging effect.

As illustrated in Fig 5.6 (b), the SEM images both show that the microelectrodes are almost totally destroyed due to FIB drift caused by the build-up of ions on the surface. Previous research [170, 171] suggested that decreasing the beam current or reducing the beam energy can alleviate

the shift. However, we found that this method helps only during a short period. When the FIB milling process is extended over more than several minutes, the beam shift still happens.

As discussed before, to deposit a thin layer of metal can increase the electric conductivity of the sample's surface, but it cannot be used on a CMOS chip. We found that using a metal adhesive tape to cover the four corners on the top surface can provide much better contact with the grounded sample holder. This method can improve the overall quality of the SEM image, but does not work with the FIB milling procedure, since the FIB is focused on a relatively small area that is usually far away from the 4 corners. Some ions in the target area do not migrate to the corner, so beam drift still occurs.

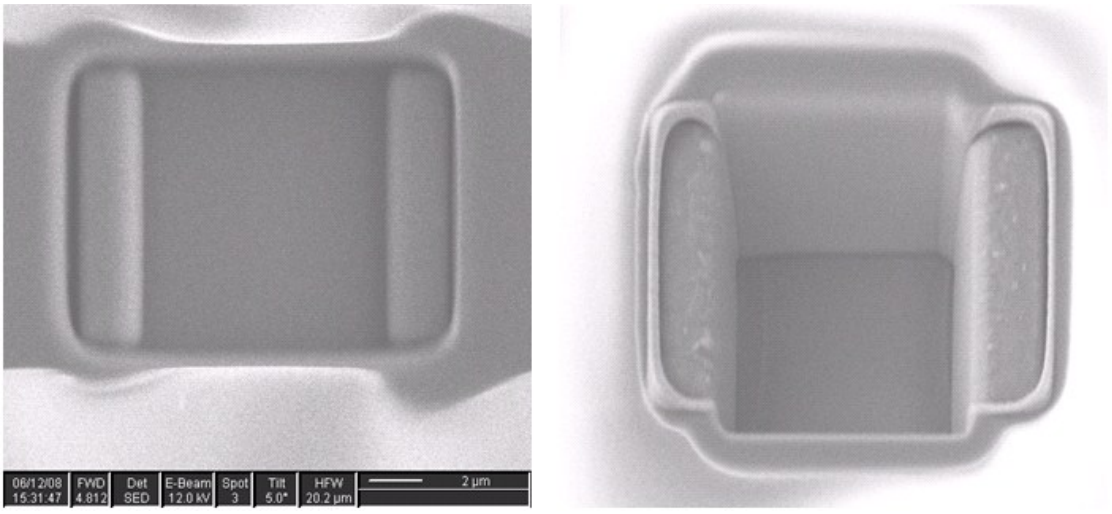

(a) (b)

Fig 5.7: SEM images of improved FIB milling results when applying a charge neutralization procedure

We found that the more effective way to eliminate the charging effect is to neutralize the build-up of electrons/ions periodically during a long time FIB milling session. For instance, when a relatively long observation with SEM is required, in the middle of the observation, a low dose FIB out of focus scan, typically 5 pA beam current and dwelling time of 1 µs, can effectively neutralize built-up electrons caused by SEM. Meanwhile, a low dose SEM out of focus scan during the FIB drilling process is also helpful to neutralize the charge associated with ion

accumulation. The improvement on the SEM image and FIB milling results that were obtained are shown in Fig 5.7.

5.3.2.2 FIB re-deposition

Another significant artefact induced by the FIB milling procedure is the re-deposition phenomena. [172~174].Although most of the sputtered material, in this case silicon or silicon oxide, is rapidly pumped away into the vacuum system, some sputtered atoms may redeposit onto the freshly milled surface of the sample. Gallium is also included in significant concentrations in the material that has been re-deposited, which will change the electrical properties of the electrodes and may cause shorts between two electrodes, thus leading to failure of the detection circuit.

As shown in Fig 5.8, the re-deposition phenomena can be observed clearly on the surface around the entrance of the milled holes. The milling time is 2 hours on the left image and 30 minutes on the right one. The images indicate that a longer milling process tends to produce more re-deposition artefacts surrounding the targeted area.

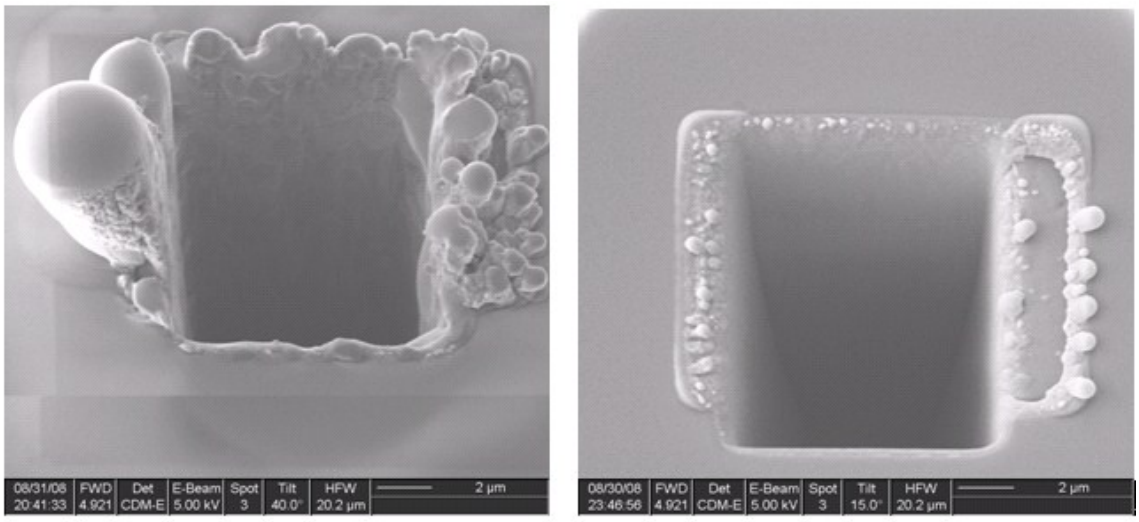

(a) (b)

Fig 5.8: FIB re-deposition effect when drilling deep into the sample

In both images (a, b), we can see that the artefacts not only cover the surface of the electrode, but also get into the milled channel and cover the sidewall of the electrodes. The metal and via layer cannot be discerned from the image. The performance of the microelectrode could be

significantly compromised. An effective way to eliminate the re-deposition needs to be found to protect the microelectrodes.

In this research, initially, we tried several conventional ways to address this problem. As adopted in a previous research [175], we tried to minimize the re-deposition by decreasing beam current and dwelling time. However, lower beam current significantly increased of the milling time in our case. Referred to another study [176], we tried to eliminate the re-deposition problem by performing a final cleaning FIB mill at a reduced accelerating voltage. This approach may help to remove a portion of the damaged layer and reduce the extent of re-deposition. Again due to the deep milling depth required, the method didn't work well in our study.

Eventually, we solved the problem by using the GIS system. By choosing the proper GIS beam chemistry and corresponding material file, the re-deposition effect could be removed totally. In our experiments, we found that when the milling depth is less than 100 μm, the re-deposition is almost totally avoidedby utilizing the GIS. Fig 5.9 shows some results after a long time milling procedure (2 hours and 19 minutes). However, when deeper milling is required, GIS is not completely successful at eliminating the re-deposition problem. The reason is that when the milling process is close to the GIS nozzle, it works effectively to pump out artefacts; when the milling process goes deep into the hole, far from the GIS nozzle, the artefacts cannot be sucked into the GIS nozzle effectively. In our experiments, we found that decreasing dwell time is a more effective way to remove artefacts when the milling process is deep into the channel.

Based on our experimental results, we suggest to use GIS and relatively long dwell time, typically, 10~20 μs when the milling depth is less than 100 μm. When a deeper milling is required, the dwelling time should be shortened, 1 μs was used in this research, while still using the GIS.

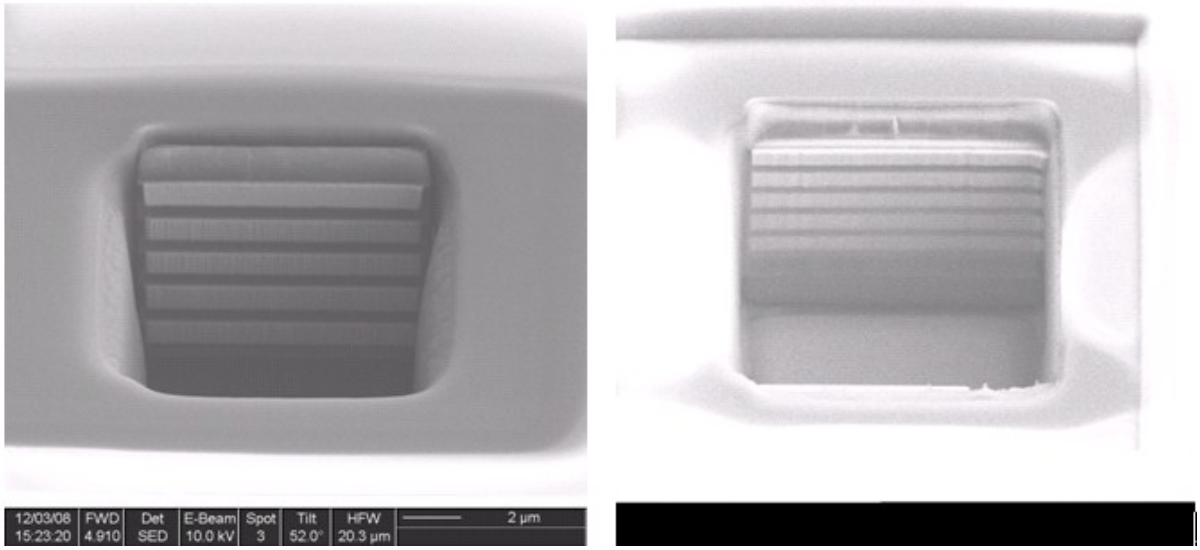

Fig 5.9: The re-deposition effects are almost eliminated after applying the GIS when the drilling depth is less than 100 µm. Electrodes are released without artefacts. Drilling depth is 20µm (left) and 12µm (right) on the SEM Micrographs

5.3.2.3 Maximum milling depth of FIB

FIB is generally used as a tool for Transmission Electron Microscope (TEM) sample preparation, micro-circuit surgery, thin film deposition and nanostructure fabrication. To the best of our knowledge, the achievable maximum milling depth of FIB has not been investigated before. To utilize FIB for constructing through substrate microchannels or vias also has not been reported on. According to the working principle of the FIB, the maximum depth that can be milled depends on several parameters, including ion dose, ion beam current, dwelling time, overlap ratio, milling time and milling area.

In this research, a dummy CMOS die using the same CMOS fabrication technology was used to determine a set of optimized parameters suitable for deep milling. Note that the aim is to mill through a silicon substrate of 325 µm thickness. The experimented parameters are reported in Table 5.2. The first set of experiments is designed to determine the maximum milling depth using maximum beam current supported by the FIB system. The line profile is chosen in order to have maximum beam density per area. The other set of parameters that were experimented are also listed in Table 5.2. The milling depth is checked by SEM after breaking one side of a CMOS chip

manually. In those experiments, a square pattern of 300 µm by 300 µm is etched as deep as possible, as shown in Figure 5.10 (a). The SEM images of the milling results are presented in Fig 5.10 (b, c, d) (using ion beam current of 20 nA). In the second test, a beam current of 7 nA is used. The parameters used for the experiments and the resulting measured milling depths are listed in Table 5.3. Note that using a 7 nA beam current, the expected milling time is significantly increased as compared with the experiment done with a 20 nA beam current. In both tests, the measured depths are much less than the one predicted by the software provided with FIB system. Even when we set the milling depth to 500 µm with the beam current of 20 nA, after 10 hours milling, the measured depth was only 116 µm, far from the expected milling depth. Note that depth is the same as the one that was measured after 3 hours and 46 minutes. Based on these experimental results, even with the maximum beam current offered by the system, milling through the original silicon substrate of 325 µm thickness cannot be achieved as the milled depth saturates to 116 µm. Note that in this set of experiments, the minimum dwelling times (1 µs) is chosen to minimize the re-deposition effect in a deep trench.

Table 5.1: Maximum beam current (20 nA) vs milling depth

Beam Current (nA)	Estimated Milling Time (:hour:minute)	Dwelling Time (µs)	Beam Overlap (%)	Gas Injection	Material File	Expected Milling Depth (µm)	Measured Depth (µm)
20	1:09	1	50	On	Si	100	21.4
20	1:45	1	50	On	Si	150	55.94
20	2:19	1	50	On	Si	200	92.29
20	3:46	1	50	On	Si	325	116.21

Table 5.2: Beam current (7 nA) vs milling depth

Beam Current (nA)	Estimated Milling Time (:hour:minute)	Dwelling Time (µs)	Beam Overlap (%)	Gas Injection	Material File	Expected Milling Depth (µm)	Measured Depth (µm)
7	3:19	1	50	On	Si	100	19.5
7	4:58	1	50	On	Si	150	42.31
7	6:38	1	50	On	Si	200	62.86
7	10:47	1	50	On	Si	325	81.92

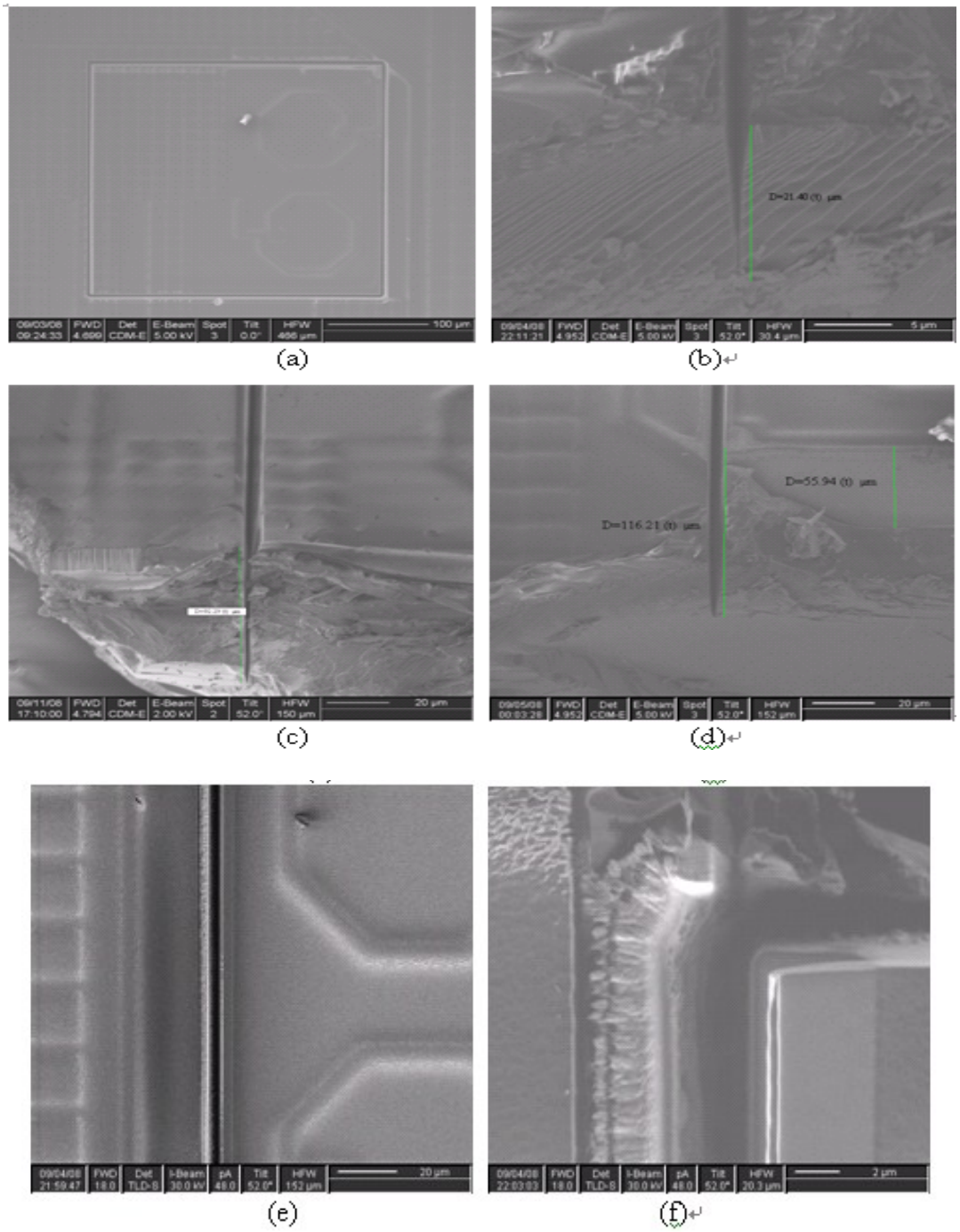

Fig 5.10: SEM images of FIB milling results (a) top view of the drilling area on a CMOS die using same TSMC 0.18µm fabrication technology; (b, c, d) cross section view of the drilling result, V shape trench can be observed; (e, f) close up view of the re-deposited artefacts at the edge of the trench.

From Fig 5.10 (e,f), it seems that the re-deposition is the main reason restricting the FIB beam from milling deeper. The artefacts accumulated on the surface of the milled structure leads to the prevention of the further milling process. Indeed, when the milling procedure is conducted near the surface of CMOS chip, the GIS needle is very close to the milling location, around 30-50 µm above the surface, thus, the re-deposition can be eliminated effectively. However, as the beam mill deeply into the substrate, the GIS cannot reach the milling region. It becomes clear that the sputtered silicon atoms cannot get out the narrow microchannel. They probably collide with the incoming Ga^+ ions, leading to some significant decrease of the Ga^+ ion's energy. It results in a gradually narrowed V-shape trench as shown in Fig 5.10 (b, c, d). The maximum milling depth is always around 120 µm in these experiments.

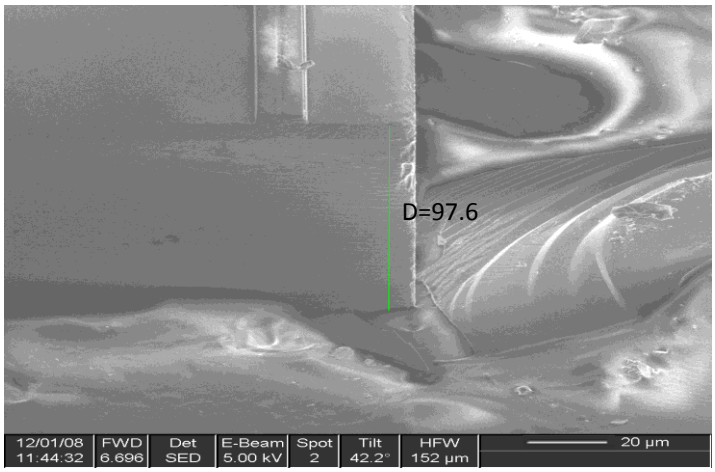

Fig 5.11: SEM micrographs showing the thickness of the CMOS die mounted on a silicon wafer used as a sample holder after a RIE thinning process.

However, based on the results achieved with the dummy CMOS dies, if the substrate thickness can be thinned from the original 325 µm to around 100 µm, there is still a chance to mill microchannels through the substrate using the FIB technology. Without access to chemical mechanical polishing equipment, which is a conventional tool used to thin wafers, RIE technology was used to thin the CMOS substrate to around 100 µm from the backside. The result is shown in Fig 5.11. The detailed RIE procedure will be introduced in the next section.

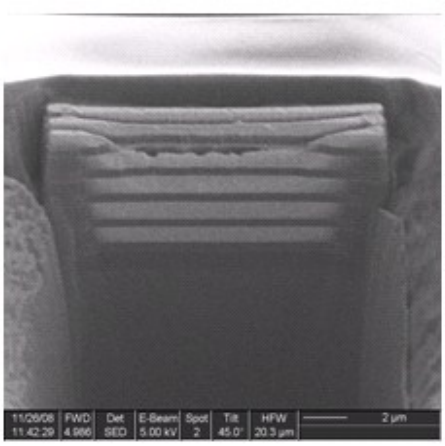

(a)

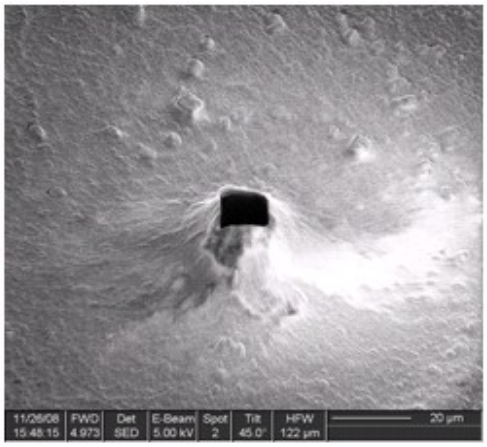

(b)

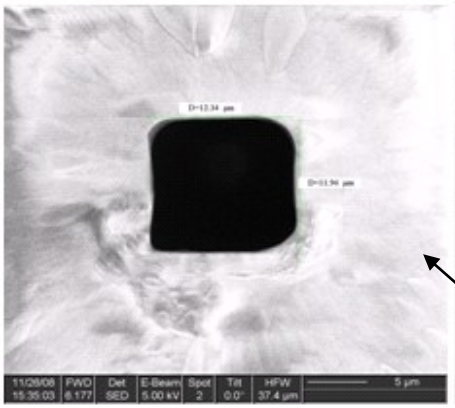

(c)

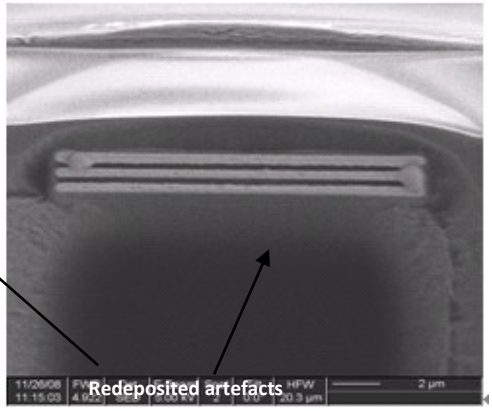

(d)

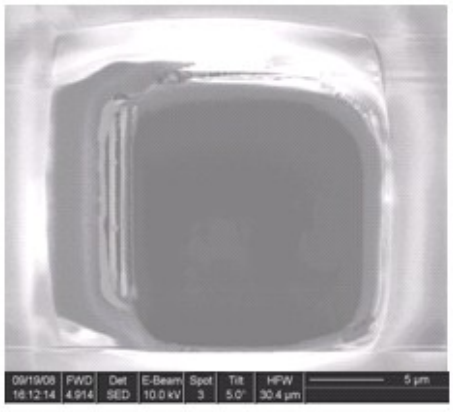

(e)

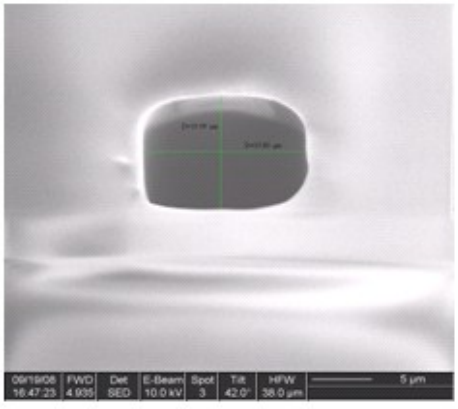

(f)

Fig5.12: SEM micrographs of through substrate microchannels and microelectrodesafter the FIB milling process. (a) A microelectrode is partially damaged during the 3 hours 19 minutes FIB milling process. The size of the microelectrode is 16µm x 8µm x 2µm (Length x Height x Thickness). The cross-section of the microchannel in between two microelectrodesw is a 16µm square. (b) SEM image from the backside of the CMOS die showing the through substrate microchannel. (c) SEM image of the microchannel after polishing from the backside with FIB. (d) Even with the low dose, FIB milling from the backside, the induced re-deposition covers the surface of the microelectrodes. (e) Top view (e) and bottom view (f) of a through substrate microchannel with a cross-section area of 10µm by 10µm. This required more than 4 hours milling procedure and one of the microelectrodes was damaged due to the ion beam shift.

After the wafer thinning process, through substrate micro channels were successfully milled by FIB. This is illustrated in Fig 5.12. This Figure shows that two micro channels of 10 µm by 10 µm, and 16 µm by 16 µm cross section were formed under different conditions.

We found that when the cross section of the microchannel is smaller than 10 µm square, the experimental results show that even the thinned CMOS substrate cannot be milled through without damaging the microelectrodes on the wall. In another typical experiment, after more than 6 hours FIB milling, the FIB cannot penetrate an 80 µm thick CMOS die with an opened window of 5 µm by 5 µm. Meanwhile, for larger microchannels cross section, longer milling time is expected, but through substrate microchannels can be achieved. The experimental results also suggest that three stages using different beam currents should be adopted when a deep milling procedure (more than 100 µm) is required. 1) For removing the silicon dioxide, a small beam current should be utilized to avoid damaging the microelectrodes. While, the milling window should be exactly the same size as the microchannel cross section to fully expose the metal microelectrodes. 2) In the procedure of underneath silicon etching, strong beam current can be adopted to accelerate the milling procedure. However, smaller milling window (1 to 1.5 µm smaller than the actual opened window) should be used to avoid the damage on the released microelectrodes due to the beam shift. 3) Before the ion beam fully penetrates the substrate, smaller beam current should be used, otherwise, the strong ion bombardment may create a hollow

micro needle, as illustrated in Fig 5.12(b). Indeed with a constant beam current of 20 nA, the surrounding area of the micro channel is perturbed out of the surface leading to an uneven backside of the chip. When the beam current is decreased to 6 nA before completely milling through, the hollow microneedle effect is eliminated. The resulting smooth backside is shown in Fig 5.12(f).

So far, the best results we achieved using FIB is with a 10 µm x 10 µm cross section through substrate microchannel. Typically, it takes around 4 hours to get through substrate microchannel on a CMOS chip thinned to 100 µm thick. The amount of time consumed is acceptable for rapid prototyping experiments. However, if a large microelectrode array needs to be released as part of experimental research work; extremely long FIB processing time can be expected. The time and cost are major disadvantages of adopting FIB for this task. Hence, in the next section, as an alternative approach, DRIE technology is introduced.

5.4 Deep reactive ion etching

DRIE is a highly anisotropic etch process used to create deep, steep-sided holes and trenches in wafers, with aspect ratios of 30:1 or more [176]. The system used in this project can achieve aspect ratio up to 30:1 with a silicon wafer [178]. Compared with reactive-ion etching (RIE), DRIE can etch much deeper and faster, up to 600 µm or more with rates of up to 20 µm/min, while practical etch depths for RIE would be limited to around 10 µm at a rate up to 1 µm/min.

In order to achieve high aspect ratio etching with straight sidewall, different technologies are adopted to protect the sidewalls during the etching procedure. Based on the technologies used, DRIE technology is classified as two main processes: Cryogenic and Bosch [177, 178]. More detailed can be found in Appendix 2.

As described in the previous section, silicon dioxide between each pair of microelectrodes should be removed first. However, DRIE of glass (silicon dioxide) requires high plasma power, which makes it difficult to find suitable mask materials for truly deep etching. Polysilicon or nickel is usually used as mask for 10–50 µm etched depths.

The preliminary tests with DRIE were conducted in the cleanroom of University of Sherbrooke. Two DRIE systems were used for two separate etching steps: 1) Advanced Oxide Etch (AOE)

Plasma Etching System for silicon dioxide etching, and 2) Advanced Silicon Etch (ASE) Plasma Etching System for silicon substrate etching.

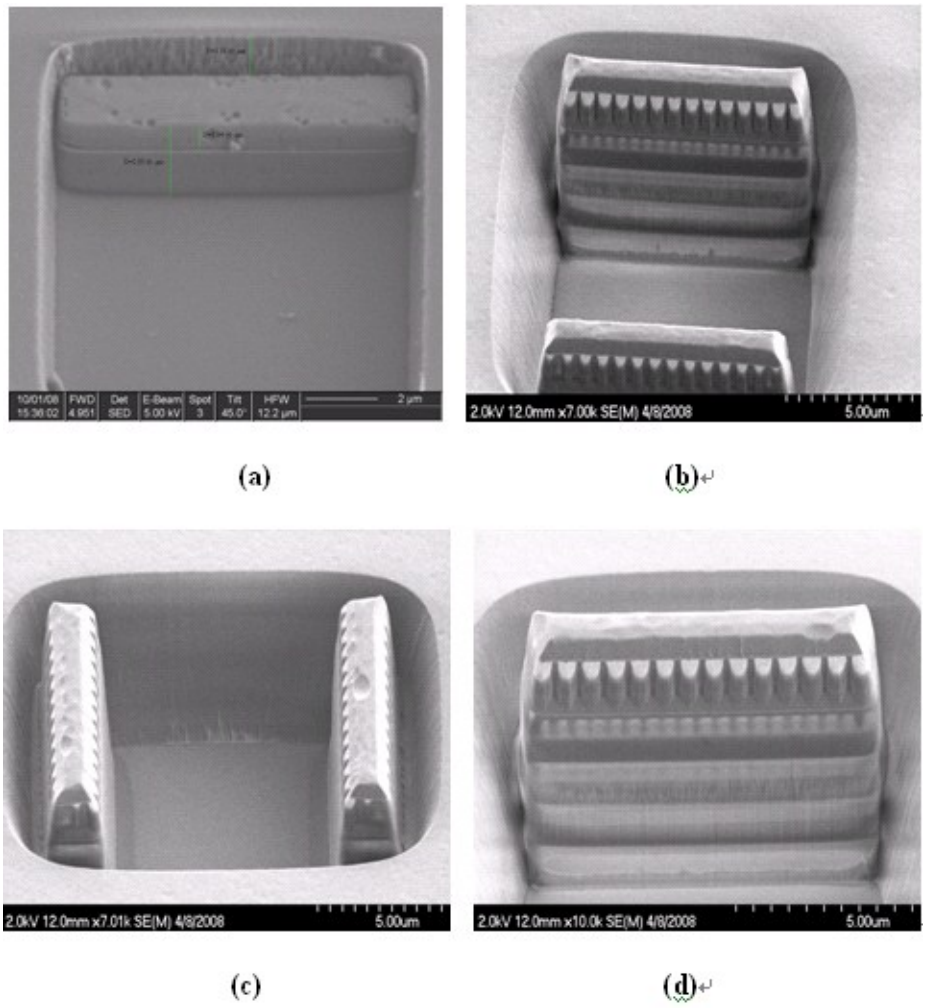

Fig5.13: SEM micrograph of silicon dioxide etching with DRIE without any additional protection layer. (a) Original CMOS die from fabrication foundry (b) After silicon dioxide was etched by AOE, a pair of microelectrodes is released. (c) Notice that the outer side of the microelectrode is also partly etched off. (d) A close-up view of the released microelectrode shows that the top metal layer is partially damaged.

5.4.1 DRIE etching without additional protection layer

Our experiment with DRIE began with silicon dioxide etching. Recall that there are three passivation layers patterned on the top metal layer by the CMOS foundry. The first test is to evaluate the selectivity of DRIE with respect to the passivation layer and the silicon dioxide. If the passivation layer can survive after the silicon dioxide etching process and still remain thick enough to protect the integrated structures during the subsequent silicon etching, a thinner, or even no additional protection layer may be required. The etching results with AOE are given above.

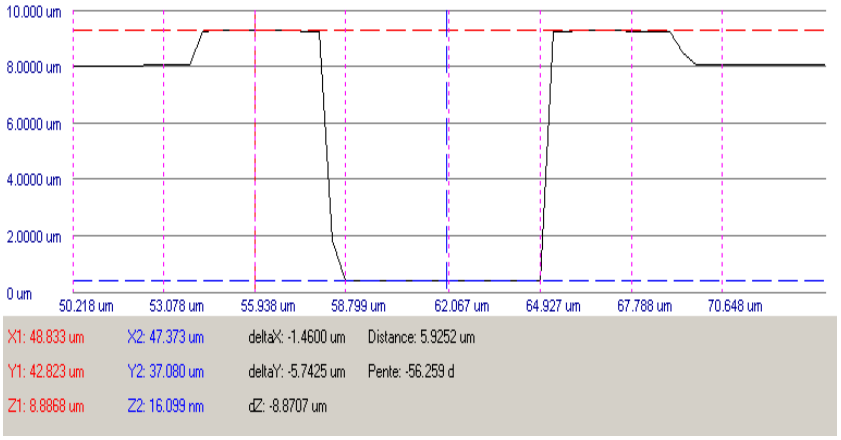

Fig 5.14: Profile of the released microelectrode pair and microchannel in between.

The SEM images in Fig 5.13 combined with the profile measurement, shown as Fig 5.14, indicate that the passivation layer on the CMOS chip is not sufficient to protect the electrodes during the silicon dioxide etching procedure with AOE. The microelectrodes, previously recessed below the surface, as shown in Fig 5.13(a), protrude after the AOE etching step, as illustrated as Fig 5.13(b, c). This observation is confirmed by the surface profile measurement, shown as Fig 5.14. The microelectrode pair is apparently out of the top surface. The profile measurement indicates that 1.2 μm of top surface was removed, which means almost all of the three original passivation layers were etched off. The SEM images also show that even the top metal layer is thinned by the DRIE silicon dioxide etching procedure. Notice that the silicon dioxide layer is only around 8 μm in height, and there is still 325 μm thick silicon underneath that needs to be penetrated. Therefore, an additional protection layer must be patterned on the CMOS chip if

DRIE technology is adopted for CMOS post processing. This extra protection layer should also cover the top of the metal microelectrodes to avoid undercut on the outer side of microelectrodes. The thickness of the protection layer depends on the aspect ratio, etching depth and selectivity [179, 180]

5.4.2 DRIE etching with photoresist based protection layer

A dedicated optical mask was fabricated first, which is designed to expose the microchannel area only. There are several issues that have to be considered:

To coat a uniform layer of photoresist is crucial for the following photolithograph steps. However, the size of the CMOS die is very small. It is very difficult to coat the die with a uniform photoresist layer. Generally, the photoresist on the edge of the die is thicker than the center of the die, induced by the surface tension of the liquid photoresist on the edge of the die or wafer, so called edge-bead effect [181]. Moreover, the surface of the fabricated CMOS chip is not flat, especially with the pad windows opened between pairs of microelectrodes. These issues can lead to the uneven spread of the photoresist on the surface of the CMOS chip if a standard spin-coating process is used.

A thick photoresist layer is required to protect the chip while through wafer channels are etched. Precise alignment with the optical mask and suitable dose of UV exposure are essential for patterning windows on the photoresist layer. A major problem encountered is the reflection of the top metal layer, which was supposed to be covered by the passivation layers. The induced light scattering makes alignment with optical mask very difficult. Determining the proper UV exposure dose is also difficult because of the uneven thickness of the photoresist layer on the top of the CMOS die.

A conventional spin-coating process was used first. Different AZ thick photoresist [182] were tested. Based on the selectivity of DRIE etching on silicon dioxide, silicon and photoresist, a photoresist layer thickness of around 10 μm was selected. However, due to the small size of the CMOS die, a photoresist layer with uniform thickness could not be obtained. Misalignment and lack of uniformity of exposed and developed photoresist are the two major issues that lead to failure of our attempts to pattern the AZ thick photoresist.

An alternative approach is to use a dry film photoresist (DFP) [183], which is a kind of thin UV sensitive dry film. The thickness of commercially available DFP films can be controlled very well thus very uniform films can be obtained.

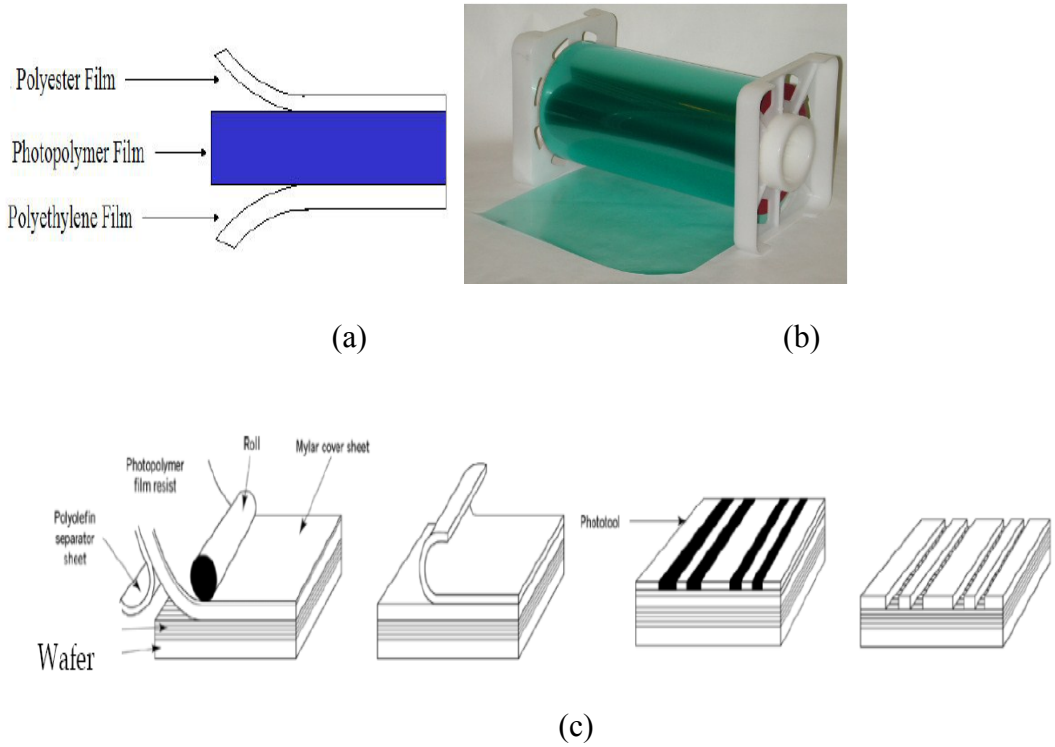

Fig 5.15: (a) Dry film structure,(b) a roll of dry film(c) dry film lamination procedure [185]

Generally, a typical DFP is a three-layer structure, as illustrated in Fig 5.15 (a). It typically includes a polyester support base membrane, a photoresist layer, and a polyethylene layer on the top. Typically, DFP is wound up as a roll that is several hundred meters long (Fig 5.15 (b)). The polyethylene is needed to prevent the photoresist from sticking to the polyester of the preceding lap during roll formation. Dry photoresist is applied on the samples using a dry lamination process. A typical lamination process is depicted as Fig 5.15(c). Firstly, the sample is fixed on a glass or silicon wafer, then fed into a laminator previously cleaned very well, where photoresist is evenly rolled across the surface of the wafer with a controlled pressure and temperature. During the lamination procedure, the polyethylene is first removed while the photoresist remains on the polyester support. After the lamination procedure, the polyester has to be peeled off for the

following exposure and development steps. The main objective of the lamination process is to create smooth and close contact between the wafer surface and the photoresist film [184].

A MX 5015 DFP (DuPont Electronic Technologies, USA) was used for the purpose of patterning a protection layer on the top of the CMOS die. This type of film is a negative tone, aqueous processable photoresist available in a three-layer composite format. The photopolymer emulsion, 15 µm in thickness, is protected by two other layers. The top layer is an extra clear polyester film with a thickness of 18.5 µm. The bottom layer, or base, is a low-density polyethylene film.

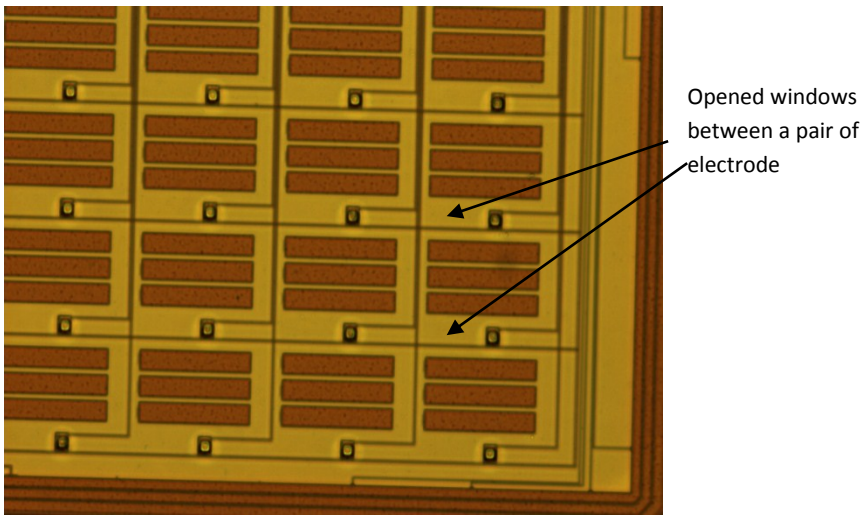

Fig 5.16: Microscopy image of a CMOS die covered with a dry film photoresist, after a photolithography process, opened windows between microelectrodes can be observed in the image

The lamination procedure was developed. A standard 4-inch (100 mm) single-side polished Si wafer was cleaned with the standard cleaning procedure with RCA1 and RCA2. After the cleaning step, the wafer surface was free from dust particles and other contaminants. The CMOS die was put in the middle of the silicon wafer. Then, the wafer carrying the CMOS die was brought into the laminator, with the photoresist facing the CMOS die. Conformation was achieved by hot roller and suitable pressure. After that, the wafer was subjected to a post-

lamination bake to enhance film adhesion on extra smooth surfaces. Before the UV exposure procedure, the top polyester sheet was first removed without tearing the photoresist out of the CMOS die. A chromium photomask was used to form patterns on dry film. After the post-exposure and development procedure, the CMOS die covered with the photoresist protection layer is air dried and ready for test. The result is shown as Fig 5.16. The opened windows between a pair of microelectrodes can be observed.

The measured thickness of the patterned photoresist is around 18 μm, which is enough to survive during the following DRIE SiO2 and Silicon etching steps. Next, the AOE machine is used for silicon dioxide etching. However, after an extensive long etching time, more than 4 hours, we found that the silicon oxide between pairs of microelectrodes was not being fully removed.

The first hypothesis is that the photoresist is not very well developed, thus a residue of photoresist is stacked on top of the silicon dioxide. Several methods were tried to obtain a complete development of the photoresist, for example, changing the exposure time, tuning the baking time, developing time and temperature. Oxygen plasma was also used to thin the entire photoresist layer by several micrometers in order to get rid of the undeveloped photoresist in the opened windows after the photolithography process. However, the silicon oxide still could not be etched off successfully by the AOE equipment.

Another hypothesis explaining this phenomenon is the refraction of the exposed metal microelectrodes. Refraction shifts the UV light away from the dark field. The reflection at the surface of metal microelectrodes and the diffraction at the edge of dark field lines of the mask make significant differences in the channels widths and taper angle [185].This may lead to some residue of photoresist left after development.

Another possible reason is the presence of the air gap between the photoresist and silicon dioxide, which can also contribute to the UV light refraction causing the increased path length and change of light propagation direction. Cross-sectional analysis may provide more details about the contour of the photoresist layer before and after the lithography procedure, however, it was very difficult to acquire clear optical images of the sidewalls because the dry film peeled off from the silicon surface during cleavage and cross sectioning of the CMOS die.

After more than 4 months extensive research, we could not find a right solution to release the microelectrode pairs on the CMOS die by using DRIE process. Due to the limited time and budget, this job is left to future investigation.

Although the expected results were not achieved with the DRIE process, compared with the FIB technology, we still believe that DRIE is more suitable for constructing arrays of through substrate channels. The main reason is that DRIE can process through substrate channels on the same die of wafer simultaneously. The etching results are more uniform and predictable than FIB which has to be adjusted each time when changing the drilling position. Compared with FIB, DRIE doesnot introduce re-deposited material or the artefacts can be easily removed, which make it more compatible with microelectronic circuits when used to achieve high aspect ratio through silicon via. Hence, more efforts were needed to develop a practical recipe for etching arrays of channels with DRIE.

5.5 Packaging

A specific package was developed in this research to offer a user friendly interface (Input/Output) for the proposed system. The interfaces include two parts: a) Electrical interface for inputs, outputs, control signals; b) Fluidic interface for sample injection and waste collection. As introduced in chapter 4, the liquid sample, potentially containing target pathogen or bacteria, is supposed to be injected onto the chip and flow through the microchannel array. Hence, the on-chip electrical circuit, including pads, bonding wires should be isolated from the liquid sample. In the meantime, the material used in the proposed system should be biocompatible to avoid any interference with the target bacteria or pathogens. On the other hand, in order to protect the microelectrode array from chemical corrosion induced by the injected sample, a protection layer should be coated onto the surface of the microelectrodes.

In our system, Parylene C [186] is coated on microelectrodes as a passivation layer for isolating the liquid medium from contacting the microelectrodes. As described in Chapter 3 and 4, a thin layer of Parylene also plays a very important role to form a coupling capacitor for measuring the impedance change between a pair of electrodes. Parylene is a very popular dielectric material widely adopted in PCB fabrication. Not only has it a good dielectric property, it is also a biocompatible material [187]. Our experiments proved that the 2.5nm to 3nm is thick enough to

serve as a dielectric layer for the isolation of bonding wire and pads. In this research, 4nm of Parylene C is coated to provide protection to microelectrode and function as a capacitor in the sensing circuitry.

The detailed packaging steps are described in Section 3.5. The packaged Lab-on-Chip microsystem is shown as Fig 5.17.

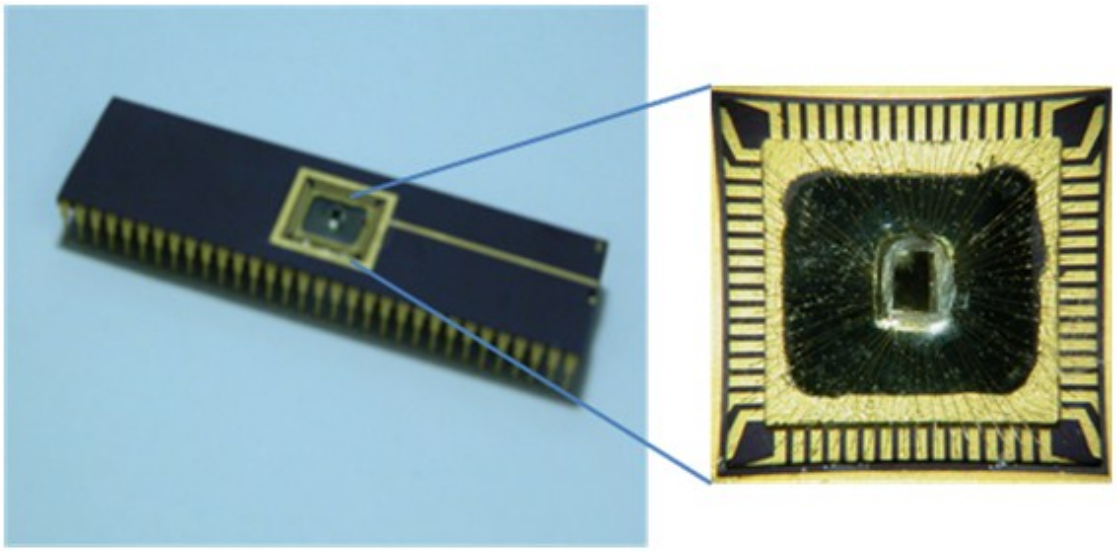

Fig 5.17: The packaged Lab-on-Chip System

5.6 Conclusion

The main objective of CMOS post processing is to release the microelectrode array and construct through substrate microchannels. In this chapter, two approaches, DRIE and FIB based post-processing were evaluated respectively. The experiment results demonstrated that FIB is a low cost maskless rapid prototyping method that can be used to create through wafer channels and release small number of microelectrodes. Different sizes of microelectrodes, as small as 5µm x 5µm, were released without patterning an additional protection layer. The experiments also validate the idea of using FIB milling through the CMOS dies after thinning the silicon substrate from the other side. Through substrate individual microchannels, with cross section of 16 µm x 16 µm and 10 µm x 10 µm were successfully fabricated. However, constrained by the maximum

milling depth due to the re-deposition issue, it is extremely difficult to form through substrate microchannels with aspect ratio larger than 10:1.

Meanwhile, DRIE, as an alternative technology, was experimented as a means to release all the microelectrodes at the same time without an extra protection layer. The experiments demonstrated that the original passivation layers on the CMOS chip are not thick enough to protect the underlying layers. Therefore, an additional photomask was fabricated to pattern a protection layer by a standard photolithographic process. Dry film photoresist is preferred because of the uniform thickness and comparably simple lamination procedure. However, the refraction, caused by the exposed top metal layer and uneven topology of the CMOS chip, made the precise alignment and effective exposure a very challenging task. More efforts would be required to find a proper recipe in the future.

To isolate the metal pads and bonding wires from the conductive sample medium, a Parylene coating is chosen to protect the microelectrodes and make the CMOS chip biocompatible. The testing chip, processed by FIB technology, was packaged in a custom modified chip carrier. Then, the CMOS die is encapsulated by a transparent and biocompatible epoxy. A microchamber is formed on top of the microeletrode array. Liquid samples can be injected into the microchamber and pass through CMOS die through microchannels.

CHAPTER 6 EXPERIMENTAL AND TESTING RESULTS

6. 1 Introduction

In this chapter, experimental setup and test results of two microfluidic devices are presented. The first set of results relate to the rapid prototyping of a microfluidic chip integrated with a planar in-channel microelectrode array. With this chip, microbeads are used to determine the sensitivity of the microelectrode array with assistance of a desktop impedance analyzer. The main objective of this chip is to validate the physical model and FEM simulations presented in Chapter 4 and to explore whether single bacterium detection can be realized by planar microelectrode pairs. On the other hand, this chip was also used to provide guidance for a future system integrated with MTB used as bio-carriers. The experimental results agree very well with the simulation results. The testing results also indicate that integration of microelectronic circuit into a microfluidic device is probably the only way to achieve single microbead or bacterium detection on chip without assistance of complex desktop instruments such as an impedance analyzer.

The functionality and performance of the on-chip sensing circuitry integrated on the microfluidic CMOS hybrid Lab-on-Chip are first evaluated. Then, the sensitivity of the microelectrode array is investigated and characterized. The microfabrication results validate the concept and feasibility of the proposed vertical, face to face microelectrode structure and CMOS post processing procedure. The preliminary experimental data also prove that a high sensitivity can be realized through proposed sensing circuitry and microelectrodes array. The testing results also indicate that the CMOS post process should be optimized in order to achieve more reliable and repeatable detection results.

The concept of using MTB as bio-carriers to achieve sensing specificity is also evaluated. The controllability, minimum magnetic field required and average thrust force of a single MTB are deduced from experiments. Finally, results of a MTB pushing a microbead under the control of external magnetic field are presented.

6.2 Rapid prototyping of a lab-on-chip device

Rapid prototyping of the microfluidic device shown in Fig.6.1 was done. It consisted of designing and fabricating the device for proof of concept experiments. This device was then tested experimentally and results were compared with simulation results presented in Chapter 4. The experimental setup and protocol is given first, followed by the results and analysis. Based on these experiments, we concluded that it is possible to detect single bacterium with assistance of a desktop instrument, such as an impedance analyzer; however, to reach the ultimate goal of having a lab-on-chip system with similar capabilities, integration of microfluidics with microelectronics may be the only solution for this kind of biosensors.

6.2.1 Experimental materials and procedure

The microchip was fabricated by Micralyneusing their MicraGEM process, which uses Pyrex glass as the substrate material and gold as in-channel metal microelectrodes. The microchip consists of a microchamber (3 mm x 3 mm), inlets for injecting samples, and microchannels connected to the microchamber that have a cross section of 52 μm x 12 μm (Width x Height).

The entire microfluidic device (excluding the inlets) is sealed by a layer of single crystal silicon. Twelve pairs of microelectrodes (20 μm x 20 μm) are patterned in planar orientation on the bottom of the microchannels. The center to center separation of the microelectrode pairs is 50 μm. The size of the microelectrode and dimension of the microchannel are chosen based the smallest feature size allowed in this process. Custom pads were fabricated on a printed circuit board (PCB) to allow connection between the microelectrodes and external impedance measurement equipment. The microelectrodes are connected to the PCB pads using a wire bonder. A precision impedance analyzer (Agilent 4924A, US) is connected to the PCB pads and used to measure the impedance signal across a microelectrode pair. The impedance analyzer is programmed to produce a sinusoidal signal of 0.5 V at a frequency of 1 MHz with 400 points per cycle. The microfluidic chip is placed under an optical microscope with an attached camera for observation during impedance measurements.

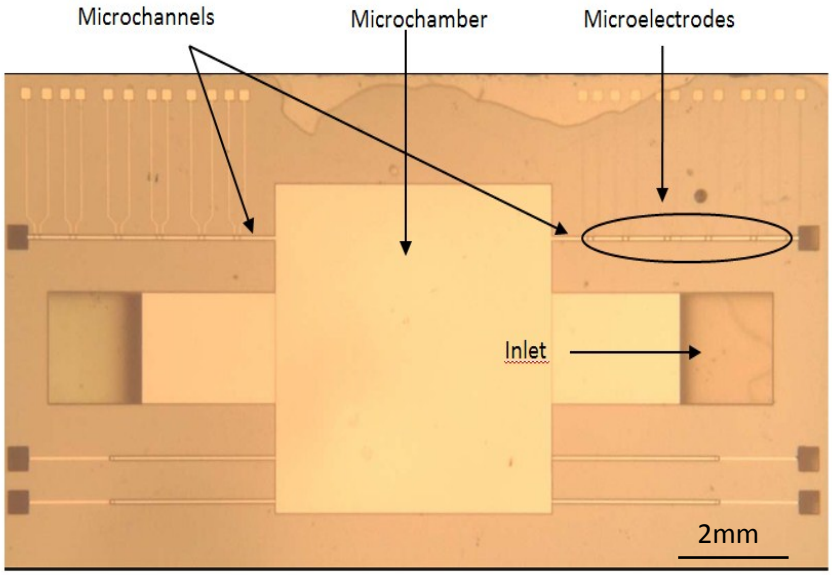

(a)

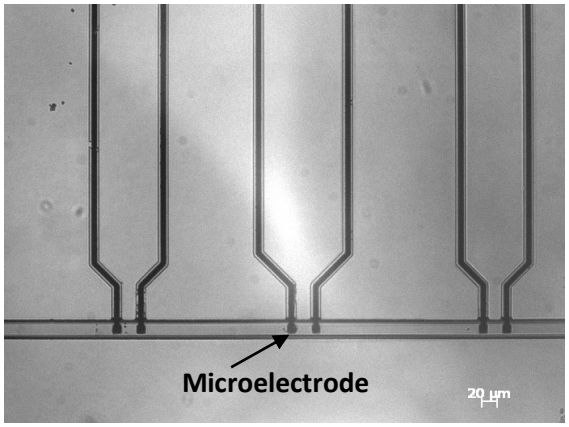

(b)

Fig 6.1: (a) Optical microscopy image of the fabricated micro-device used to detect microbeads. The image shows the microchannel and inlets where the solution was introduced, the microchannel where, through capillary action, the solution travelled, and (b)the microelecrode arrays used to perform the impedance measurements.

A key experiment was performed with a low concentration of 8 µm polymer microbeads diluted with de-ionized water. This solution was injected into the microchamber through one of the inlets. Through capillary force, the solution moves down the microchannel and the beads flow over the

microelectrode pairs. The impedance is constantly measured and the data array saved as the microbeads flow through the channel. As a microbead moves over a microelectrode pair, an increase in the impedance is detected as a pulse on the impedance plot. The impedance change is calculated by comparing the highest value of the pulse observed when a bead passes and the average impedance observed before the microbead enters the sensing region as the reference. The experimental noise was also calculated using the average and standard deviation of the reference signal.

6.2.2 Rapid prototyping experimental results and simulations

Preliminary experiments were performed with a fabricated microfluidic chip comprising embedded in-channel microelectrodes. Microbeads with a diameter of 8 μm were introduced into the microchannel. They were successfully detected using an impedance analyzer to monitor the impedance signal. The impedance signal resulting from 2 microbeads sticked together passing simultaneously through the detection zone is shown in Fig6.2 and Fig6.3. The relative increase in impedance is approximately 2.7% at the pulse's peak, or about 1.35% for a single microbead, as shown in Table 6.1. Using FEM simulation, the experimental microfluidic chip was modeled and the relative impedance increase was calculated for a pair of 8 μm beads passing through the detection region. The simulation, as shown in Table 6.1, gave a relative increase of 2.8% for 2 microbeads and 1.4% for 1 microbead, which is in good agreement with the experimental results. This shows that the simulation is able to adequately predict experimental results, and so it can be used confidently to aid in the design of the biosensor. It should be clarified that we were never successful at recording the impedance change induced by a single microbead after many tries. Single beads were observed passing through a pair of electrodes, but the signal change was immersed in the background noise, thus could not be recorded by the impedance analyzer.

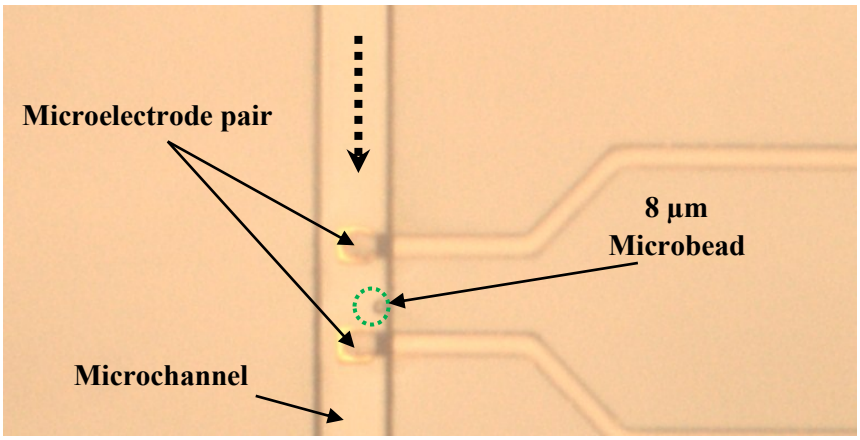

Fig6.2: Optical microscope image of an 8 µm microbead passing in between the planar microelectrodes in the detection channel of the microfluidic device.

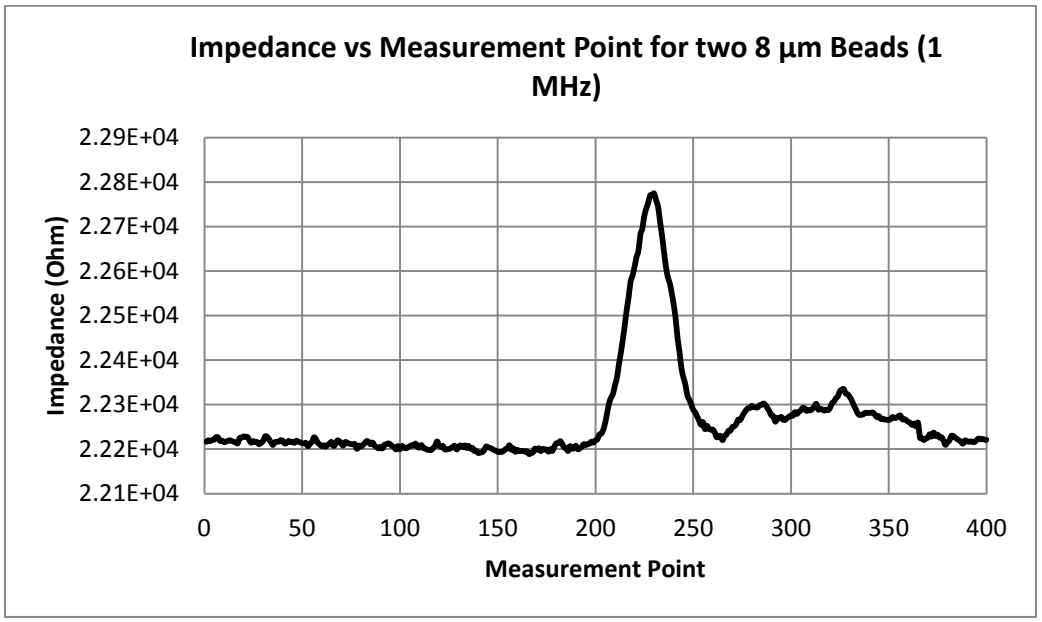

Fig.6.3: Graph showing the experimental impedance pulse recorded for two 8 µm beads passing simultaneously through the detection region.

Table 6.1: Various data obtained both experimentally and by simulation.

	8 µm Bead (x2)	8 µm Bead (x1)	MTB with *E. coli* fromRef. Solution	MTB Carrier without *E. coli* from Ref. Solution
Noise (%)	0.043	0.043	0.043	0.043
Exp. Impedance Change (%)	2.70	1.35	N/A	N/A
Sim. Impedance Change (%)	2.80	1.40	0.14	0.089

The fabricated microchip and experimental conditions are slightly different from those used to perform the optimization and MTB system simulations presented in the chapter 4. In order to compare the accuracy of experimental and simulated results, the simulation must adequately represent the experimental conditions. The simulation was modified so that the model had the same microchannel and electrode geometry as the fabricated chip. Also, the medium was changed to de-ionized water, which was measured to have a conductivity of 0.0001948 S/m and a relative permittivity of 78. The relative impedance change was calculated using a polymer microbead of 8 µm in diameter. As shown in Table 6.1, these excellent correspondences between simulation results and experimental results confirm that these simulations accurately reflect how the biosensor works. Thus, such simulations can be used with high confidence to support design and optimization of biosensors.

Similar simulations were also used to investigate the signal that a MTB carrier with an attached bacterium would produce. As shown in Table 6.1, the noise variation using the impedance analyzer was calculated to be 0.043%, based on a set of experiments which means that the sensor can potentially detect changes in impedance as small as 0.043%. Other simulations show that an impedance increase of 0.142% is expected when an MTB carrier attached to an E. coli is present in the detector, indicating that, in principle, it is possible to detect a bio-carrier system with an E. coli attached using the current experimental setup. A single MTB carrier without an attached bacterium could also be detected. Indeed, according to simulations, the expected impedance increase of 0.0890%. Thus, with the current setup, the system can distinguish between a single MTB carrier and one which carries the target bacterium. Note however that, as

we were never able to directly measure a single bead that should have produced a 1.4% change, these measurements appear to be very difficult to do, at least with the impedance analyser that we used.

6.2.3 Conclusions

Based on reported simulation and experimental results, it seems possible to implement an impedimetric system capable of single bacterium detection using the MicraGEM technology. Firstly, our experiments have shown that the current device is able to detect an increase in impedance of 2.7% when a pair of 8 μm beads (1.35% for a single bead) passes through the detection zone. This was done using an impedance analyzer to record the impedance signal. This experiment also validates the FEM simulations and shows that they are able to accurately predict experimental results. The simulation predicted an increase in impedance of 2.8% for a pair of 8 μm beads (1.4% for a single bead) travelling through the detection zone, which is in good agreement with the experimentally determined value. In conclusion, these results confirm that the FEM simulations can be used confidently in the design optimization process, and that this detection method can produce functional biosensors capable of detecting the various types of target objects and biological samples. However, the ultimate goal of this research is to develop a completely on-chip bacteria detection system. The impedance analyzer is a large and expensive piece of equipment that could not be used directly in an on-chip sensor. Instead, a microelectronic sensing circuit has to be developed in order to perform the required accurate impedance measurements completely on chip.

6.3 CMOS microfluidics hybrid lab-on-chip

The goal of the CMOS post-processing is to release the microelectrode array and to form the through substrate microchannels. That remains true, even if the initial results presented in chapter 5 showed that it is difficult to fulfill the task of etching through the CMOS substrate with FIB and DRIE. Chapter 5 showed that FIB technology was successfully used to mill two microchannels, through the substrate of a CMOS die integrating the required control and detection electronics. The cross-section of the channels that were produced is 10 μm by 10 μm and 16 μm by 16 μm respectively. Meanwhile, pairs of microelectrodes with different sizes were fully released. Hence, the main focus of the test is to verify the functionality of the microelectrodes and sensing circuits,

instead of the full functionalities of the proposed system, which is expected to detect single cell contained in an aqueous medium passing through the microchannel.

6.3.1Experimental procedure

As introduced in Chapter 3 and 4, the output signal of the sensing circuit is in digital format, complicated signal processing circuits or dedicated PCB are not required. The experimental set-up is shown in Figure 6.4.

The set-up of the experiment includes the packaged lab-on-chip system, two power supplies (Agilent E3632A, USA), a digital oscilloscope (Tektronix TDS7154, USA) for measuring the output signal, a signal generator (Agilent 33120A, USA) for sending control signal to the on-chip sensing circuit. The prototype lab-on-chip is installed on a test bread board, where a current source (LM 234, National Semi, USA), several resistors, capacitors and electrical wires are connected.

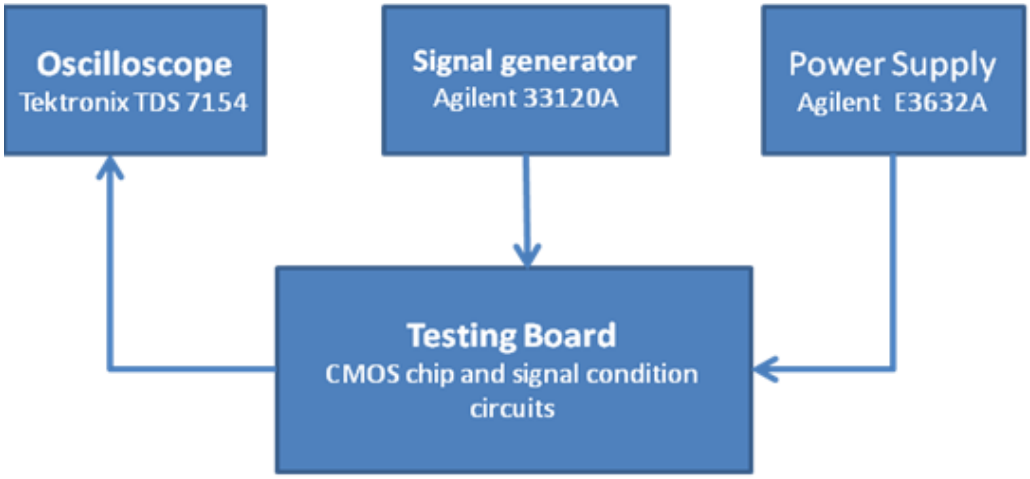

Fig 6.4: Experimental set-up

The test procedure consists of 3 steps: 1) Test of interface circuits, multiplexers, to ensure that each pair of microelectrodes can be reached and the sensing signal can be output to external instruments; 2) Test of sensing circuits: a) Adjust the frequency and amplitude of the input current, b) Configure the threshold of the output circuit, c) Adjust the circuit charging and discharging time; 3) Evaluate the performance of the microelectrodes with different bead sizes.

Liquid medium of varied conductivity were used to verify the functionality and sensitivity of the microelectrode and sensing circuits. Since we only have two through substrate microchannels, any blockage of the channels that could be caused by improper medium or beads should be avoided. Instead of microbeads or bacterial cells, we used medium of various conductance in this test. Recall that the sensing circuits are designed to detect changes of the impedance (resistivity) between the electrodes. The resistivity change induced by changing the conductive medium is equivalent to expected impedance changes that would occur if the circuit was used to detect bacteria or microbeads. The exact medium conductivities are measured by a multimeter (Thermo Scientific, Orion 5 Star Multimeter, USA). Medium with the following conductivities were prepared and measured: 0.22 ms/cm, 0.478 ms/cm, 0.733 ms/cm, 0.792 ms/cm, 0.875ms/cm, 1ms/cm, 1.4 ms/cm, 2.6 ms/cm, 3 ms/cm, 3.06 ms/cm, 3.18 ms/cm, 3.34 ms/cm and 3.48 ms/cm. For reference, the normal blood conductivity is around 6.67ms/cm [188], sea water has a conductivity of 32.7 ms/cm (equals to 25g salt in 1Kg water) [189], and de-ionized waterconductivity is 1.0~0.1μs/cm.

Tests were conducted at room temperature. The procedure consists of: a) cleaning the packaged CMOS chip with DI water and dry it before each test; b) prepare the conductive medium, making sure it is very well mixed before being injected into the microchamber and measuring its exact conductivity with a multimeter before the test; c) immediately after the sample injection, cover the microchamber with a piece of glass coated with a thin layer of PDMS to avoid medium evaporation, which would lead to concentration of the medium and gradual variation of its conductivity; d) apply a small vacuum, generated by a syringe, from the bottom of the packaged CMOS chip to force the medium to flow from the top microchamber into the through substrate microchannel; e) after each test, the chip is rinsed in DI water and dried with air to remove debris that could be caused by the NaCl solution.

6.3.2 Experimental results

6.3.2.1 Interface circuit functionality test

The test and results analysis part were conducted together with Jaouad El-Fouladi, who was also responsible for circuit design, simulation and test in this research. As illustrated in Fig 6.5, four independent sensing and interface circuits are located on four corners of the CMOS die. Each of

them is responsible for testing 30 of the 120 microelectrode pairs present on the CMOS die. By configuring the external control signal of on-chip multiplexers, each microelectrode pair and relevant sensing circuit are selected, then, the input current from the external current source is injected into the correspondent sensing circuitry. In the meantime, the impedance is measured. Impedance is reflected as the pulse width of the waveform present on the output pin, which is connected to an external oscilloscope.

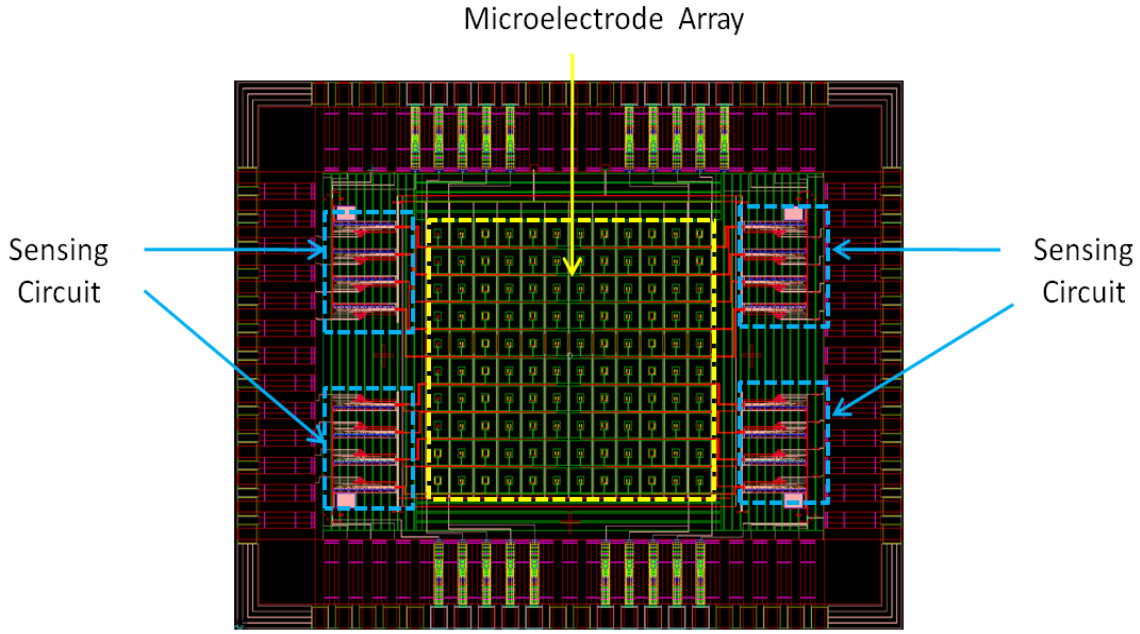

Fig 6.5: Layout of the CMOS Lab-on-Chip system. The microelectrode array is located in the center of the chip. Four reconfigurable sensing circuit modules, working independently, are implemented on both sides.

In this test, a NaCl solution with conductivity of 0.9s/m was injected onto the microchamber constructed on the top of the microelectrode array. We proved that each pair of microelectrodes can be addressed and impedance can be measured. The impedance variations between microelectrodes are transferred to the output processing circuit and then displayed through an oscilloscope. Some testing results are shown as Fig 6.6. The performance of the microelectrodes with different sizes produces different results, reflected as the width of the pulse under the same input conditions. These test results confirm that the thin Parylene film functions as a capacitor in the sensing circuitry.

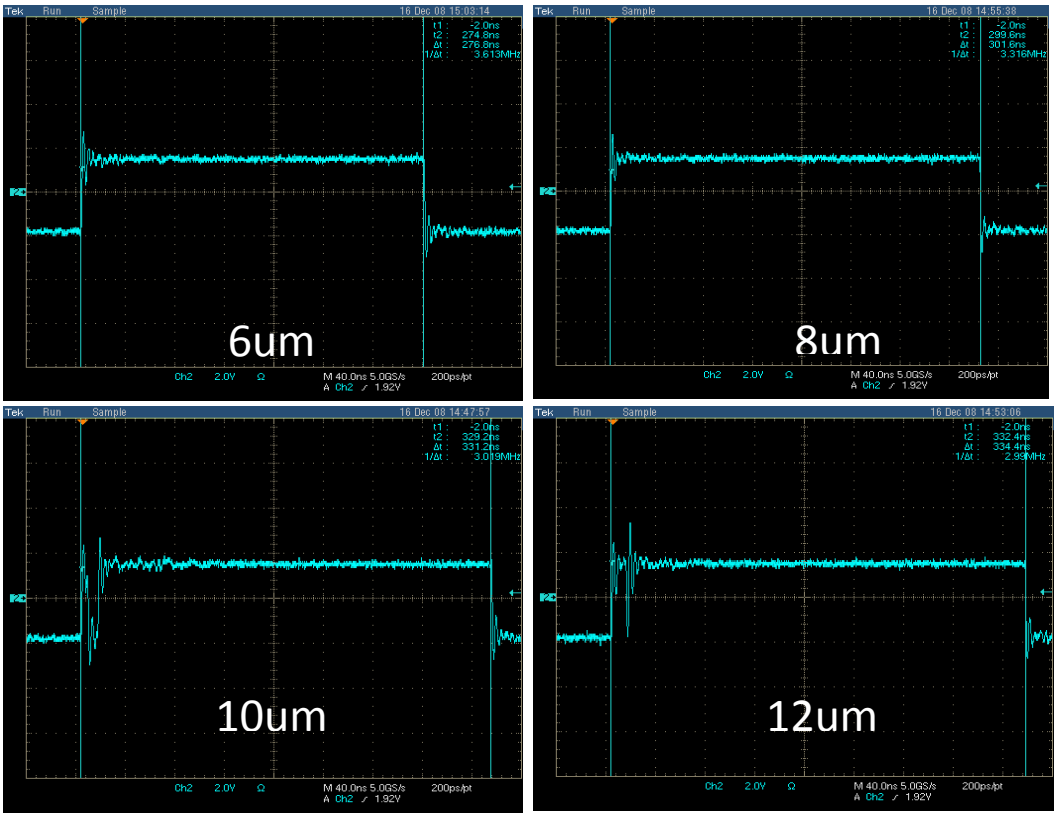

Fig 6.6: Pulses obtained with an oscilloscope for various microelectrode pairs that can be reached individually through dedicated selection pins.

6.3.2.2 Performance of microelectrodes and sensing circuit.

The ultimate goal of this research is to detect and identify a single micrometer size bacterium or particle. Based on the simulation results shown in Chapter 4, in order to achieve such a resolution, the size of targeted bacterial cell or particle should be comparable to the size of the microchannel and microelectrode. However, it is of interest that the size of pathogenic bacteria is in the range of 1µm to 10µm. As described in chapter 5, we were not able to fabricate 10µm through substrate microchannel with enough reliability and repeatability. The test began with the two through substrate microchannels with microelectrode pairs released on their wall. The cross section of the microchannels were 16µm x16 µm and 10µm x 10µm respectively. The dimensions of microelectrodes are respectively 10µm (L) x 8µm (H) x 2µm (W) and 16 µm (L) x 8 µm (H) x 2µm (W) for the 10 µm and 16 µm channels.

Following the procedure described in section 5.3, the medium was expected to flow into the through substrate microchannel. However, we were not able to observe that the liquid medium went through the substrate, even when we applied relatively large vacuum on the back side of the chip. We could not obtain consistent output signals from either microelectrode pairs on the wall of the two through substrate microchannels. The possible reasons for this failure are analyzed in the next section.

The results shown in Table 6.2 were obtained from microelectrodes pairs (10μm x 8μm x 2μm. L x H x W) in adjacent microcavities (10μm X 10μm X 10μm) under the following conditions: electric current: 1.25μA and charging/discharging frequency: 1MHz, 3MHz and 8.5MHz.

Table 6.2: Pulse Width (ns) observed for various conductivities

Conductivity (ms/cm) / Frequency(MHz)	Air	3	3.06	3.18	3.34	3.48	4.1
1	196	85	85	86	85	85	86
3	128	117	115	114	113	112	111
8.5	34.6	25	25	25	25	24	25

According to the circuit analysis and simulation described in Chapters 3 and 4, the magnitude of the injected current, the charging/discharging time and the threshold of the output buffer can be adjusted to control the sensing circuit. With a consistent input electric current and charging/discharging cycle, as well as fixed threshold of the output buffer, a larger conductivity should induce shorter high pulses on the digital output pin of the CMOS chip. The experimental results indicate that the system works as expected when the charging/discharging frequency is 3MHz, but the system could not differentiate the conductivity variations at 1MHz or 8.5MHz.

Using the same pair of microelectrodes, when the current is decreased to 0.125μA and the charging/discharging frequency is set at 0.8MHz, the system discriminated the change of conductivity very well, as illustrated in Table 6.3.

Table 6.3: Pulse width (ns) vs. conductivity (injected current is 0.125 μA)

Length of Microelectrode (μm)	Frequency (MHz)	Conductivity (ms/cm)	Pulse Width (ns)
10	0.8	0.40	196
10	0.8	0.73	194
10	0.8	0.79	191
10	0.8	0.87	189
10	0.8	1.0	187
10	0.8	1.4	183
10	0.8	2.6	177

The relative detection sensitivity of the system can be determined by equation 6.1 to define the system relative resolution:

$$relative\_resolution = \frac{(Cond_{sample} - Cond_{ref})}{Cond_{ref}} \times 100\% \tag{6.1}$$

Based on the test results shown in Table 6.2 and Table 6.3, we can deduce that the system relative resolution can reach 2%, which means that a 2% change of conductivity between a pair of microelectrodes (10μm x 8μm x 2μm, L x H x W) can be identified by the sensing circuits. As simulated in Chapter 4, a bacterium of 5μm diameter should cause 10.7% change of the conductivity between a pair of microelectrodes with a detection volume of 10μm by 10μm by 10μm size in between. Thus, the sensitivity achieved by the proposed system is good enough for single bacterium detection.

It should be mentioned that the above results were acquired during the very first experiments when they were repeatable if the experiment was performed with same medium. However, the next day and using the same chip and experimental setup, the previous experimental results could not be repeated and the output signals were irregular and random. There are several possible explanations for this behaviour: a) the on-chip sensing circuits were damaged during the test, b) the surface condition of the microelectrodes was changed by the medium and c) the microcavity between the microelectrode pair was blocked in some way. During the following test, when the input signals were changed, the outputs did respond accordingly, but in an irregular manner, which indicates that the circuit is functional nonetheless. So, a close inspection of the tested CMOS chip was undertaken.

6.3.2.3 Analysis

The CMOS chip was inspected using an SEM. It was found that there was lots of debris left on the surface and microelectrode array. Some of the debris accumulated at the entrance of the microcavity, as illustrated in Fig 6.7(a). The presence of the debris compromised the behaviour of microelectrode array and leads to failure of the detection process. There was no output signal from the microelectrode pairs that were partially or fully covered by debris, as shown in Fig. 6.7 (b).

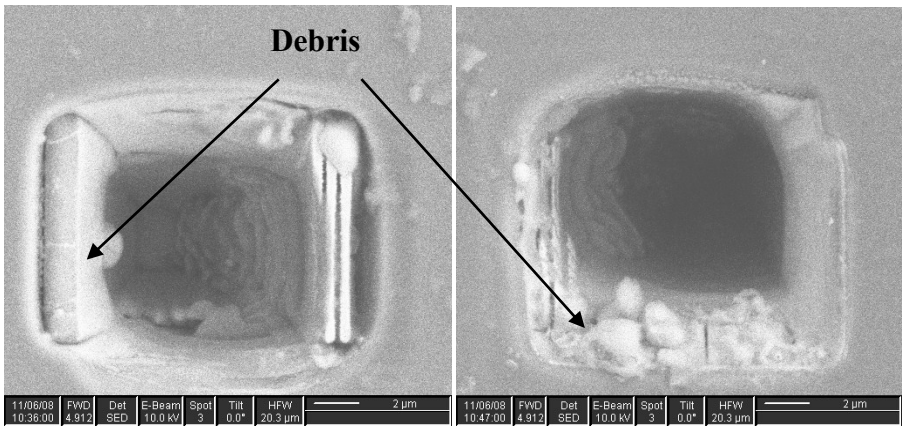

(a)

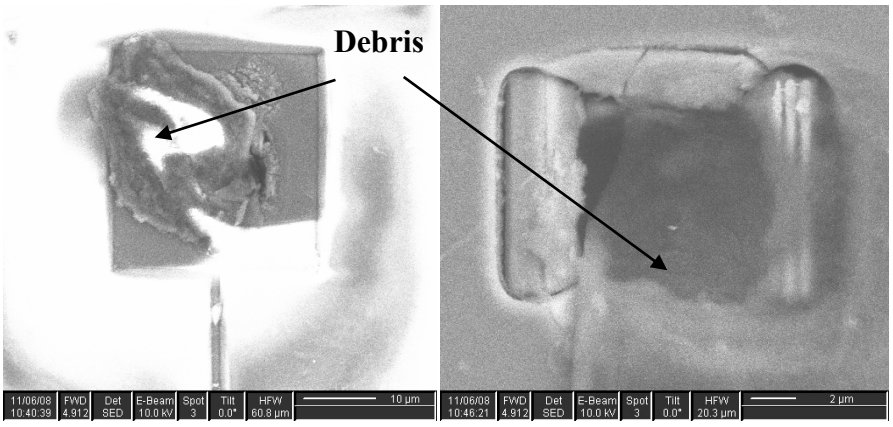

(b)

Fig 6.7: Debris left on the surface of the microelectrodes and entrance of the microchannel after the initial test.

Since the conventional wafer cleaning procedures usually adopt strong acid or alkaline solution, neither of them is compatible with CMOS chip and the packaging material. Several other methods were used to try to remove the debris, including ultrasonic bath, oxygen plasma cleaning, and long-time rinse in DI water with magnetic agitation. However, not much improvement was achieved. The only effective way to get rid of the debris is to remove them manually; however, the debris in the microcavity on the inner side of the microelectrodes cannot be reached even with the smallest probe tips.

In order to continue our evaluation of the proposed system, a second CMOS die was processed with FIB and packaged as was the first one. On this chip, several pairs of microelectrodes were released, but without through substrate microchannels, as shown in Fig6.8. Under the same experimental conditions, the previous experiment was repeated on the second CMOS chip, which validated the experimental results and system sensitivity. Again, as the first chip, the second chip was covered with debris and became unstable after several tests.

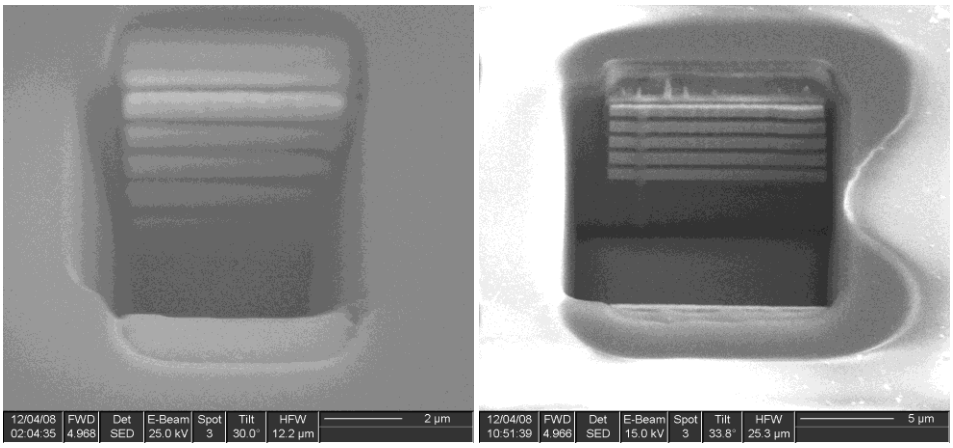

Fig 6.8: SEM micrograph of released microelectrode pairs and microcavities

6.3.3 Discussion

The experimental results achieved with two CMOS Lab-on-Chip microsystems validate the concept of the face-to-face microelectrode structure and functionalities of the on-chip sensing circuit. We can conclude that the sensitivity of the proposed system is as least 2% of conductivity change in the microcavity. The sensitivity reached with the microelectrode pair in a microcavity

also proved that rapid detection of a single bacterium (~10μm) is feasible using the proposed microsystem. The experimental results also indicate that the sensitivity of the each pair of microelectrodes depends on the size of the microelectrode, the charge/discharge time of the sensing circuit, the threshold of the output buffer, and the magnitude of the injected electrical current. Optimizing these parameters is required to maximize the performance of the microsystem. More work is required to improve the system and make it work more efficiently and reliably. Several issues encountered need further investigation and are discussed below.

As described in Chapter 5, reliable and repeatable CMOS post processing should be developed to form through-substrate microchannels and release microelectrodes on the walls. Secondly, consistent and continuous flow in the microchannels should be established. However, since the CMOS die is thinned to around 100 μm, the silicon substrate becomes very fragile, which prevents us from applying deeper vacuum from the bottom of the CMOS die to induce flow in the microchannel. Theoretically and with such a small microchannel (10μm by 10μm in this case), the capillary force should generate the flow in the microchannel if the surface of the microchannel is hydrophilic. In this research, Parylene is coated all over the CMOS die, covering the surface of microelectrodes and inner sides of the microchannels, but Parylene is a highly hydrophobic material, without applying relatively high pressure in the microchannel, it is difficult to introduce flow in two through substrate microchannels formed by FIB technology.

In the case of microcavities, where the microelectrode pairs are released but through substrate channels were not formed. When the liquid sample is injected into the microchamber on the top of the microelectrode array, the liquid sample does not always fill the whole microcavity due to the hydrophobic Parylene coating or air bubble trapping. Thus, the microelectrodes on the walls may have partial or even no contact with the liquid sample. As illustrated in Fig 6.9, there are three potential contact modes: a) no contact, b) partial contact, and c) full contact. Without reliable contact between the microelectrode and the sample, the performance of the microelectrodes is compromised and the test results may not be uniform. The depth of the liquid sample going into the microcavity could not be well controlled. Among other things, it depends on the fabrication process of the microcavity as well as the Parylene coating process.

When a CMOS chip is under test, it is very difficult to investigate the contact condition between the liquid sample and microelectrodes in the microcavity by observation, for example, using microscope. Different methods were tried to investigate the contact effect on the performance of the CMOS chip, for instance, applying various pressure on the top of the microchamber to change the access depth of the liquid sample in the microcavities. By real-time monitoring the output waveform, if the change of the access depth is changed, the conductivity will be changed accordingly, reflected as the change of the output waveform. This method works well with microelectrodes of different sizes, but, in terms of the same microelectrode pair in the same microcavity, the output waveforms changes appear to be random, which suggests that the liquid access depth is irregular each time and that we could not control it.

However, during our tests, the experiments were repeatable on pairs of microelectrodes with the same size on two different CMOS chips, the pressure changes had almost no effect on the output waveform. The particular size of microelectrode is 10μm (length) X 8 μm (height) X 2 μm (width) and the 2% percent system resolution was estimated based on this. From our experimental results, we observed immediate change of the output signal when the liquid sample is injected into the microchamber, which means that the situation when there is no liquid in between the microelectrodes was not occurring, thus the only explanation is that the microcavity is fully filled with liquid, which is the same condition as the liquid sample flowing through substrate microchannel. Hence, we can conclude the 2 % resolution achieved is enough to identify a single bacterium using the proposed system.

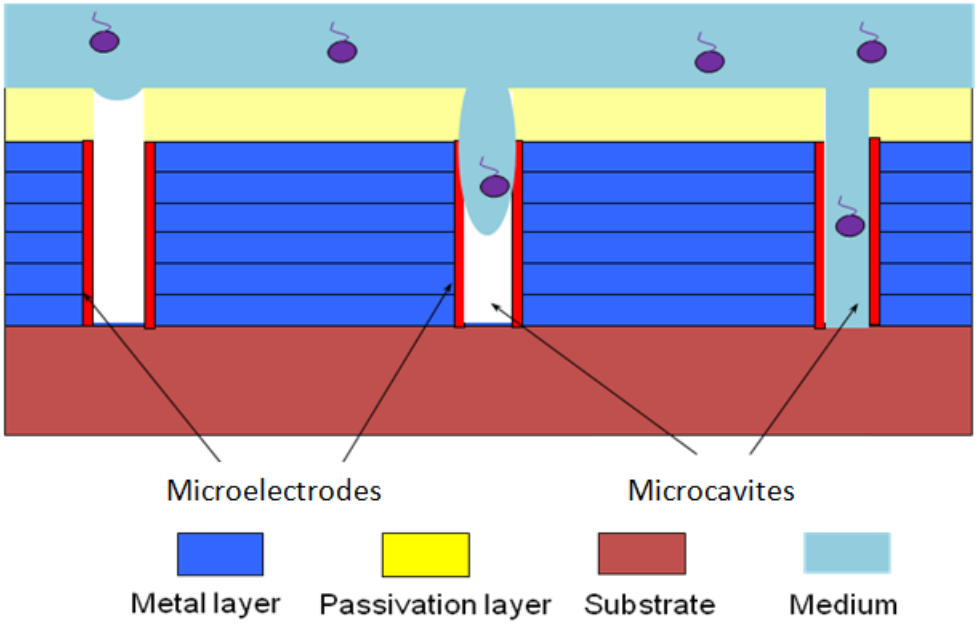

Fig.6.9: Varied depth of the medium in the microcavities between pairs of microelectrodes

6.4 Experiments of using MTB as bio-carrier

In Chapter 4, the simulation results indicated that, using MTB and microbead, the proposed system should be able to realize detection specificity and that the sensing circuit is capable of differentiating whether the target bacterium is caught on the microbead pushed by a MTB. Since the technology of binding two different kinds of antibody, one for MTB and one for target bacteria, is still under development, the experiments presented below are the initial research that focuses on the characterization of MTB as bio-carrier in a microfluidic environment.

6.4.1 Characterization of MC-1 MTB

In order to evaluate the potential of using MTB [190] as bio-carriers, MC-1 MTB [191] has been selected for our experiments [188,189]. The cell of MTB MC-1 is 1 to 2 μm in diameter and highly motile, having two bundles of flagella located on one side of the cell (see Fig 6.10). Observed under a TEM, typically, in each cell there are 5 to 14 magnetic nanoparticles, called magnetosome. As other magnetotactic bacteria (e.g. Magnetospirillum magnetotacticum), MC-1 cells use a chain of magnetic nanoparticles as a compass to find favorable environmental

conditions. MTB MC-1's migration pattern displays a polar preference. They swim only to one direction along the magnetic field lines, either south or north, called unidirectional movement. Another significant advantage of considering MC-1 MTB as bio-carriers is that they can achieve a high swimming speed, from approximately 50μm/s up to 300μm/s. In this section, the thrust force and the effects of microenvironment on the mobility of MC-1 are investigated.

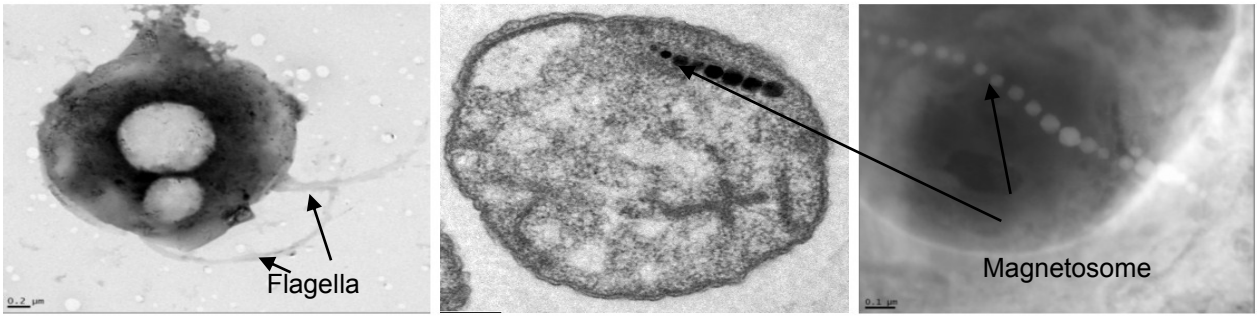

Fig 6.10: Transmission electronic microscope (TEM) images of the MC-1 bacterium and magnetosome

6.4.1.1 Thrust Force and Speed of the MTB MC-1

In order to evaluate the maximum payload of the MC-1 MTB, the average thrust force of a single MC-1 bacterium has been investigated. The motion of a MC-1 bacterium in a viscous medium is characterized by a very low Reynolds number [192]. In a very low Reynolds number regime, also known as creep flow condition, the inertial effects can be neglected. Stoke's law describes the equation of the hydrodynamic drag force for a spherical particle in a viscous medium [192]. Given the diameter of an MC-1 bacterium to be approximately 2μm, the average swimming speed to be 210μm/s, the dynamic viscosity of sea water to be 1.005mPa·s, and assuming that the thrust force used to propel the bacterium is equivalent to the drag force exerted by the medium, we have

$$F = 6\pi\mu\upsilon R \approx 4pN \tag{6.2}$$

The calculated average thrust force of 4 pN for a single MC-1 bacterium is much larger than that provided by other motile bacteria, such as Salmonella and E-Coli (~0.2 pN). Furthermore, as a worst case condition, if we assume that the flagella motor of each MC-1 bacterium maintains the

same rotation rate, hence maintaining the same thrust force after being attached to a microbead, their swimming speed will decrease according to the increase in hydrodynamic drag force as the frontal surface area increases. Based on the experimental data shown in Fig 6.11, the relationship between the swimming speed of the bacteria and the diameter of the microbead being propelled is calculated based on Stoke's law and illustrated in Fig 6.12.

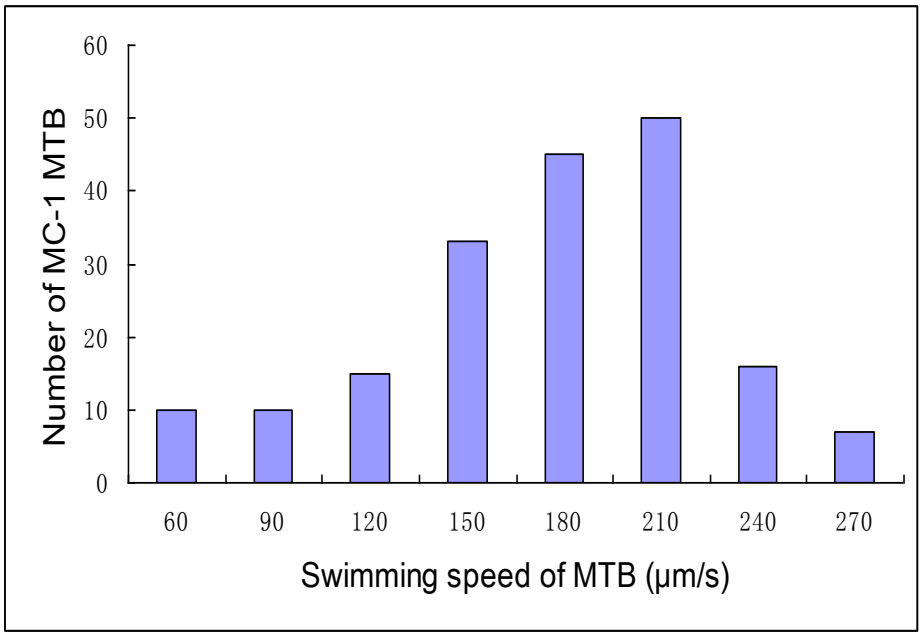

Fig6.11: Swimming speed measured from a sample of 180 MC-1 bacteria in unbounded sea water conditions. The results were achieved using a high speed camera installed on a microscope

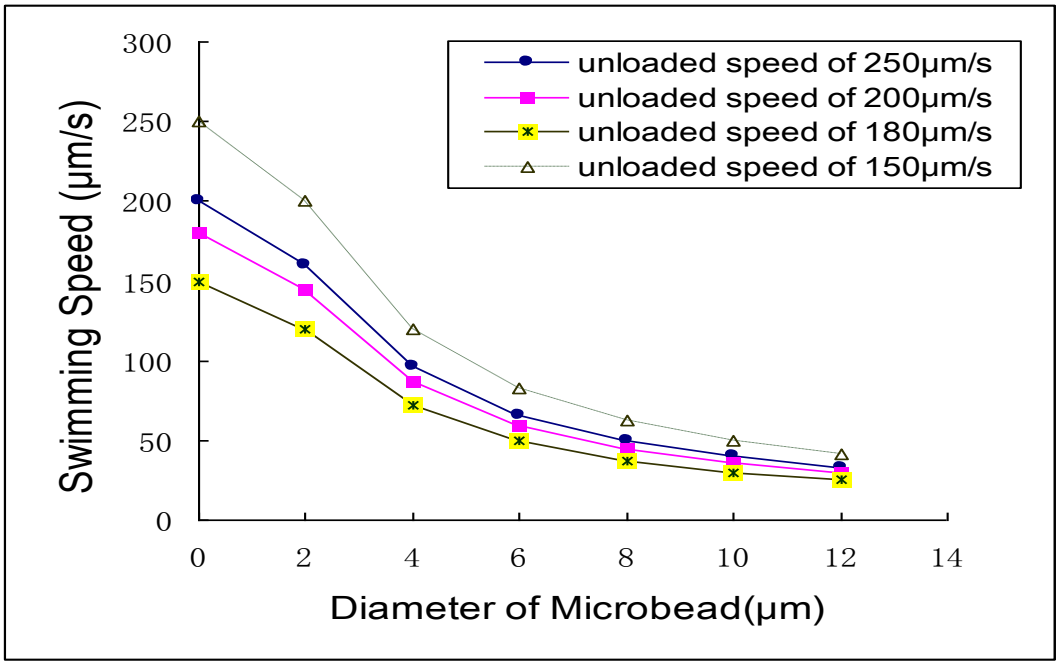

Fig 6.12: Measured average swimming speed of the MC-1 MTB as a function of the diameter of the attached microbead, estimated based on Stoke's law[192].

6.4.1.2 MTB MC-1's speed in microchannel

In microfluidic systems such as lab-on-chip and μTAS, an important issue that needs be considered for micro or nano-transport is the wall effect. The wall effect is characterized by an increase in the drag force acting against the bio-carrier as the dimensions of the microsystem approach that of the carrier. This is caused by the proximity of the walls of the microchannels and micro-chambers for *in vitro* experiments, or capillaries and lymphatic vessels for *in vivo* applications. This effect becomes more significant as the diameter of the microchannel approaches the diameter of the bio-carrier, according to [193]:

$$\frac{v}{v_\infty} = \{\frac{1-(\frac{d}{D})}{1-0.475(\frac{d}{D})}\}^4 \tag{6.3}$$

Where d is the diameter of the micro-carrier, D is the inner diameter of the channel, v is the velocity of the micro-carrier, and v_∞ is the velocity under the unbounded condition. As depicted

in Fig. 6.13, as the diameter of the microchannel decreases and approaches the size of the bacteria, the swimming speed drops significantly. For example, in a channel with a diameter of 10μm, the average swimming speed of the MC-1 bacterium is expected to decrease from 200 μm/s in an unbounded environment to 122μm/s in the channel. A similar theoretical result is confirmed by another model proposed in [194], in which a velocity of119μm/s is obtained using the same conditions.

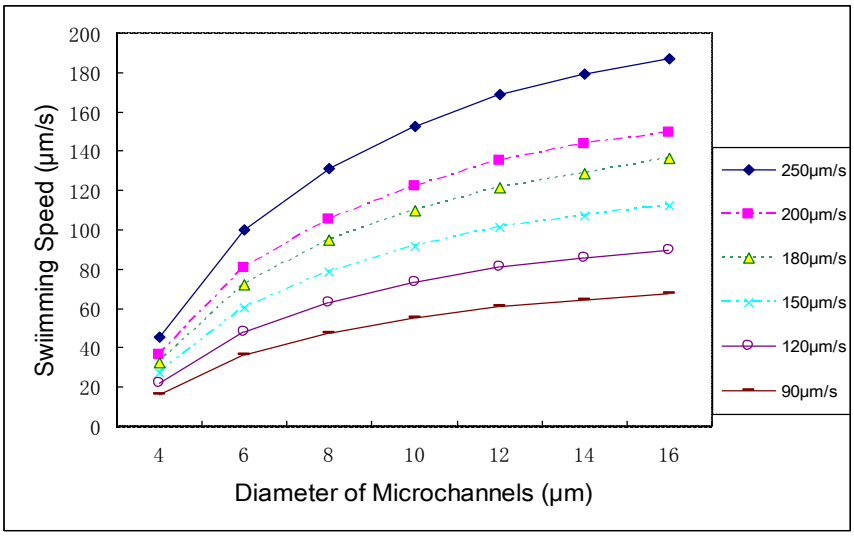

Fig 6.13: Theoretical wall effect on the swimming speed of the MC-1 bacteria in microchannels with various diameters.

The influence of the wall effect on the mobility of the MTB is experimentally investigated. In this experiment, a microchannel with widths ranging from 12 μm to 4 μm, representative of numerous possible environments, such as a micrometer-sized channel, capillary, or microchamber, is used to investigate this effect. The microfluidic device used to perform these measurements is illustrated in Fig 6.14 a). An interesting phenomenon is observed when the MCB are directed to swim through the microchannel and their speed is monitored. As shown in Fig 6.14 (b), in most cases, as the channel size decreases the speed of the bacteria also decreases, but remains much higher than the speeds predicted previously by Stoke's Law. This seems to suggest that the MC-1 bacteria can compensate for the wall effect by increasing their effective thrust force.

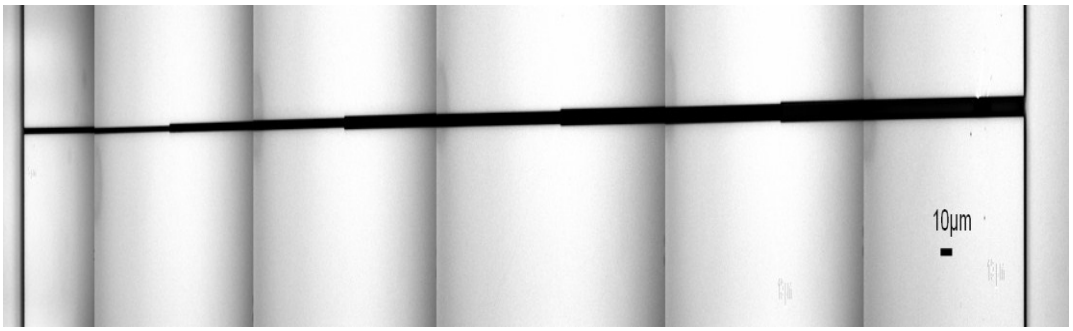

(a)

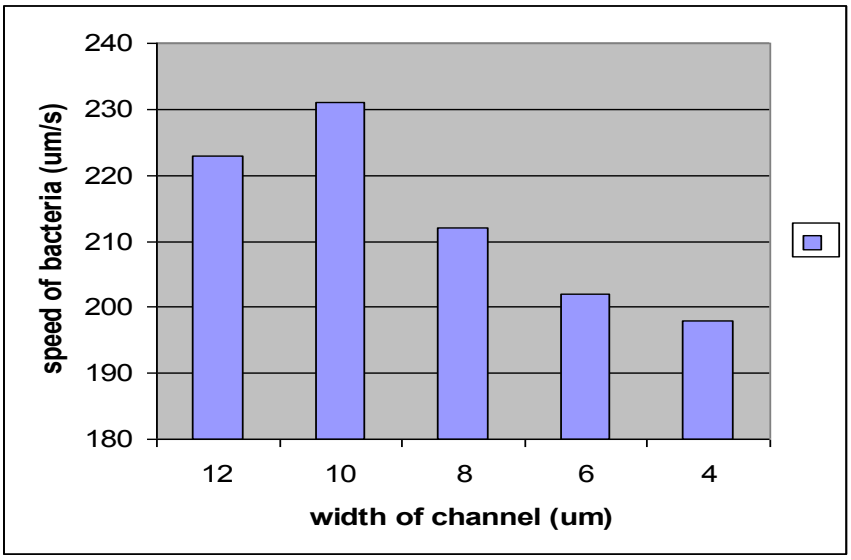

(b)

Fig6.14: (a) Microchannel with various widths, from 4 to 12 μm(b) Observed average swimming speed of 50 MC-1 bacteria in each microchannel

6.4.2 Medium viscosity effect on the MTB MC-1 mobility

Since the MTB MC-1 is supposed to be used in different medium for bacteria detection and the viscosity of the medium has a direct impact on the efficiency of the MC-1 bio-carrier, the performance of MC-1 in different viscosity needs to be investigated. A glycerol solution is added into the MC-1 medium with an initial viscosity of 1.005 mPa·s. When the amount of glycerol in the medium is increased, the viscosity of the solution increases, which results in a decrease in swimming speed of the bacteria. The measured swimming speed of MC-1 bacteria decreases

significantly and is much lower than the theoretical values predicted by Stoke's law, as shown in Fig 6.15. One possible reason is that due to the lower nutrition and oxygen level in the medium with the increased glycerol content, the MC-1 bacteria are stressed and their motility is consequently reduced. This result implies that MTB MC-1 appear to work more efficiently as a bio-carrier in an oxygen rich and less viscous medium.

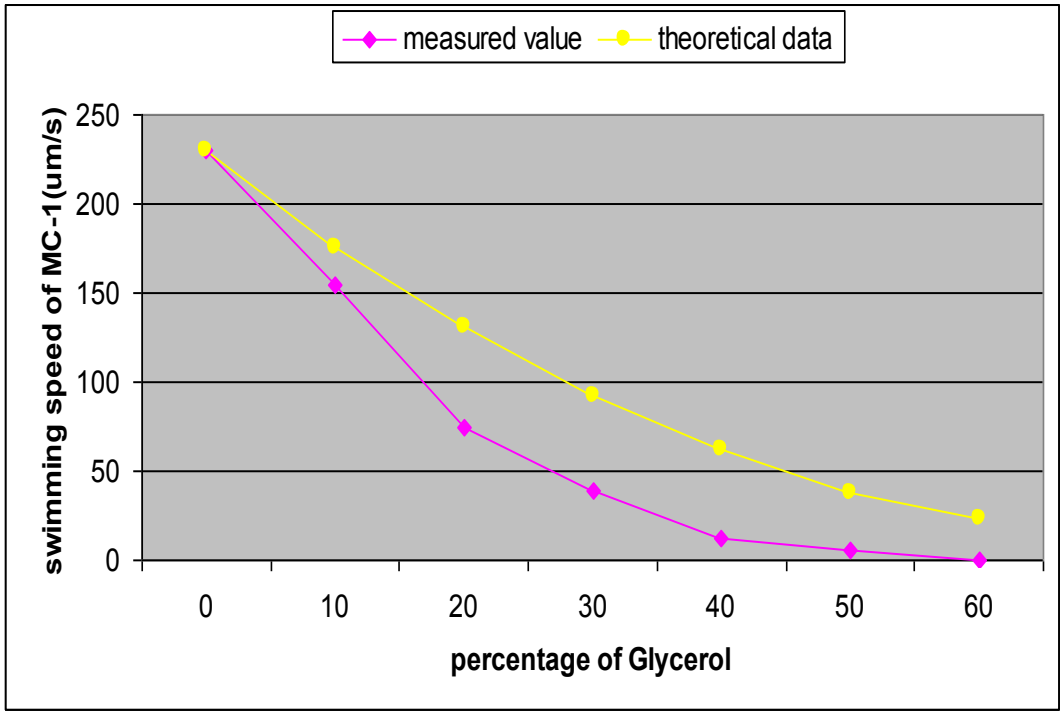

Fig 6.15: The swimming speed of MC-1 bacteria as a function of solution viscosity.

6.4.3 Controllability of MTB MC-1 in microchannels

As an initial assessment, the controllability of the MC-1 MTB inside microchannels is validated through the use of an applied magnetic field. A microfluidic device was fabricated on a Pyrex glass wafer, with the minimum feature size (width and height) of the microchannel being 20μm. First, MC-1 bacteria are injected into the microchannel with a syringe. After stabilization of the flow in the microchannel, the MC-1 bacteria navigated as depicted in Fig 6.16, when guided using a permanent magnet. A field intensity of 10 Gauss was used during the experiments.The field magnitude was validated with a Gauss meter (Lakeshore model 450, USA). At 10 Gauss, most bacteria could be controlled efficiently for navigation in the microchannels. As shown in

Fig 6.16, changing the direction of the external magnetic field led to an immediate corresponding change in the swimming direction of the MC-1 bacteria in the microchannels.

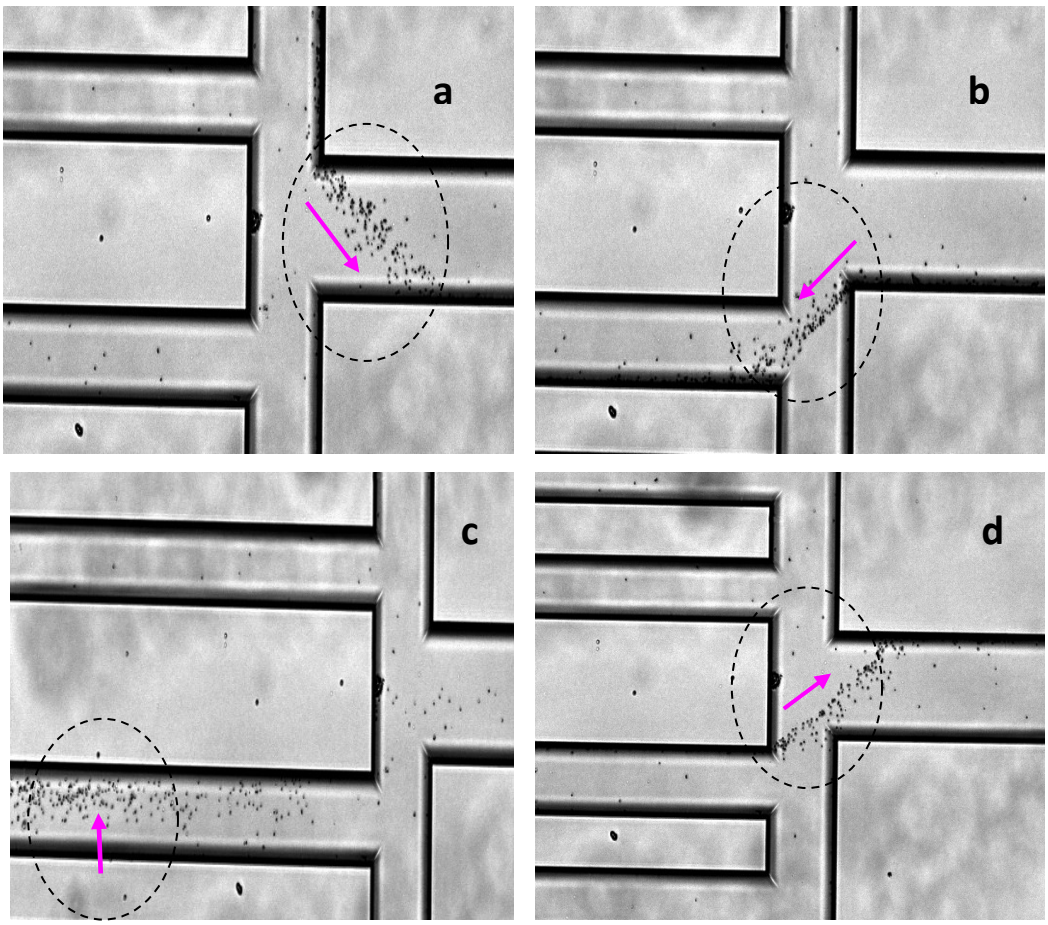

Fig 6.16: Control of MC-1 bacteria in microchannels. (a) With the magnetic field set to -45^{o} with respect to the parallel channel (far left image), the bacteria begin to swim into the central microchannel (width of 100 μm) from the upper corner. (b) The magnetic field is then switched to -135^{o} and immediately the bacteria in the central channel begin to migrate into the lower channel (width of 50 μm). (c) The bacteria swim from the bottom of the microchannel to upside and stay after the magnetic field is set at 90^{o}. (d) The bacteria reverse their swimming direction after the magnetic field is set to 45 ^{o} (second image from right) and swim back to the central channel (far right image).

6.4.4 Loading of the bacteria with microbeads

Another important issue in the design of a system based on MTBs used as bio-carriers is a suitable method to attach the MTB to functional micro- or nanobeads. A dedicated protocol, which is described below, was developed to coat the nano/microparticles with MC-1 specific antibodies in an attempt to increase the binding efficiency of the MTB to the nano/microspheres.

Step 1: Polyclonal antibody production. Anti-MC-1antibodies were collected from rabbits, and they were injected into media containing heat-inactivated MC-1 bacteria as antigens.

Step 2: Preparation of polyclonal Antibody-Coated Fluorescent Beads; Polyclonal Anti-MC-1 antibodies were added to the pre-washed FluoSphere® beads (2% solids, Invitrogen), then washed three times in PBS-1X and one time with BPS-2X. MC-1 attachment to the beads is achieved by introducing the microorganisms into the bead suspension at a concentration of approximately double that of the bead concentration. The suspension of beads and MC-1were left for no longer than 30 minutes before experimentation, by which time a sufficient number of MC-1 had attached to the surface of the bead, as illustrated in Fig 6.17.

Because of the specificity of the MC-1 antibodies, only the MC-1 bacteria can attach to the coated microparticles. Binding of the antibody to the MC-1 bacterial cells depends on hydrogen bonding, electrostatic attractions, and Van der Waals interactions. These bonds are weak compared to covalent bonds, but a stable complex is reached between the MC-1 MTB and antibodies in the presence of a high number of these bonds. Depicted in Fig 6.18 is the ability of the MC-1 to push a 2μm polystyrene microsphere, attached using antibodies, through a pre-programmed path. It was observed that the MC-1 is able to push the bead through the pre-programmed path without becoming removed from the microbead due to the antibodies that we have fabricated. Our experimental results have shown that after coating the microbeads with an MC-1 antibody, the efficiency of the attachment has increased from 1% with other methods to more than 10%. The method of increasing binding efficiency and combining two types of antibodies on the same microbeads is in development.

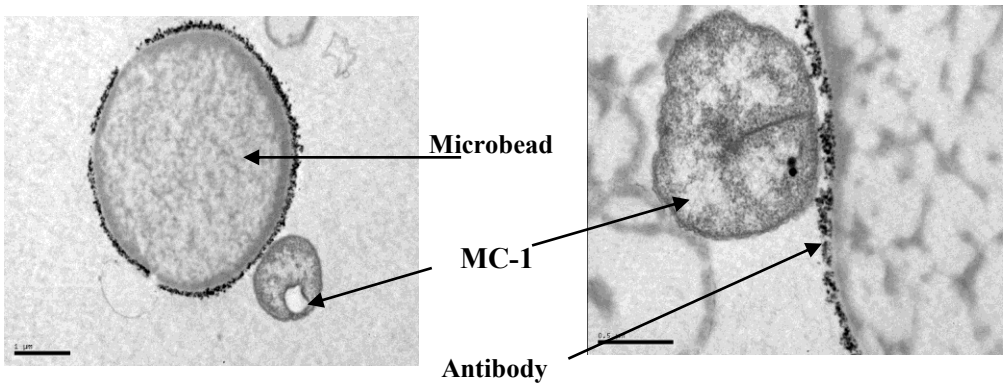

Fig 6.17: TEM images of a single MC-1 bacterium attached to a 5 μm microsphere through antibodies.

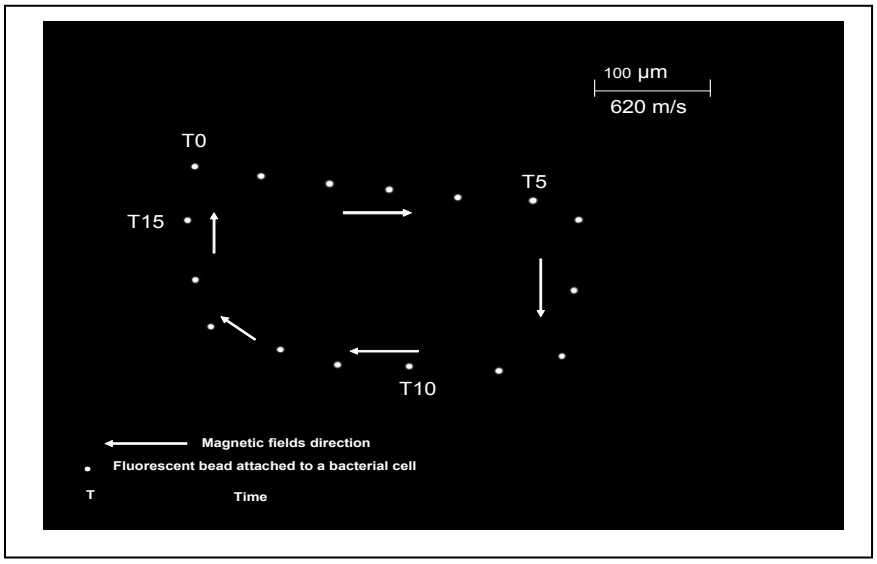

Fig 6.18: Displacement of a 2μm bead being pushed by a single MC-1 cell under control of a directional magnetic field. The antibodies were used as the attachment mechanism, and fluorescent microscopy was used to image the movement of the microbead.

6.4.5 Conclusion in relation to the potential of using MC-1 as a bio-carrier

In conclusion, the MC-1 MTB has shown to be a powerful bio-carrier for controlled manipulation and transportation. The average 4 pN thrust force of a single MC-1 bacterium is sufficient to push a microbead with a speed in the range of100 μm/s. Under the control of a magnetic field of less

than 10 Gauss, MC-1 MTB can transport the loaded microbead to the desired destination rapidly and precisely.

CHAPTER 7 CONCLUSION AND OUTLOOK

7.1 Conclusions

In this thesis, various means of implementing biosensor systems for single bacterium detection have been investigated. A system based on a CMOS chip comprising a microelectrode array as well as stimulation and recording circuitry was proposed. This system was prototyped using a CMOS chip post-processed to release the microelectrode array. Many challenges were encountered in relation to biocompatibility, to effective transduction to detect a single bacterium using microelectrodes, and to achieve chip functionality. To make this possible, a novel approach for constructing vertical face-to-face microelectrode pairs was developed and implemented on a CMOS chip. The single bacterium detection is realized through on chip sensing circuits. As envisioned, detection specificity would be achieved by introducing magnetotactic bacterial complex combining the bacteria with a microbead that has a functionalized surface. The experimental results indicate that a 2% impedance variation, caused by the conductivity change between a pair of microelectrodes, can be detected by the proposed system.

7.2 The CMOS advantages

Throughout the course of this research, the question was often raised, why CMOS? CMOS posses some very useful advantages, in particular multiplexing, on-chip signal processing, leading to capabilities of handling large microelectrode array sizes. In the field of pathogenic bacteria detection, the ultimate goal is to detect various pathogen species in real-time with high accuracy and specificity. To increase the screening speed, the signal collected on the microelectrodes should be processed in a parallel manner. By increasing the number of the microelectrodes, the accuracy and throughput are improved. Without multiplexing, the number of microelectrode pairs is limited to the number of interfaces to the outside(e.g. commercial systems typically offer 64 electrodes). Furthermore, processing (saving and transferring) the large volume of data produced by a large electrode array is cumbersome if the system is not integrated. On-chip circuitry could be used to implement on-chip signal processing algorithms to reduce the

volume of data. For example, circuitry could be used to detect impedance variations and the chip output could be the waveform width or event frequency. On the other hand, CMOS is relatively expensive to develop and post-processing is complex. If only a few measurements are necessary, the cost of a CMOS system may not be justifiable. Finally, the complexity of working with CMOS technology may preclude its widespread use by biologists or biochemists.

7.3 Main achievements

The ultimate goal of this research was to develop a field-exploited, automatic and integrated biosensor for single pathogenic bacterium or microparticle detection. In this research, we were trying to address several essential aspects which include sensitivity, throughput, specificity of detection, automation and cost effectiveness. The main achievements of this thesis are summarized below.

1) Sensitivity

As a kind of biosensor, sensitivity is one of the most important parameters. Traditional methods using electrochemical detection all depend on bench top instruments to realize the sensitivity needed to detect single microparticle or bacterium. In this research, we proposed and validated two solutions to provide the required sensitivity. Firstly, face to face electrodes were used to enhance the sensitivity of electrodes. Compared with planar electrodes, face to face orientation shrinks the detection volume and decreases the crosstalk among electrodes, thus increases the signal to noise ratio. Secondly, a novel sensing circuit was developed. Considering the dielectric property of most biological cells, instead of using complex signal conditioning and process circuitry, the proposed sensing mechanism is relatively simple but extremely sensitive to the impedance variations caused by the bacterial cells. By monolithically integrating the microelectrode array directly into a CMOS chip, the environmental impacts and background noise are significantly minimized. The simulation of the physical model and electric circuit and preliminary experiment results all proved that the feasibility of detecting single bacterial cell or microparticles.

2) Throughput

Bacteria, especially when they are pathogen, must be identified as soon as possible. This is very critical in food industry, battle field or hospital. Biosensors capable of detecting them are required, and such biosensor would be invaluable if they were able to process samples in parallel and to report results as soon as possible. To address these issues, we proposed a novel electrode structure, which not only allows high density of microelectrode to be implemented, but allows continuous detection by flowing aqueous samples through microchannels between electrodes, which would significantly increase the throughput. By using traditional planar electrode array, a sample amplification step is required, generally taking from several hours to days. It is also quite time consuming to wait for the targeted bacterial cells to approach the detection area, mostly by diffusion, which is a very slow process under the condition of low Reynolds numbers. Although more experimental validation is required, with the proposed structure, targeted bacterial cell or microparticles could be brought to a detection area by injecting a sample flow directly into the microchannels with electrode pairs on the wall. The requirement for pre-amplification is minimized and signal collected on each electrode pairs can be processed timely by on-chip circuitry, the detection results can be available almost in real-time.

3) Integration and Automation

This research is the first exploration of a monolithic integrated system that embeds an array of face to face microelectrodes into a CMOS chip. As simulation results have shown in Chapter 4, a face to face microelectrode array offers better sensitivity than a planar microelectrode array, but the conventional face to face electrode fabrication process is complex and expensive. This research proposed and validated a novel fabrication method using CMOS technology to fabricate large arrays of face to face microelectrodes and sensing circuits on a single CMOS chip. By monolithic integration with CMOS, the on-chip circuits are directly connected with the on-chip electrode array, where signals are extracted and processed automatically. By this means, the impact of the environment is greatly reduced. Benefiting from the well developed CMOS technology, signal processing and analysis can be realized easily on chip and detection results can be presented to end-users in real time; by integrating with sensors, e.g. optical sensor or chemical sensor, the functionalities of the bio-sensor can be expanded further. Moreover, it is

expected that such an integrated biosensor would produce more reliable and repeatable results. It is also potentially very cost effective for mass fabrication.

4) Specificity

Besides measuring the concentration of some bacterial in a sample, an effective biosensor should also be able to distinguish different types of bacteria. In this research, a new method of using bio-carriers to achieve specificity was investigated. This approach combined conventional an antibody-antigen binding method with a magnetotactic bacterial based bio-carrier to realize rapid and specific detection. Different from widely adopted microbead based immunoassay, magnetotactic bacterial are introduced to accelerate the binding process and to enhance sensing efficiency. Controlled by external magnetic field, groups of magnetotactic based bio-carriers, functionalized with specific antibody, screen the sample and catch the target bacteria, then bring them to the detection area, where the microelectrode array is implemented. Fundamental research has been conducted to characterize the chosen magnetic bacteria, MC-1. Experimental results achieved so far indicated that MC-1 is the fastest magnetic bio-carrier ever reported. The quick response time, high controllability and ease of cultivation, make MC-1 a very promising bio-carrier in the proposed biosensor.

5) Through CMOS substrate via fabrication process

This research explored the feasibility of using the FIB technology to realize through substrate via structure on a CMOS die. Experimental results indicated that through via array with aspect ratio up to 10: 1 can be constructed on a thinned CMOS die by FIB technology, which offers an option to researchers who are not able to access DRIE equipment. Our research allowed us to obtain a maximum drilling depth of 100 μm using FIB, which to the best of our knowledge, has not been reported before in literature.

7.4 Future work

The achievements listed above validated the proposed concepts. The reported preliminary experimental results are promising. In order to reach the ultimate goal, several improvements need to be considered as future efforts. .

First of all, a reliable, repeatable and cost effective CMOS-post processing method needs to be developed to implement a large through substrate microchannel array on a CMOS die. More efforts need to be invested to implement TSV on a CMOS die that would be compatible with the proposed electrode structure with small feature size, e.g., less than 10 μm. As discussed in Chapter 3 and Chapter 6, the size of the microchannel, as the detection volume, directly affect the sensitivity of the biosensor. DRIE technology is widely adopted to fabricate TSVs on silicon substrate. The DRIE process offers a capability of fabricating large TSV arrays on a CMOS chip all at the same time, which was a major challenge in our research. With the rapid development in 3D-IC industry, the size of TSV is getting smaller and density of TSV on a single CMOS chip is increasing. If the same technology could be used in this research, it would further increase the sensitivity and throughput of the biosensor proposed. It should be noted that TSV technologies emerged while we were conducting this research and they were certainly not available for us to use in a timely way. If some vendors now offer TSV technologies, it is not routinely available as a standard option on widely available CMOS technologies and the compatibility of these techniques with the proposed electrode structure remains to be demonstrated.

Secondly, the long-term reliability of the CMOS lab-on-chip should also be investigated. For example, issue that need consideration include: erosion on the microelectrode array, contamination on the package (particularly the sodium ions that are known to be very harmful), clogging in the microchannel induced by samples, etc.. They will have impact on the performance and reusability of the biosensor. At this stage, reusability of the biosensor appears to be an elusive goal and the type of proposed biosensor will probably first appear in the form of expendable components with lifetimes measured in minutes and possibly hours.

Thirdly, although the magnetic bacteria based bio-carriers are expected to achieve sensing specificity, this method also introduces more complexity: The biocompatibility of the magnetic bacteria with targeted pathogenic bacteria needs further investigation. In the meantime, an efficient and reliable bio-affinity protocol should be developed in order to immobilize two different kinds of antibodies (one for the MTB, the other for targeted bacterium) on the same microbead to realize the specific detection. Hence, a more efficient and reliable way to achieve specificity should be developed, which is a challenge faced by almost all electrochemical based

biosensors. One possible solution is to functionalize the microelectrode array directly instead of introducing microbeads, for example, binding antibody or biotin on the surface of the microelectrode to capture the target bacterium. However, one of the major constrains of this solution is that only one type of bacteria can be detected on a chip, since only one kind of antibody or biotin can be bound on a microelectrode array and the chip cannot be reused. Still, it may be worth using this method when dealing with highly contingent and fatal pathogens. Another approach to address this problem is to establish a bacterial electrochemical properties database using the proposed biosensor; by measuring the impedance of the different strains of bacteria, the electrochemical properties of a single bacterium are collected, sorted, and built into a database. With the database in each system, by measuring the electrical properties of the bio-entity passing between a pair of microelectrode and compare the signal with on-chip bacterial database, the specific detection can be realized. This method will not require additional surface functionalization and parallel detection can be achieved. It will be more efficient and independent than traditional bio-affinity methods. By this means, the biosensor will become a multi-bacteria detection platform for high throughput screening of pathogens and the chip itself could be reusable. However, to establish the database, significant time and efforts need to be invested.

Finally, a dedicated package needs to be developed for field deployed of the biosensor, the package will not only provide a fluidic interface for introducing sample and sample and maintaining the flow through the microchannels, but also provide an electronic interface to connect to the outside world for the purpose of results analysis, data readout and storage. With the increase density of TSV/Microchannels, the package should also provide enough mechanical strength to support the CMOS die.

Although more efforts need to be invested, we have a strong belief that combining the microfluidics with CMOS will be the main success factor for biosensors. With the development of multiple chip module and 3D IC technology, a stand-alone lab-on-chip system, comprising a power module, sensing and signal processing module, and wireless communication module, will be able to detect single pathogenic bacterium automatically and in a real-time manner. Such a system could find numerous applications in food and agricultural industry, clinical trial, point of care, disease control and prevention.

REFERENCES

[1] PS. Mead, L.Slutsker , V. Dietz , LF.McCaig, Js.Bresce, C.Shapieo, PM.Griffin, RV.Tauxe , "Food-Related Illness and Death in the United States," Emerging Infectious Diseases journal, vol. 5, No. 5, pp. 607-625 , 1999.

[2] J. Meng, and M.P. Doyle, "Emerging and evolving microbial foodborne pathogens," Bulletin de L'Institut Pasteur, vol. 96, pp.151-164, 1998.

[3] R.L. Buchanan, M.P.Doly. "Foodborne desease significance of E.Coli O157:H7 and other enterohemorrhagic E.Coli," Food Technol., vol. 51, No. 10, pp. 69-76, 1997.

[4] K, Helrigh, Official Methods of Analysis of the association of official analytical chemists, Vol. 2, 15th ed., AOAC, Arlington, VA, pp.425-497, 1990.

[5] D. Ivnitski et al., "Application of electrochemical biosensors for detection of food pathogenic bacteria," Electroanalysis, vol. 12, No. 5, pp.317-325, 2000.

[6] J.I. Prosser, "Molecular marker systems for the detection of genetically modified microorganisms in the environment". Microbiology, vol. 140, pp. 5–17, 1994.

[7] J. Happel, H. Brenner, "Low Reynolds number hydrodynamics: with special applications to particulate media", 1st pbk. Ed, edn. M. Nijhoff (Distributed by Kluwer, Boston), The Hague Boston Hingham, MA, USA, 1983.

[8] J. P. Brody, P. Yager, R. Goldstein and R. H. Austin, "Biotechnology at Low Reynolds Numbers", Biophys. J., vol. 71, pp. 3430–3441, 1996.

[9] H.C. Berg. "Random Walks in Biology", Princeton University Press", Princeton, NJ, 1993.

[10] G. Fuhr, R. Hagedorn, T. Müller, W. Benecke, B. Wagner, and J. Gimsa, "Asynchronous travelling-wave induced linear motion of living cells," Studia Biophysica , No. 140, pp. 79-102, 1991.

[11] R. Hagedorn, G. Fuhr, T. Müller, and J. Gimsa, "Travelling wave dielectrophoresis of microparticles," Electrophoresis, No. 13, pp. 49-54, 1992.

[12] J. Suehiro and R. Pethig, “The dielectrophoretic movement and positioning of a biological cell using a three-dimensional grid electrode system,” Journal of Physics D, Applied Physics, No. 31, pp. 3298-3305, 1998.

[13] L. Cui and H. Morgan,” Design and fabrication of travelling wave dielectrophoresis structures,” J. Micromech. Microeng., No. 10, pp. 72–79, 2000.

[14] H. Morgan, M.P. Hughes, and N.G. Green, “Separation of submicron bioparticles by dielectrophoresis,” Biophys. J., vol. 77, pp. 516–525, 1999.

[15] J. Yang, Y. Huang, X.B. Wang, F.F. Becker, and P. Gascoyne, “Cell separation on microfabricated electrodes using dielectrophoretic/gravitational field flow fractionation,” Anal.Chem., vol. 71, pp. 911–918, 1999.

[16] C. Iliescu, L. Yu, G. Xu, and F. E. H. Tay,” A Dielectrophoretic Chip With a 3-D Electric Field Gradient”, J. Microelectromechinical Microsystems, vol. 15, No. 6, pp.1506-1513, 2006

[17] U. Seger-Sauli, M. Panayiotou, S. Schnydrig, M. Jordan, and P. Renaud, "Temperature measurements in microfluidic systems: Heat dissipation of negative dielectrophoresis barriers ", Electrophoresis, No. 26, pp. 2239-2246, 2005.

[18] M. Yamada and M. Seki, “Microfluidic particle sorter employing flow splitting.and recombining,” Anal. Chem., vol. 78, pp. 1357–1362, 2006.

[19] M. P. MacDonald, G. C. Spalding, and K. Dholakia, “Microfluidic sorting in an optical lattice” Nature, vol. 426, pp. 421-424, 2003.

[20] H. Watarai, M. Suwa, and Y. Iiguni," Magnetophoresis and electromagnetophoresis of.microparticles in liquids". Anal.Bioanal.Chem., vol. 378, No. 7, pp.1693–1699, 2004.

[21] PS. Mead, L.Slutsker , V. Dietz , LF.McCaig, Js.Bresce, C.Shapieo, PM.Griffin, RV.Tauxe , “Food-Related Illness and Death in the United States,” Emerging Infectious Diseases journal, vol. 5, No. 5, pp. 607-625 , 1999.

[22] J. Meng, and M.P. Doyle, “Emerging and evolving microbial foodborne pathogens,” Bulletin de L'Institut Pasteur, vol. 96, pp.151-164, 1998.

[23] R.L. Buchanan, M.P.Doly. “Foodborne disease significance of E.Coli O157:H7 and other enterohemorrhagic E.Coli,” Food Technol., vol. 51, No. 10, pp. 69-76, 1997.

[24] FDA, Food Protection Plan. Department of health and human services. Maryland: U.S. Food and Drug Administration; 2007.

[25] Y.Okon, S.L. Alerecht, and R.H. Burris, " Methodds for Growing Spirillum lipoferum and for counting it in pure culture and in association with plants", Applied and Environmental microbilooty, vol, 33, pp. 85-88, 1977.

[26] K. Helrich, "Official Methods of Analysis of the Association of Official Analytical Chemists", Microbiological Methods, vol. 2, pp. 425–497, 1990

[27] C.W.Kaspar, C. Tartera, "Methods for detecting microbial pathogens in food and water", Methods Microbiol. vol.22, pp. 497–530, 1990

[28] M.Tietjen, D.Y.C.Fung, "Salmonella and food safety", Crit. Rev. Microb. vol.21, pp.53–83, 1995

[29] B. W.Brooks, C. L J. Devenish, D.Lutze-Wallace, R. Milnes, H. Robertson, and G. Berlie-Surujballi, "Evaluation of a monoclonal antibody-based enzyme-linked immunosorbent assay for detection of Campylobacter fetus in bovine preputial washing and vaginal mucus samples", Vet. Microbiol. vol.103, pp. 77-84, 2004

[30] T. E. Besser, B. L. Richards, D. H. Rice and D. D. Hancock, "Escherichia coli O157:H7 Infection of Calves: Infectious Dose and Direct Contact Transmission," Epidemiology and Infection, vol. 127,pp. 555-560, 2001

[31] B.H.Pyle, S.C. Broadaway, and G.A. McFeters ,"Sensitive detection of Escherichia coli O157:H7 in food and water by immunomagnetic separation and solid-phase laser cytometry", Applied and Environmental Microbiology, vol. 65, pp.1966–1972, 1999

[32] K.Mullis, F. Faloona, S.Scharf, R. Saiki, G.Horn, H.Erlich, Cold Spring Harbor Symposia on Quantitative Biology 51, pp,263–273.1986

[33] I. Smolina, C.Lee, and M. Frank-Kamenetskii , "Detection of Low-Copy-Number Genomic DNA Sequences in Individual Bacterial Cells by Using Peptide Nucleic Acid-Assisted Rolling-Circle Amplification and Fluorescence In Situ Hybridization", Appl Environ Microbiol, vol. 73, pp.2324–2328, 2007

[34] J.Zhou, "Microarrays for bacterial detection and microbial community analysis", Current Opinion in Microbiology, vol.6, pp.288-294, 2003

[35] E.M. Southern, "Detection of specific sequences among DNA fragments separated by gel electrophoresis", Journal of Molecular Biology, vol. 98, pp. 503-517, 1975

[36] Rodr´ıguez-L´azaro, D., D. A. M., Herrewegh, A., Pla, M., Cook, N., Ikonomopoulos, J., 2005. Int. J. Food Microbiol. 101, 93–104.

[37] A.Jofr´e, M. B., M.Garriga, M.Hugas, M.Pla, D. Rodr´ıguez-L´azaro, T.Aymerich, "Simultaneous detection of Listeria monocytogenes and Salmonella bymultiplex PCR in cooked ham", Food Microbiol. vol.22, pp. 109–115, 2005

[38] E. Howeand G. Harding, "A comparison of protocols for the optimisation of detection of bacteria using a surface acoustic wave (SAW) biosensor", Biosensors and Bioelectronics, vol.15, pp.641-649, 2000

[39] A.K.Deisingh, T.M. ," Strategies for the detection of Escherichia coli O157:H7 in foods", J. Appl. Microbiol. vol.96, pp.419–429, 2004

[40] J.M.Simpson, and D.V.Lim, "Rapid PCR confirmation of E. coli O157:H7 after evanescent wavefiber optic biosensor detection," Biosens. Bioelectron. vol.21, pp.881-887, 2005

[41] A. Touron, B.T., B.Pawlak, F. Petit, "Detection of Salmonella in environmental water and sediment by a nested-multiplex polymerase chain reaction assay",Res. Microbiol. vol.156, pp. 541–553, 2005

[42] N.C.Cady , M.V.S. Kunnavakkam, C.A. Batt, "Real-time PCR detection of Listeria monocytogenes using an integrated microfluidics platform", Sens. Actuators B. vol.107, pp. 332–341, 2005

[43] L.Yang, Y. Li, G.F.Erf, "Impedance Immunosensor for Detection of Escherichia coli O157:H7", Anal. Chem. vol.76, pp.1107–1113, 2004

[44] B.M.Willardson, J.F.Wilkins, T.A.Rand,J.M.Schupp,K.K.Hill,P.Keim, P.J.Jackson, , ," Development and Testing of a Bacterial Biosensor for Toluene-Based Environmental Contaminants", Appl. Environ. Microbiol.Vol.63, pp.1006–1012, 1998.

[45] J. Tschmelak, G.Proll, G. Gauglitz, "Ultra-sensitive fully automated immunoassay for detection of propanil in aqueous samples: steps of progress toward sub-nanogram per liter detection.",2004. Anal.Chim. Acta, vol.519, pp.143–146, 2004

[46] Y.M.Bae, B.K.Oh, W.Lee,W.H. Lee, J.W.Choi, "Detection of insulin-antibody binding on a solid surface using imaging ellipsometry", Biosens. Bioelectron., vol.20, pp. 895–902, 2004

[47] Marion G. Macey, Flow Cytometry: Principles and Applications, Humana Press; 1 edition, 2007

[48] F.F. Mandy, M.Bergeron, D.Recktenwald, C.A. Izaguirre, “A simultaneous three-color T cell subsets analysis with single laser flow cytometers using T cell gating protocol comparison with conventional two-color immunophenotyping method”, Journal of Immunological Methods, vol.156, pp.151-162, 1992

[49] M. Zourob, Principles of Bacterial Detection: Biosensors, Recognition Receptors and Microsystems, Springer , 2008

[50] M.A.Cooper, “Label-free screening of bio-molecular interactions”, Anal. Bioanal. Chem., vol 377, pp. 834–842, 2003

[51] X.D. Hoa, A.G. Kirk, M. Tabrizian, “Towards integrated and sensitive surface plasmon resonance biosensors: A review of recent progress”, Biosensors and Bioelectronics, vol.23, pp. 151-160, 2007

[52] A.D.Taylor, Q.Yu, S.Chen, J.Homola, S.Jiang, “Comparison of E. coli O157:H7 preparation methods used for detection with surface plasmon resonance sensor”,. Sens. Actuators B, vol.107, pp.202–208, 2005.

[53] B.K.Oh,W.Lee, B.S.Chun, Y.M.Bae, W.H. Lee, J.W. Choi, “The fabrication of protein chip based on surface plasmon resonance for detection of pathogens”, Biosens.Bioelectron. vol.20, pp.1847–1850, 2005

[54] J.R.Crowther, ELISA Theory and Practice. Humana Press Inc., USA, 1995

[55] H.Ueda, K.Tsumoto , K. Kubota1, E.Suzuki, T.Nagamune, H. Nishimura, P.A. Schueler, G.Winter, I.Kumagai and W. C. Mahoney ,”Open sandwich ELISA: A novel immunoassay based on the interchain interaction of antibody variable region”, Nature Biotechnology vol.14, pp.1714 – 1718, 1996

[56] Y.Mine, “Separation of Salmonella enteritidis from experimentally contaminated liquid eggs using a hen IgY immobilized immunomagnetic separation system”, J. Agric. Food Chem. vol.45, pp.3723–3727, 1997

[57] A. M. Gijs,”Magnetic bead handling on-chip: new opportunities for analytical applications”, Microfluid Nanofluid, vol.1 pp.22–40, 2004

[58] S. K. Sia and G. M. Whitesides, “Microfluidic devices fabricated in PDMS for biological studies”, Electrophoresis, vol. 24, pp.3563–3576, 2003

[59] K. L. Helton and P. Yager, “Interfacial instabilities affect microfluidic extraction of small molecules from non-Newtonian fluids,” Lab on a Chip, vol.7, pp.1581–1588, 2007

[60] A. E. Kamholz, B. H. Weigl, B. A. Finlayson and P. Yager, “Quantitative analysis of molecular interaction in a microfluidic channel: the T-sensor”, Analytical Chemistry,vol.71, pp.5340–5347, 1999

[61] D.R. Baselt, G.U.Lee, M.Natesan, S.W.Metzger, P.E.Sheehan, R.J. Colton, “A biosensor based on magnetoresistance technology”,Biosens. Bioelectron. vol.13, pp.731–739, 1998

[62] P.A. Besse, G. Boero, M. Demierre, V. Pott, R. Popovic, Detection of a single magnetic microbead using a miniaturized silicon Hall sensor, Appl. Phys. Lett., vol.80, pp.4199-4201, 2002

[63] A.L.Olivier , F. Javier Del Campob, F. Xavier Mu˜noz, “ Pathogen detection: A perspective of traditional methods and biosensors “, Biosensors and Bioelectronics, vol. 22, pp. 1205–1217, 2007

[64] Eggins, B.R., 2002. Chemical Sensors and Bisensors.John Wiley & Sons Ltd.

[65] E. Katz and I. Willner, “Probing Biomolecular Interactions at Conductive and Semiconductive Surfaces by Impedance Spectroscopy: Routes to Impedimetric Immunosensors, DNA-Sensors, and Enzyme Biosensors,” Electroanalysis, vol.15, pp. 913-947, 2003.

[66] I. Abdel-Hamid, D. Ivnitski, P. Atanasov, E.Wilkins,” Flow-through immunofiltration assay system for rapid detection of E. coli O157:H7”, Biosens. Bioelectron. vol.14, pp.309–316, 1999

[67] P. Bergveld,” Thirty years of ISFETOLOGY, What happened in the past 30 years and what may happen in the next 30 years”, Sens. Actuators B Chem. vol.88, pp.1–20, 2003

[68] J.Munoz, C.Jimenez, A.Bratov, J.Bartroli, S.Alegret, C.Dominguez, “A fully electronic label-free dna sensor chip”, Biosens. Bioelectron. vol.12, pp.577–585, 1997

[69] J.R.Sandifer, J.J.Voycheck, “ A Review of Biosensor and Industrial Applications of pH-ISFETs and an Evaluation of Honeywell's DuraFET”, Mikrochim. Acta., vol.131, pp. 91–98, 1999

[70] E. Barsoukov, J.R.Macdonald, Impedane Spectroscopy Theory, Experiment and Applications. John Wiley & Sons Ltd., Hoboken, New Jersey. 2005

[71] C. Gabrielli, Identification of Electrochemical Processes by Frequency Response Analysis. Solartron Analytical, 1990
http://www.solartronanalytical.com/technicalsupport/technicalnotes/index.php.

[72] E. Katz and I. Willner, “Probing Biomolecular Interactions at Conductive and Semiconductive Surfaces by Impedance Spectroscopy: Routes to Impedimetric Immunosensors, DNA-Sensors, and Enzyme Biosensors,” Electroanalysis, vol.15, pp. 913-947, 2003.

[73] L.Yang, Y.Li, G.F.Erf, "Impedance Immunosensor for Detection of Escherichia coli O157:H7", Anal. Chem. 76, 1107–1113, 2004

[74] Grimnes, S., Martinsen, O., 2000. Bioimpedance and Bioelectricity Basics.Academic Press.

[75] V. M. Mirsky, M. Riepl and O. S. Wolfbeis," Capacitive monitoring of protein immobilization and antigen-antibody reactions on monomolecular alkylthiol films on gold electrodes", Biosenors Bioelectron.vol.12, pp. 977–989, 1997.

[76] E.C.Alocilja, S.M.Radke, "Market analysis of biosensors for food safety", Biosens. Bioelectron., vol.18, pp.841–846, 2003

[77] Z. Muhhammad-Tahir, E.C. Alocilja, "A conductometric biosensor for biosecurity",2003. Biosens.Bioelectron.,vol.18, pp.813–819, 2003

[78] K. G. Ong, C. A. Grimes, C. L. Robbins, and R. S. Singh, "Design and application of a wireless, passive, resonant-circuit environmentalmonitoring sensor," Sens. Actuators A, Phys., vol. 93, pp. 33–43, 2001

[79] S.M. Radke and E.C. Alocilja, "A high density microelectrode array biosensor for detection of E. coli O157:H7", Biosens. Bioelectron.,Vol. 20, pp.1662-1667, 2005

[80] L.G. Carrascosa, M. Moreno, M. Álvarez and L.M. Lechuga, "Nanomechanical biosensors: a new sensing tool 2006",. Trac-Trends Anal. Chem. vol.25, pp.196–206, 2006

[81] L. Murphy,"Biosensors and bioelectrochemistry", Curr. Opin. Chem. Biol., vol.10, pp.177–184, 2006

[82] X. Zhao, L. R. Hilliard, S. J.Mechery, Y. Wang, R. P. Bagwe, S. Jin, and W. Tan, "A rapid bioassay for single bacterial cell quantization using bioconjugated nanoparticles ", PNAS, vol. 101, pp. 15027~15032, 2004

[83] R. Go´mez, R. Bashir, A. Sarikaya, MR. Ladisch, J. Sturgis, JP. Robinson, ...S. Wereley, "Microfluidic Biochip for Impedance Spectroscopy of Biological Species", Biomed. Microdevices, vol.3, pp. 201–209, 2001

[84] J.J Gau, E.H.Lan, B.Dunn, C.-M.HO, J.C.S.Woo, "A MEMS based amperometric detector for E. coli bacteria using self-assembled monolayers", Biosens. Bioelectron.16, 745–755, 2001

[85] R. Gomez, R. Bashir, A.K.Bhunia, "Microscale electric detection of bacterium metabolism", Sens. Actuators B Chem., vol.86, pp.198–208, 2002

[86] , E.T.Lagally, J.R.Scherer, R.G. Blazej, N.M.Toriello, B.A. Diep, M.Ramchandani, G.F.Sensabaugh, L.W.Riley, R.A. Mathies, "Integrated portable genetic analysis microsystem for pathogen/infectious disease detection", Anal. Chem. Vol.76, pp.3162–3170, 2004

[87] C. Zhang, D. Xing, Y.Li, "Micropumps, microvalves, and micromixers within PCR microfluidic chips: Advances and trends", Biotechnology Advances, vol. 25, pp.483-514, 2007

[88] C. Zhang, J. Xu, W. Ma, ,"PCR microfluidic devices for DNA amplification", WBiotechnol Adv.vol. 24, pp. 243-84, 2006.

[89] J. Yakovleva, R. Davidsson, M. Bengtsson, T. Laurell, J. Emnéus, "Microfluidic enzyme immunosensors with immobilised protein A and G using chemiluminescence detection", Biosens Bioelectron. vol.19, pp. 21-34, 2003

[90] P. S. Dittrich and P. Schwille,"An Integrated Microfluidic System for Reaction, High-Sensitivity Detection, and Sorting of Fluorescent Cells and Particles", Anal. Chem., vol. 75, pp. 5767–5774, 2003

[91] S. Gawad S, L.Schild, Ph. Renaud, " Micromachined impedance spectroscopy flow cytometer for cell analysis and particle sizing", Lab on a Chip 2001;vol.1, pp. 76–82, 2001

[92] J.H. Nieuwenhuis, F. Kohl, J.Bastemeijer, P.M.Sarro, M.J.Vellekoop, " Integrated Coulter counter based on 2-dimensional liquid aperture control", Sens Actuators B vol.102,pp. 44–50, 2004

[93] D.K.Wood, G.B. Braun, J.L. Fraikin, L.J. Swenson , N.O.Reich, A.N.Cleland,"A feasible approach to all-electronic digitallabelling and readout for cell identification", Lab Chip, vol. 7, pp. 469–474, 2007

[94] H. Morgan, D. Holmes, NG. Green, "High speed simultaneous single particle impedance and fluorescence analysis on a chip,"urr Appl Phys, vol. 6, pp. 367–370, 2008

[95] R. Rodriguez-Trujillo, O. Castillo-Fernandez, M. Garrido, M. Arundell , A.Valencia , and G. Gomila, "High-speed particle detection in amicro-Coulter counter with two-dimensional adjustable aperture", Biosens Bioelectron., vol. 24, pp. 290–296 ,2008

[96] K. Cheung, S. Gawad S, and Ph. Renaud ," Impedance spectroscopy flow cytometry: on-chip label-free cell differentiation", Cytometry A vol 65A, pp. 124–132, 2005

[97] C. Kittel , E. Nascimento, N. Demierre, T. Silva, T. Braschler, Ph. Renaud, and A.G. Oliva ," Label-free detection of Babesia bovis infected red blood cells using impedance spectroscopy on a microfabricated flow cytometer,". Acta Trop, vol. 102, pp. 63–68, 2007

[98] GA. Ferrier, S F. Romanuik , D J. Thomson , G.E. Bridges , and M R. Freeman," A microwave interferometric system for simultaneous actuation and detection of single biological cells",. Lab Chip, vol.9, pp. 3406–3412, 2009

[99] J.D.Plummer, M.D. Deal, P.B. Griffin, " Silicon VLSI Technology: Fundamentals, Practice, and Modeling", 1st ed. , US: Prentice Hall, 2000.

[100] Sherif Sedky, " Post-Processing Techniques for Integrated MEMS", US: Artech House Publishers, 2005.

[101] H. Anthony, D. Graham, C.R. Bowen, J.Taylor and J.Robbins, "Neuronal cell biocompatibility and adhesion to modified CMOS electrodes", Biomed Microdevices vol. 11, pp.1091–1101, 2009

[102] K. T.C. Chai , P.A. Hammond, D.R.S. Cumming, " Modification of a CMOS microelectrode array for a bioimpedance imaging system", Sensors and Actuators B vol.111–112, pp .305–309, 2005.

[103] S. Ayers, K.Berberian, K. D. Gillis, M. Lindau, and B. A. Minch, "Post-CMOS fabrication of working electrodes for on-chip recordings of transmitter Release", IEEE Transactions on Biomedical Circuits and Systems, vol. 4, no. 2, pp. 86~92, 2010

[104]L. Berdondini, P.D. van der Wal, N.F. de Rooij, M. Koudelka-Hep, "Development of an electroless post-processing technique for depositing gold as electrode material on CMOS devices", Sensors and Actuators B, vol.99, pp. 505–510, 2004

[105] "TSMC 0.18 Micron CMOS process flow", provided by MOSIS

[106] "TSMC 0.18 Micron CMOS design rules" , provided by MOSIS

[107] K. Asami , "Dielectric imaging of biological cells", Colloid Polym Sci vol. 273, pp.1095-1097,1995.

[108] K. Asami, " Characterization of biological cells by dielectric spectroscopy," Journal of Non-Crystalline Solids vol.305, pp. 268–277, 2002

[109]S. Gawad, L. Schild and Ph. Renaud, " Micromachined impedance spectroscopy flow cytometer for cell analysis and particle sizing", Lab on a Chip, vol.1, pp.76–82, 2001.

[110] J. Noordegraaf, “Conformal Coating Using Parylene Polymers,” Med. Device Technol., 8(1), pp.14-20, 1997.

[111] G.L. Schnable, L.J. Gallace, H.L. Pujol, “Reliability of CMOS Integrated Circuits," Computer, vol. 11, no. 10, pp. 6-17, 1978.

[112]G. L.Schnable, K.M. Schlesier, C. P. Wu.Comizzoli, and R.B.Comizzoli, “Reliability implications of lateral alkali-ion migration in MOS integrated circuits”, Journal of the Electrochemical Society, vol.141, no.11, pp. 3250-3253,1994

[113]T.Y. Chang, V.G. Yadav, S. De Leo, A. Mohedas, B. Rajalingam, C.L. Chen, S. Selvarasah, M.R. Dokmeci and A. Khademhosseini, “Cell and protein compatibility of parylene-C surfaces” , Langmuir , vol. 23, pp. 11718–11725, 2007

[114] http://engineering.tufts.edu/microfab/index_files/docs/Parylene.pdf

[115] http://www.vp-scientific.com/parylene_properties.htm

[116] C.Hassler, R.P. von Metzen, P. Ruther, T.Stieglitz, “Characterization of parylene C as an encapsulation material for implanted neural prostheses”, Journal of Biomedical Materials Research Part B: Applied Biomaterials, vol. 93B, Issue 1, pp. 266-274, 2010.

[117] L.Yang, Y.Li, Erf GF, “ Interdigitated Array microelectrode-based electrochemical impedance immunosensor for detection of Escherichia coli O157:H7”, Anal Chem. Vol.15, no.76(4), pp.1107-1113, 2004

[118] L.Yang, R. Bashir,“ Electrical/electrochemical impedance for rapid detection of foodborne pathogenic bacteria”, Biotechnol Adv.vol. 26, no.2, pp.135-150. 2008

[119] K. Dill, D. D. Montgomery, W.Wang, J/. C. Tsai,” Antigen detection using microelectrode array microchips”, Analytica Chimica, vol. 444, pp. 69–78, 2001

[120] S.M. Radke, and E. C. Alocilja,” Design and Fabrication of a Microimpedance Biosensor for Bacterial Detection”, IEEE SENSORS JOURNAL, Vol. 4, no. 4, pp. 434-440, 2004

[121]J.El Fouladi, Z.Lu, Y.Savaria and S.Martel, “An integrated biosensor for the detection of bio-entities using magnetotactic bacteria and CMOS technology”, 29th Annual International

Conference of the IEEE Engineering in Medicine and Biology Society (EMBS), Lyon, France, Aug. 23-26, 2007

[122] Z.Lu and S. Martel, "Controlled bio-carriers based on magnetotactic bacteria", The 14th International Conference on Solid-state Sensors, Actuators and Microsystems Lyon, France, June 10-14,pp.683-686, 2007

[123] R. Denomme, Z.Lu, and S. Martel, "A microsensor for the detection of a single pathogenic bacterium using magnetotactic bacteria-based bio-carriers: simulations and preliminary experiments", 29th Annual International Conference of the IEEE Engineering in Medicine and Biology Society (EMBS), Lyon, France, Aug. 23-26, 2007

[124]Z.Lu, and S. Martel, "Preliminary investigation of bio-carriers using magnetotactic bacteria," Proceedings of the 28th IEEE-EMBS Annual International Conference of the Engineering in Medicine and Biology Society, pp. 3415-3418, New York, Aug 30 – Sept. 3, 2006.

[125] Z. Lu and S.Martel "Microfluidic system for assessing the controllability of MC-1 magnetotactic bacteria as carriers in micro-channels," The Nanotechnology Conference and Trade Show (NSTI) Nanotech, Boston, MA, USA, May 7-11, 2006.

[126] R D. Cook, D S. Malkus, M E. Plesha, and R J. Witt Concepts and Applications of Finite Element Analysis, 4th Edition Wiley, 2001

[127] C C. Mcintyre and W M. Gril ,"Finite Element Analysis of the Current-Density and Electric Field Generated by Metal Microelectrodes"Annals of Biomedical Engineering, Vol. 29, pp. 227–235, 2001

[128] J R. Buitenweg, W L.C. Rutten, and E. Marani, "Geometry-Based Finite-Element Modeling of the Electrical Contact Between a Cultured Neuron and a Microelectrode", IEEE Transactions on Biomedical Engineering, vol. 50, no. 4, pp. 501-509 2003

[129] S. Cho and H. Thielecke, " Design of electrode array for impedance measurement of lesions in arteries",Physiol. Meas., vol. 26, pp.19–26, 2005

[130] J W. Wang, M. Wang, and L. Jang, "Effects of electrode geometry and cell location on single-cell impedance measurement", Biosensors and Bioelectronics, vol 25, 6, pp.1271-1276, 2010

[131] D S. Gray, J L. Tan, J. Voldman, and C S. Chen, “Dielectrophoretic registration of living cells to a microelectrode array” , Biosensors and Bioelectronics, vol 19, 12, pp. 1765-1774, 2004

[132] W E. Morf, M. Koudelka-Hep, and N. F. de Rooij, “Theoretical treatment and computer simulation of microelectrode arrays”, Journal of Electroanalytical Chemistry, vol 590, 1, pp.47-56, 2006

[133] R. Field, and M. Ghovanloo, “Finite element analysis of planar micromachined silicon electrodes for cortical stimulation,” IEEE EMBS Special Topic Conf. On Microtechnologies in Med. and Biol., pp. 297-300, 2006

[34] X. Huang, D. Nguyen, D W. Greve, and M M. Domach, “Simulation of Microelectrode Impedance Changes Due to Cell Growth”, IEEE SENSORS JOURNAL, vol 4, 5, pp. 576-583, 2004

[135] C. Gabrielli, M. Keddam, P. Rousseau, V. Vivier, “Numerical Simulation of the Electrochemical Impedance of a Microelectrode using FEMLAB”, Proceedings of the COMSOL Multiphysics User's Conference, Paris, 2005.

[136] CMC microsystem, MicraGEM user guide, 2007

[137] C. D. Ferris, Introduction to Bioelectrodes, Plenum Press, New York, 1974

[138] K. H. Schoenbach, F. E. Peterkin, S. J. Beebe, D. Byars, R. W. Alden, III, P. Adolphson, and T. Turner, “Effect of pulsed electric fields on micro-organisms: experiments and applications”, IEEE Transcations on Plasma Science, vol. 25, 2, pp.284-292, 1997.

[139] H. Huelsheger, J. Potel, and E.-G.Niemann, “Electric field effects on bacteria and yeast cells,” Radiat. Environ. Biophys., vol. 22, p. 149, 1983.

[140] T.B. Jones, Electromechanics of Particles, Cambridge: Cambridge University Press, 1995.

[141] L. Conyers, “Relative Dielectric Permittivity (RDP),” University of Denver, 1989

[142] J.J Licari, L.A. Hughes, Handbook of Polymer Coatings for Electronics, 2nd ed., n.p.: William Andrew Publishing/Noyes, 1990.

[143] K. Cheung K, S.Gawad, and Ph. Renaud Ph, “Impedance spectroscopy flow cytometry: on-chip label-free cell differentiation”, Cytometry A vol 65A, pp 124–132, 2005

[144] S. Gawad , L. Schild L, and Ph.Renaud, “Micromachined impedance spectroscopy flow cytometer for cell analysis and particle sizing”, Lab on Chip, vol 1, pp 76–82, 2001

[145] S.Gawad S, T. Sun , NG.Green, and H.Morgan ," Impedance spectroscopy using maximum length sequences: application to single cell analysis", Rev Sci Instrum vol. 78, pp 054301 - 054301-7 ,2007.

[146] S. Gabriel, RW. Lau and C. Cabriel, " The dielectric properties of biological tissues: II. Measurements in the frequency range 10Hz to 20GHz", Phys. Med. Biol vol 41, pp 2251-2269, 1996

[147] P. Mirtaheri, S. Grimnes and Ørjan G. Martinsen, " Designing a PtCO2 sensor based on conductivity measurements", IFMBE Proceedings, Vol 17, Part 9, pp 300-303,2007

[148] G J. Tortora, B R. Funke, and C L. Case, Microbiology: An Introduction, 8th edition, Benjamin Cummings; 2003

[149] K. Asami, T. Hanai and N. Koizumi,"Dielectric analysis of Escherichia coli suspensions in the light of the theory of interfacial polarization", Biophysical Journal, Vol 31, 2, pp.215-228, 1980

[150] T.B. Jones, Electromechanics of Particles, Cambridge: Cambridge University Press, 1995.

[151] S. Gawad, K. Cheung, U. Seger, A. Bertsch, and P. Renaud, "Dielectric spectroscopy in a micromachined flow cytometer: theoretical and practical considerations," Lab on a Chip, vol. 4, pp. 241-251, 2004.

[152] www.cmc.ca

[153] www.mosis.com

[154] C L. Dai, "A maskless wet etching silicon dioxide post-CMOS process and its application", Microelectronic Engineering, vol.83, pp.2543-2550, 2006

[155] F.Heer, W. Franks, A. Blau, S. Taschini, C. Ziegler, A. Hierlemann and H. Baltes, "CMOS microelectrode array for the monitoring of electrogenic cells", Biosensors and Bioelectronics, vol. 20, pp. 358-366, 2004

[156] B. Eversmann, M. Jenkner, C. Paulus, F. Hofmann, R. Brederlow, P. Fromherz, F. Brenner, M. Schreiter, R. Gabl, K. Plehnert, M. Steinhauser, G. Eckstein, D.Schmitt-Landsiedel, R. Thewes, "A 128 × 128 CMOS bio-sensor array for extracellular recording of neural activity ", 2003 IEEE Int. Solid State Circuits Conf., pp. 222–223, 2003

[157] B.Warneke and K. S. J. Pister, "In situ characterization of CMOS post-process micromachining", Sensors and Actuators A: Physical, vol. 89, pp. 142-151, 2001

[158] O. Tabata, R. Asahi, H. Funabashi, K. Shimaoka and S. Sugiyama, “Anisotropic etching of silicon in TMAH solutions ”, Sensors and Actuators A: Physical, vol.34, pp. 51-57, 1992

[159] H. Seidel , L. Csepregi , A. Heuberger , H. BaumgSrtel “Anisotropic Etching of Crystalline Silicon in Alkaline Solutions”, J. Electrochem. Soc., vol. 137, No. 11, pp. 3612-3626, 1990

[160] L. Chang; M.Ieong and M. Yang,” CMOS Circuit Performance Enhancement by Surface Orientation Optimization.”, IEEE Transactions on Electron Devices, vol. 51, pp.1621-1627, 2004

[161]G.T.A. Kovacs , N.I. Maluf and K.E. Petersen,” Bulk micromachining of silicon”, Proc. of the IEEE, vol. 86, pp. 1536-1551, 1998

[162] R. Jacob Baker,CMOS Circuit Design, Layout and Simulation, 2nd Edition, Wiley-IEEE Press, 2004

[163]J. D. Plummer,M. D. Deal , P. B. Griffin , Silicon VLSI Technology: Fundamentals, Practice, and Modeling, Prentice Hall, 2000

[164] Stephen A. Campbell, “The Science and Engineering of Microelectronic Fabrication”, Oxford University Press, 2001

[165] C.H.Chen, C H. Fang, Y K. Yang and C W.Tang, “ A deep submicron CMOS process compatible suspending high-Q inductor”, IEEE Electron Device Letters, vol. 22, pp. 522-523, 2001

[166] xP DualBeam System User’s Guide, FEI, 2003

[167] L. A. Giannuzzi and F. A. Stevie, “A review of focused ion beam milling techniques for TEM specimen preparation”, Micron, vol.30, pp. 197-204, 1999

[168] C. R. Musil, J.L. Bartelt, and J. Melingailis, "Focused Ion Beam Microsurgery for Electronics", IEEE Electron Device Letters, vol. EDL-7, pp. 285-287, 1986

[169] C.A.Volkert and A.M. Minor,”Focused Ion Beam Microscopy and Micromachining”, MRS Bulletin, vol. 32, pp. 389-395, 2007

[170]Richard WIRTH, “Focused Ion Beam (FIB): A novel technology for advanced application of micro- and nanoanalysis in geosciences and applied mineralogy”,European Journal of Mineralogy; vol. 16; no. 6; pp. 863-876, 2004

[171]R.R. NistalaTan, C.W. Hua, and Y.N. Zhao, “Development of FIB-based Charge Reduction Methods for Auger Electron Spectroscopy and Their Application in Failure Analysis”,

13th International Symposium on the Physical and Failure Analysis of Integrated Circuits, Singapore pp.67-70, 2006

[172] J.M.Cairney and P.R. Munroe, Redeposition effects in transmission electron microscope specimens of FeAl-WC composites prepared using a focused ion beam miller", Micron, vol.34, pp. 97–107, 2003

[173] J.M.Cairney, R.D.Smith, and P. R. Munroe, "Transmission electron microscope specimen preparation of metal matrix composites using the focused ion beam miller ". Microsc. Microanal.vol. 6, pp.452–462, 2000

[174] Y.Q. Fu, N.K.A. Bryan, O.N. Shing and N.P. Hung," Influence of the Redeposition effect for Focused Ion Beam 3D Micromachining in Silicon", Int J. Adv. Manuf. Technol., vol. 16, pp.877–880, 2000

[175] S. Rubanov and P. R. Munroe," FIB-induced damage in silicon" , Journal of Microscopy , vol. 214, , pp. 213–221, 2004

[176] http://www.alcatelmicromachining.com/amms_en/download/docs/news/doc180.pdf

[177] C. M. Waits, B. Morgan, M. Kastantin, R. Ghodssi, "Microfabrication of 3D silicon MEMS structures using gray-scale lithography and deep reactive ion etching ", Sensors and Actuators A: Physical, vol.119, , pp. 245-253, 2005

[178] C.D. Natale, A. D'Amico, and P. Siciliano, "Advances in Deep Oxide Etch Processing for MEMS-mask Selection", Sensors and microsystems: proceedings of the 5th Italian Conference, Italy, pp. 300-307, 2000

[179] C H. Lin, G B. Lee, B W, Chang and G L. Chang, "A new fabrication process for ultra-thick microfluidic microstructures utilizing SU-8 photoresist", J. Micromech. Microeng. vol. 12, pp. 590–597, 2002

[180] http://www.az-em.com/

[181] K. Stephan, P. Pittet, L. Renaud, P. Kleimann, P. Morin, N. Ouaini and R. Ferrigno, "Fast prototyping using a dry film photoresist: microfabrication of soft-lithography masters for microfluidic structures ",J. Micromech. Microeng. vol.17, 2007

[182] http://www2.dupont.com/APL/en_US/assets/downloads/pdf/DryFilmSolutionforTSV.pdf

[183] J. Zhang, M B. Chan-Park and R. Conner, "Effect of exposure dose on thereplication fidelity and profile of very high aspect ratio microchannels in SU-8," Lab on a chip, vol.4 pp. 646-653,2004

[184] J. Noordegraaf, “Conformal Coating Using Parylene Polymers,” Med. Device Technol., vol.8, pp. 14-20,1997.

[185] T.G. Yuen, W.F. Agnew, L.A. Bullara, “Tissue Response to Potential Neuroprosthetic Material Implanted Subdurally,” Biomaterials, vol. 8, pp. 138-141, 1987.

[186] F. Jaspard and M. Nadi,” Dielectric properties of blood: an investigation of temperature dependence”, *Physiol. Meas.* Vol 23, pp. 547, 2002.

[187] www.ocean-sci-discuss.net/7/773/2010/osd-7-773-2010.pdf

[188] R P. Blakemore, “Magnetotactic bacteria”, Science, vol 190, pp. 377, 1975.

[189] D.A. Bazylinski and RB. Frankel, “magnetosome formation in prokaryotes”, Nat Rev Microbiol.vol2, pp. 217-30, 2004

[190] F C. Meldrum et al, “Electron Microscopy Study of Magnetosomes in a Cultured Coccoid Magnetotactic Bacterium”, Proceedings: Biological Sciences, vol. 251, pp.231-236, 1993

[191] R B Frankel, et al, “Magneto-aerotaxis in marine coccoid bacteria”, J.Biophys., vol. 73, pp. 994-1000, 1997.

[192] E.M. Purcell, “life at Low Reynolds Number”, American Journal of Physics, vol 45, pp. 3-11, 1977.

[193] A. W. Francis, “Wall effect in falling ball method for viscosity”, Physics, vol 4: 403-406, 1933.

[194] J. Happel, “Low Reynolds number hydrodynamics”, Hingham, NY: Kluwer Boston, 1983

APPENDIX 1: Focused Ion Beam

A focused ion beam system (FIB) is a relatively new tool for microfabrication. It has some degree of analogy with a scanning electron microscope (SEM) or a transmission electron microscope (TEM). In SEM or TEM systems, the electron beam is accelerated and focused onto the surface of samples, and upon interaction with the material composing the surface, it generates electrical signals that are collected to create highly magnified images of the sample. The details of a sample can be observed and analyzed over a wide range of magnifications. Fig a.1 presents many similarities of typical SEM and FIB systems.

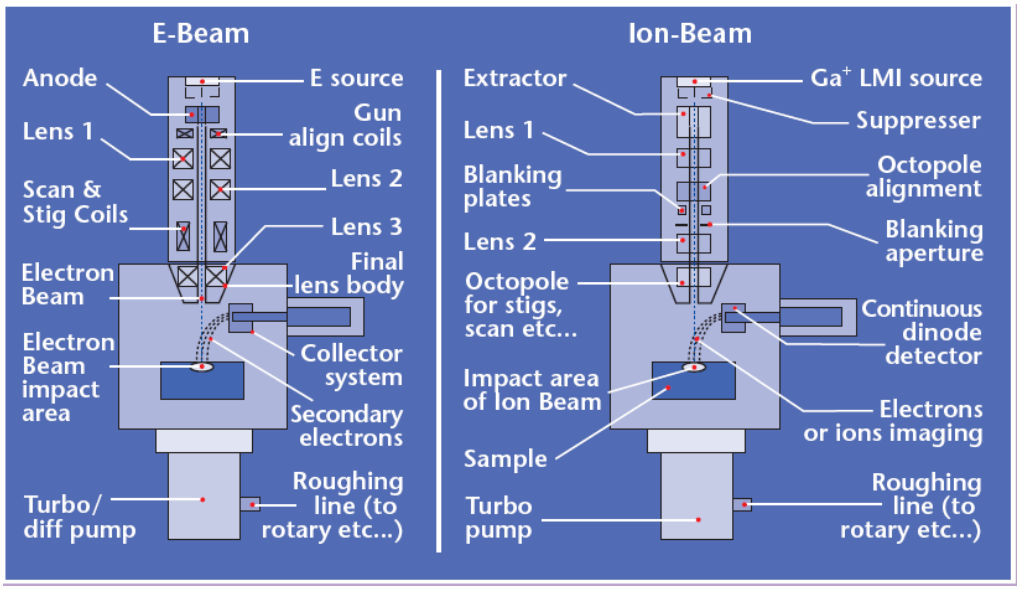

Fig a.1: Schematic presentation of the similarities between SEM and FIB systems [ref]

The main difference between SEM and FIB systems is the use of different particles to create the primary beam that bombard the surface of the sample. As the name indicates, SEM uses electrons and FIB uses ions. The major consequences of the use of ions instead of electrons are: 1) ions are larger than electrons. The size of ions is much larger than electrons, so they cannot easily penetrate deeply into the sample. 2) Ions are also much heavier than electrons. Therefore, they can gain a high momentum. When an ion hits an atom, its mass is comparable to the mass of the sample atom, and as a consequence, the target atom hit by an ion can gain enough energy and speed to cause it to be removed from the material lattice. This phenomenon is called sputtering and milling. 3). Ions are positive and electrons are negative. The sign of the particles need to be

considered only when the charging phenomenon occurs when observing isolating samples, such as glass. Table a.1 presents a quantitative detailed comparison of FIB and SEM systems.

Table a.1 Comparison between FIB and SEM system [ref]

		FIB	SEM	Ratio
Particle	type	Ga+ ion	electron	
	elementary charge	+1	-1	
	particle size	0.2 nm	0.00001 nm	20.000
	mass	$1.2 .10^{-25}$ kg	$9.1.10^{-31}$ kg	130.000
	velocity at 30 kV	$2.8.10^{5}$ m/s	$1.0\ 10^{8}$ m/s	0.0028
	velocity at 2 kV	$7.3.10^{4}$ m/s	$2.6.10^{7}$ m/s	0.0028
	momentum at 30 kV	$3.4.10^{-20}$ kgm/s	$9.1.10^{-23}$ kgm/s	370
	momentum at 2 kV	$8.8.10^{-21}$ kgm/s	$2.4.10^{-23}$ kgm/s	370
Beam	size	nm range	nm range	
	energy	up to 30 kV	up to 30 kV	
	current	pA to nA range	pA to uA range	
Penetration depth	In polymer at 30 kV	60 nm	12000 nm	
	In polymer at 2 kV	12 nm	100 nm	
	In iron at 30 kV	20 nm	1800 nm	
	In iron at 2 kV	4 nm	25 nm	
Average electrons	secondary electrons	100 - 200	50 - 75	
signal per 100				
particles at 20 kV	back scattered electron	0	30 - 50	
	substrate atom	500	0	
	secondary ion	30	0	
	x-ray	0	0.7	

All the current FIB systems use Gallium as the ion source. There are various reasons why Ga^{+} is the best choice: 1) It has a low melting temperature. Pure Ga is metallic and it has a low melting point near room temperature, as low as 30^{o}C, hence it requires limited heating and is relatively easy to integrate into a compact gun. During the operation, the gallium is in liquid phase, so the source is called a liquid metal ion source (LMIS). 2) With Ga^{+} ions, high brightness can be obtained which has direct relationship with the intensity of the beam. 3) As an element in the center of the periodic table, Gallium has an optimal momentum transfer capability for a wide variety of materials. 4) Although Gallium is present in the sample after the process, its impact on the Si lattice is very low (this material is a common doping).

Ref:

http://www.fei.com/uploadedFiles/Documents/Content/2006_06_FIBCapabilities_td.pdfhttp://www.fei.com/uploadedFiles/Documents/Content/2006_06_FIB_Overview_pb.pdf

APPENDIX2: DRIE Bosch and Cryogenic Technology

1. Cryogenic process

The main idea of the cryogenic process is to decrease the temperature in order to slow down the chemical reaction happening on the sidewalls of the etching spot. However, ions continue to bombard upward-facing surfaces and etch them away. In Cryo-DRIE, the wafer is chilled to −110 °C (163 K) [ref]. This process produces trenches with nearly vertical sidewalls.

2. Bosch process

The Bosch process, also known as pulsed or time-multiplexed etching, alternates repeatedly between two modes to achieve nearly vertical structures [ref]: 1) Etching mode: during this mode, the plasma contains ions that attack the wafer from a nearly vertical direction (for silicon, this is often sulfur hexafluoride (SF6)); 2) Deposition mode: Deposition of a chemically inert passivation layer. For instance, C4F8 source gas yields a substance similar to Teflon. Each mode lasts for several seconds or less. The passivation layer protects the entire substrate from further chemical attack and prevents further etching. However, during the etching phase, the directional ions that bombard the substrate attack the passivation layer at the bottom of the trench (but not along the sides). They collide with it and sputter it off, exposing the substrate to the chemical etchant.

These etch/deposit steps are repeated for many cycles resulting in a large number of very small isotropic etch steps taking place only at the bottom of the etched pits. To etch through a 0.5 mm silicon wafer, for example, 100–1000 etch/deposit steps are needed. The two-phase process causes the sidewalls to undulate with an amplitude of about 100–500 nm. The cycle time can be adjusted: short cycles yield smoother walls, and long cycles yield a higher etch rate.

Reference:

Marc J. Madou, Fundamentals of microfabrication: the science of miniaturization, CRC Press, 2002

http://www.alcatelmicromachining.com/amms_en/download/docs/news/doc180.pdf